ABSTRACT

INVESTIGATION OF THE BAROREFLEX OF THE RAT: STEADY STATE AND DYNAMIC FEATURES

by
Xiaorui Tang

The baroreflex is one of the most important feedback systems in the body to maintain

blood pressure variation within the homeostatic range. In this dissertation, the

important features of the carotid and aortic baroreflexes have been extensively

investigated on ventilated, central nervous system intact, neuromuscular blocked

(NMB) rats using different control system and signal processing tools. Studies have

demonstrated that sinoaortic denervation (SAD) caused substantial increases in the

blood pressure variability. Comparing the pre- and post-SAD blood pressure spectra,

there was a significant increase of power in the very low frequency region (0.00195 –

0.2 Hz), and a significant decrease of power in the low frequency region (0.2 – 0.6 Hz)

after SAD. The dominant power change after SAD was in the very low frequency

region of the blood pressure spectra.

The carotid and aortic baroreflexes were accessed by volumetric manipulation

of the carotid sinus and electrical manipulation of the aortic depressor nerve (ADN)

using step and sinusoidal stimulations. Myelinated ADN-A fibers and myelinated +

unmyelinated ADN-A+C fibers were accessed separately in the experiments. Results

showed that the baroreflex functions as a 'low-pass' filter, with –3dB cutoff frequency

at approximately <0.1 Hz. The major working area of the baroreflex system is in the VLF region of the blood pressure spectra. The estimated system transportation lag was 1.07s, which would cause the baroreflex system to oscillate at frequencies around 0.4 Hz.

Analyses demonstrated that it is not likely that the baroreflex is activated only occasionally, such as in response to postural shifts, but operates continuously to bring the blood pressure into balance. It is theoretically and experimentally demonstrated that the absolute gain of the open-loop baroreflex system can be predicted by the ratio of the pre- and post- blood pressure amplitude spectra.

INVESTIGATION OF THE BAROREFLEX OF THE RAT: STEADY STATE AND DYNAMIC FEATURES

by
Xiaorui Tang

A Dissertation
Submitted to the Faculty of
New Jersey Institute of Technology
in Partial Fulfillment of the Requirements for the Degree of
Doctor of Philosophy

Department of Electrical and Computer Engineering

May 2000

APPROVAL PAGE

INVESTIGATION OF THE BAROREFLEX OF THE RAT: STEADY STATE
AND DYNAMIC FEATURES

Xiaorui Tang

Dr. Stanley S. Reisman, Dissertation Advisor   Date
Professor of Electrical and Computer Engineering,
New Jersey Institute of Technology

Dr. Barry R. Dworkin   Date
Professor of Behavioral and Neuroscience,
Pennsylvania State University, Hershey Medical Center

Dr. Alan Snyder   Date
Associate Professor of Surgery and Bioengineering,
Pennsylvania State University, Hershey Medical Center

Dr. Alexander Haimovicn   Date
Professor of Electrical and Computer Engineering,
New Jersey Institute of Technology

Dr. Peter Engler   Date
Associate Professor of Electrical and Computer Engineering,
New Jersey Institute of Technology

BIOGRAPHICAL SKETCH

Author: Xiaorui Tang

Degree: Doctor of Philosophy

Date: May 2000

Undergraduate and Graduate Education:

- Doctor of Philosophy in Electrical and Computer Engineering,
  New Jersey Institute of Technology, Newark, NJ, 2000

- Master of Science in Electrical and Computer Engineering,
  New Jersey Institute of Technology, Newark, NJ, 1995

- Bachelor of Science in Information and Electronic Science
  Yunnan University, Yunnan, P. R. China, 1989

Major: Electrical and Computer Engineering

Presentations and Publications:

Barry R. Dworkin, Susan Dworkin and Xiaorui Tang,
   "Carotid and Aortic Baroreflex of the Rat I: Open-Loop Steady-State Properties
   and Blood Pressure Variability,"
   American Journal of Physiology, in press.

Barry R. Dworkin, Xiaorui Tang, Alan Snyder and Susan Dworkin,
   "Carotid and Aortic Baroreflex of the Rat II: Open-Loop Frequency Response
   and the Blood Pressure Spectrum,"
   American Journal of Physiology, in press.

Xiaorui Tang, Barry R. Dworkin, Susan Dworkin and Stanley S. Reisman
   "A New Approach Used to Extract Fluctuations in Vagal Activity – Wigner
   Distribution of Heart Rate Variability"
   *Proceedings of the IEEE 1st International BME, EMB Conference, 1999. Atlanta,
   U.S.*

Xiaorui Tang, Barry R. Dworkin, Susan Dworkin and Stanley S. Reisman
"Time Frequency Analysis of Heart Rate Variability in Rat Sleep/Wakefulness Cycles"
Proceedings of the IEEE 25th Annual Northeast Bioengineering Conference,1999. Connecticut, U.S.

Xiaorui Tang, Barry R. Dworkin, Susan Dworkin and Stanley S. Reisman
"Autonomic Nerve and Hemodynamic Response to CO2 in the Conscious Rat"
Proceedings of the 9th International Symposium on the Autonomic Nervous System,1998. Florida, U.S.

Xiaorui Tang and Stanley S. Reisman
"Signal Processing of Systolic Arterial Blood Pressure and Heart Rate Variability in Conscious Rats"
Proceedings of the IEEE 23rd Annual Northeast Bioengineering Conference,1997. New Hampshire, U.S.

Xiaorui Tang and Stanley Reisman
"Heart Rate Variability Study on Stroke Patients"
Proceedings of the IEEE 21st Annual Northeast Bioengineering Conference, 1995. Maine, U.S.

This dissertation is dedicated to the four most precious people in my life
my cherished parents, Ruiming Xia and Guiyao Tang
my aunt, Catherine, S. H. Chen, who provided me the most important opportunity to
further my education
and my beloved husband, Hai Xu.
They taught me how to love and how to aim high.
Their boundless support, guidance and encouragement have sustained me for as long as I
can remember.

ACKNOWLEDGEMENT

The author wishes to express her sincere gratitude to her advisor, Dr. Stanley S. Reisman, for his guidance, constantly support, encouragement, and reassurance. The author also would like to sincerely thank Dr. Barry R. Dworkin and Susan Dworkin for providing valuable and countless resources, guidance, and moral support throughout this research. Without their help, this thesis would never have been completed.

Special thanks are extended to Dr. Alan Snyder, Dr. Alexander Haimovich and Dr. Peter Engler for serving as members of the committee.

TABLE OF CONTENTS

TABLE OF CONTENTS
(Continued)

TABLE OF CONTENTS
(Continued)

Chapter   **Page**

LIST OF TABLES

LIST OF FIGURES

LIST OF FIGURES
(Continued)

CHAPTER 1

INTRODUCTION

The baroreceptor reflex plays an important role in maintaining an organism's systemic blood pressure at a homeostatic level. Abnormally low or high systemic blood pressure resulting from baroreflex malfunction could cause dizziness, fainting, loss of consciousness, brain damage, stroke, and various other symptoms. Although there has been substantial research on the baroreflex system, our present knowledge falls far short of providing a complete understanding of its mechanisms in regulating blood pressure in various situations. The major goal of this dissertation is to use signal processing and automatic control system engineering tools to further investigate the steady state and dynamic features of the baroreflex system. In the Introduction, the scope of the thesis is presented. Engineering and physiological backgrounds relevant to the thesis are introduced in Chapters 2, and 3. Experimental methodologies, protocols, data acquisition, data analysis, experimental results, discussion and conclusions are sequentially presented in Chapters 4-10.

1. 1 Scope of Thesis

The baroreflex is a complicated closed-loop negative feedback system, whose major role is to maintain the body blood pressure at a homeostatic level. Since a relatively complete investigation of the baroreflex system always involves large manipulation of the physiological state, and sometimes irreversible damages to the system, an animal model is importation for baroreflex cardiovascular studies. The goal of the present studies is the

1

use of open-loop approaches to extensively investigate the important features of the baroreflex system in rats. The dissertation contained three phases.

In the first phase of this research (study 1), the rats were sinoaortic denervated. Two purposes were served by the denervation: 1) To open the closed loop baroreflex negative feedback system. It is importation to recognize that the analyses of dynamic feedback systems under closed-loop conditions could very easily lead to erroneous conclusions [1], thus, it is essential to have an open-loop condition, under which the baroreflex investigations could be performed. 2) To investigate the effects of sinoaortic denervation (SAD) on the blood pressure signal. Changes in the standard deviation and spectra of the blood pressure signal before and after SAD were examined.

The second phase of this research involved two studies, study 2 and 3. In this phase, the steady state and dynamic features of the carotid sinus and aortic arch baroreflexes were investigated by using hydraulic stimulation of the carotid sinus and electrical stimulation of the aortic depressor nerve (ADN). In study 2, step stimulations were applied to the carotid and aortic baroreceptors, whereas, in study 3, sinusoidal stimulations were applied to both baroreceptors. The following goals were accomplished by study 2: 1) The stimulus-response curves between the baroreceptor stimulations and heart rate, blood pressure, mesenteric vascular conductance, femoral vascular conductance were derived. 2) The cardiovascular effects of the carotid sinus and aortic arch baroreflex stimulations were compared. 3) The linear region of the baroreflex system was estimated. 4) The pure time lag (or transportation lag) of the baroreflex system, defined as the time between the baroreceptor stimulation onset and the initiation of the blood pressure response, was calculated. 5) The blood pressure, heart rate, mesenteric vascular conductance and femoral vascular conductance baroreflex transfer

functions were derived from the transient responses of each individual cardiovascular component to the step responses. This is the first time that these dynamic features of the baroreflex system have been studied in conscious rats, the first time that extensive cardiovascular responses to the baroreceptor stimulations have been investigated simultaneously on the same preparation, and also the first time the transportation lag has been derived directly from experimental data from rats.

In order to avoid possible bias in the results, which may be caused simply by using the same data resources or a single data analysis method, stimulations at both the carotid sinus and aortic arch baroreceptors were varied sinusoidally in study 3. The mean and amplitude of the sinusoidal waves were chosen at the linear region of the system. The baroreflex transfer functions were derived by using the sine fit and power spectral analysis methods from the sinusoidal stimulation data. Details of these studies are thoroughly discussed in Chapter 4, 6 and 7.

In the last phase of this work, a new methodology was proposed to derive the absolute gain of the baroreflex system. It was theoretically and practically demonstrated that the absolute gain of the open-loop baroreflex system can be predicted by using the ratio of the amplitudes of the pre- and post- SAD blood pressure spectra. This result has provided a new simple direct approach to estimate the absolute gain of the baroreflex system. It can significantly reduce the experimental time over previous approaches; it provides a method to access the absolute baroreflex gain in the small organisms, e.g. mice, in which precise surgical manipulations and stimulations are not possible. Mice are important models for genetic studies.

All the experiments in the dissertation were conducted on neuromuscularly blocked (NMB) Long-Evan female rats, the unique chronic preparation developed by Dr.

Barry Dworkin at Pennsylvania State University, Hershey Medical Center [2]. The continuously monitored and maintained neuromuscularly blocked rats were ventilated at 72 breathes/min, with a 1:2 inspiratory/expiratory ratio, a minute volume of 200cc and fixed inspiratory gas mixture. Rats maintained normal heart rates, blood pressures, normal sleep-wakefulness cycles, intact sensory functions (i.e. to reliably discriminate between 2- and 4- kHz equi-intensity tones) and intact nervous systems. All experiments were conducted under no anesthesia.

CHAPTER 2

ENGINEERING BACKGROUND

The major contribution of this dissertation is the use of control and other various

engineering tools to investigate the steady state and dynamic features of the baroreflex

system. In the following sections, an overview of the control and other engineering

theories closely relating to the dissertation research is provided.

2. 1 Basic Concepts

There are two kinds of control systems: closed-loop system (feedback system) and open-

loop system (non-feedback system). If the output is fed back to the input of the system to

further affect the later outputs through the control loop, it is called closed-loop system,

shown as figure 2.1. If the output is not fed back to the input of the system, it is called an

open-loop system. The general structure of an open-loop system is shown in figure 2.2.
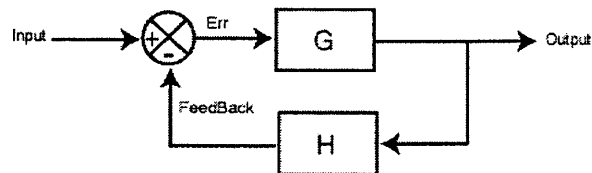
Figure 2.1 Closed-loop feedback system (from B. Kuo, *Control Systems*, 1982)
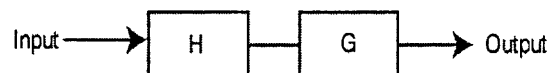
Figure 2.2 Open-loop system

The open loop system is rather unsophisticated. If parameters G and H, in the figure 2.2 are considered as constant gains, the input-output relationship of the system will simply be

$$M = \frac{Output}{Input} = G \cdot H \tag{2.1}$$

The major shortcoming of an open-loop system is that it may not satisfactorily fulfill the desired performance requirement.

Closed loop systems are much more sophisticated, accurate, and adaptive than the open loop system. As shown in figure 2.1, in the closed loop system, there is a link or feedback from the output to the input of the system. Ordinarily, the output signal is fed back and compared with the reference input, and an actuating signal proportional to the difference of the input and the output, which is called an error signal, is sent though the system to correct the error. The baroreflex system in the body is a typical feedback system. The feedback is from the blood pressure through the baroreceptors. There is a neural summing point in the central nervous system (CNS), which combines its endogenous noise with the baroafferents' output, and a hydraulic point at the baroreceptors that reflects the net action of the cardiovascular effectors relative to the sensory reference or adaptation level. The net effect of the baroreflex system is to maintain the blood pressure at a homeostatic level.

Based on the basic structure of the closed-loop system shown in figure 2.1, the input-output relation of the system is

$$M = \frac{Output}{Input} = \frac{G}{1+GH} \qquad (2.2)$$

2.2 Effects of Feedback on Overall Gain and Stability

It is evident from equation (2.2) that feedback affects the gain G of a non-feedback system by a factor of 1+GH. If GH is positive, then it decreases the gain of the overall system, and the overall system became a negative feedback system. If GH is less than 0 and greater than -1, then it increases the gain of the overall system, and the overall system is a positive feedback system. Positive feedback may cause the system to oscillate or became unstable. G and H also can be functions of frequency, for the same system, the magnitude of 1+GH can be greater than 1 in one frequency range but less than 1 in another. Therefore, feedback could be positive in one frequency range and negative in another. This frequency dependent feature clearly reflects in the baroreflex feedback system. The present study demonstrated that between 0-0.2 Hz, the baroreflex system has negative feedback, whereas between 0.2-0.6 Hz, the baroreflex system has positive feedback.

If GH = -1, the output is infinite for any finite input, and the overall system become unstable. Of course, we are only dealing with the static case here; in general GH = -1 is not the only condition for instability. One of the advantages of feedback systems is that, by incorporating feedback loop(s) to the system, an unstable system can be stabilized. Since this property of the feedback system is not closely related to the thesis, we are not going to discuss it in detail here.

2.3 Effects of Feedback on External Disturbance or Noise

Effects of feedback on external disturbance or noise depend greatly on the location at which the noise is introduced into the system. There is no general conclusion for this question. Feedback might or might not have direct effects on the signal to noise ratio of the system.
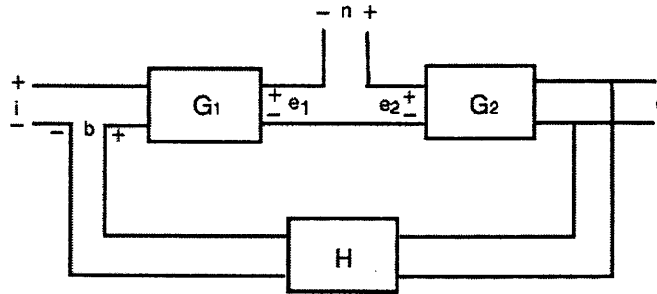
Figure 2.3 Feedback system with a noise signal (from B. Kuo, *Control Systems*, 1982)

For example, for a feedback system shown in figure 2.3, the output due to signal i and noise n acting simultaneously is

$$o = \frac{G_1 G_2}{1 + G_1 G_2 H} i + \frac{G_2}{1 + G_1 G_2 H} n \qquad (2.3)$$

The signal to noise ratio of the output is:

$$\frac{Signal}{Noise} = \frac{\dfrac{G_1 G_2}{(1 + G_1 G_2 H)} i}{\dfrac{G_2}{1 + G_1 G_2 H} n} = G_1 \frac{i}{n} \qquad (2.4)$$

From the equation, it is shown that the signal-to-noise ratio in the output is proportional to the gain G_1. To increase the signal-noise ratio, evidently we should either increase the magnitude of G_1 or i relative to n. Varying the magnitude of G_2 would have no effect on the ratio. Moreover, in this case, the feedback is shown to have no direct effect on the output signal-to-noise ratio of the system.

However, under certain conditions, feedback can improve the signal-to-noise ratio. Let us assume that in the system of the figure 2.3, if the magnitude of G_1 is increased to G_1' and that of the input i to i', with all other parameters unchanged, the output due to the input signal acting alone is at the same level as that when feedback is absent. In other words, if we let

$$o|_{n=0} = \frac{G_1'G_2i'}{1+G_1'G_2H} = G_1G_2i \tag{2.5}$$

With the increased G_1, G_1', the output due to noise acting alone becomes

$$o|_{i=0} = \frac{G_2n}{1+G_1'G_2H} \tag{2.6}$$

Now, the signal-to-noise ration becomes:

$$\frac{G_1G_2i}{\dfrac{G_2n}{(1+G_1'G2H)}} = \frac{G_1i}{n}(1+G_1'G_2H) \tag{2.7}$$

which is greater than that of the system without feedback by a factor of $(1+G_1'G_2H)$.

Therefore, from the two cases demonstrated above, it is shown that the effects of

feedback on noise could vary. The physiological body is a very complicated system, and

in the baroreflex feedback loop, physiological 'noise' is introduced along the reflex path.

Questions regarding where and how the noise is introduced into the feedback loop are

still unsolved. So far, very few papers address the noise problem in the system.

2.4 Transfer Function

In reality, all physiological systems may be nonlinear. To establish practical analysis,

whenever applicable, assumptions and approximations are made to linearize, in certain

range, the nonlinear systems, then utilize linear control theory to analyze the systems.

Similar methods were used in our baroreflex studies. In the studies, the 'linear' region of

the baroreflex system was first estimated, then the linear theory was applied to

characterize the system.

For a linear time invariant system, the input-output relationship usually is

described by a transfer function. It is well known that, in the time domain, the input-

output relationship of a linear system follows convolution theory, that is:

$$\begin{aligned} y(t) &= \int_0^t h(\tau)x(t-\tau)d\tau \\ &= x(t) * h(t) \end{aligned}$$

(2.8)

where * denotes the convolution operation.

Taking the *Laplace transform* of equation (2.8), we have:

$$Y(s) = X(s)H(s) \qquad (2.9)$$

where Y(s), X(s) and H(s) are the *Laplace transforms* of *y(t), x(t) and h(t)*, respectively.

The *Laplace transform* has transformed the real convolution process in the time

domain into an algebraic multiplication in the transform domain. *H(s)*, the *Laplace*

transform of the impulse response *h(t)*, is defined as the transfer function of the system.

$$H(s) = \frac{Y(s)}{X(s)} \qquad (2.10)$$

Under sinusoidal steady state, we set $s = j\omega$; Equation (2.10) becomes

$$H(j\omega) = \frac{Y(j\omega)}{X(j\omega)} \qquad (2.11)$$

$H(j\omega)$, a complex function of ω, is defined as the frequency response of a system,

which describes the static response of a system changes with the frequency. The $H(j\omega)$

can be expressed in terms of its magnitude and phase as:

$$H(s)\big|_{s=j\omega} = H(j\omega) = |H(j\omega)|e^{j\varphi(\omega)} \qquad (2.12)$$

where $|H(j\omega)|$ is the amplitude (gain) frequency response, and φ is the phase frequency

response.

Typical gain and phase frequency responses of a low pass system are shown in Figure 2.4, in which the gain decreases as the frequency increases. f_{co} is the cutoff frequency of a system. The cutoff frequency is the point at which only half power of the input signal passes the system. The cutoff frequency or half-power point is defined such that $|H(f_{co})| = \dfrac{1}{\sqrt{2}} = 0.707$ and roughly divides the passband ($f < f_{co}$) from the stopband ($f > f_{co}$).

It is reported that the baroreflexes of dog and rabbit behave as low pass filters [3-5], with cutoff frequencies at approximately 0.05 Hz. In this study, the spectral effects of SAD in the rat predict a similar transfer function.
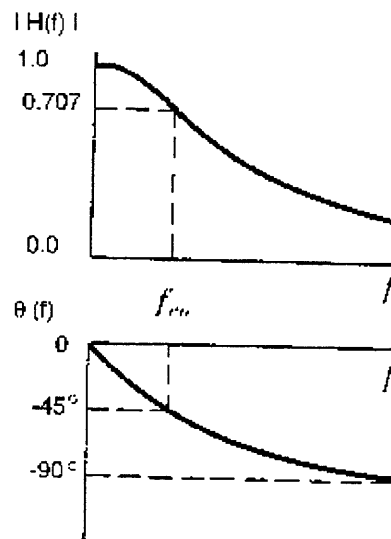
Figure 2.4 Amplitude ratio and phase shift of a low pass filter

2.5 Pure Time Lag

Pure time lag is a very important concept in system analysis. It is encountered in various types of systems, especially systems with hydraulic, pneumatic, or mechanical transmission. In these systems the output will not begin to respond to input until after a given time interval. Pure time lag exists in the baroreflex system, because when stimulating the baroreceptors, we observed that the blood pressure does not respond to the stimulation onset until a certain time lag (see figure 7.5).

Pure time lag is extremely important in a negative feedback system. Control theory states that every negative feedback system containing time lags is prone to oscillate because, as frequency increases, the output signal phase is progressively shifted from the input signal until, at a particular frequency, it is fed back positively, i.e. the output is in phase with the input [6].

Pure time lag was estimated from the blood pressure step responses in our study. Lags were estimated on 5 rats. The values for the Sinus are slightly larger than the ADN, but this difference was most likely due to mechanical delays in the balloon inflation. The mean lag for the ADN was $\approx 1.07s$, which is equivalent to a phase shift of $<10^{\circ}$ at 0.025 Hz; but 180° at 0.45 Hz. From a regular perspective, the lag would obviate the negative feedback of the baroreflex at 0.2 Hz, and reverse it at 0.45 Hz. As a remainder, 0.2-0.6 Hz corresponds to the LF region of the blood pressure spectra.

CHAPTER 3

PHYSIOLOGY BACKGROUND

3.1 The Baroreceptor Reflex System

The baroreflex is a closed loop negative feedback system, which plays an important role in restraining minute-to-minute variability of the blood pressure. The baroreflex system consists of sensory receptors (baroreceptors), afferent pathways, an integrating center in the central nervous system, efferent pathways and effector organs.

The baroreflex receptors are stretch-sensitive endings located in the carotid sinus and the aortic arch. The carotid sinus is a small dilation of the internal carotid artery just above the bifurcation of the common carotid artery. The afferent nerve fibers from the carotid sinus projects to the nucleus of the solitary tract (NTS) in the brain stem via Herring's nerve and the glossopharyngeal nerve, whose cell bodies are located in the petrosal ganglion. The afferent nerve from the aortic arch baroreceptor projects to the central nervous system by way of the aortic depressor nerve (ADN), recurrent laryngeal nerve (RLN), superior laryngeal nerve (SLN) and probably the cervical vagus (X); in all cases the cell bodies are thought to be in the nodose ganglion [7]. The sensory endings are not sensitive to intra-arterial pressure changes as such, since if an increase in intra-sinus pressure is prevented from causing distension of the vessel, then baroreceptor reflexes are not activated. In 1971, Angell provided clear evidence that aortic transmural pressure is the stimulus for aortic arch baroreceptor activation [8]. The stretching degree of the arterial wall proportionally relates to the baroreflex afferent nerve firing rate. Under normal steady state blood pressure level, the afferent nerves discharge at a certain rate. When the pressure decreases, the stretching in the arterial wall decreases, and the

nerves firing rate declines, and when the pressure increases, it increases the stretch, and thus accelerates the nerves firing rate. This stretch-sensitive feature of the baroreceptors is extremely important in our experimental design. While investigating the carotid sinus baroreflex characteristics, instead of perfusing the vessels at the carotid sinus, we inserted a balloon into the carotid sinus baroreceptor region. By inflating and deflating the balloon, we stretched the sinus vessels to different extents, and therefore stimulated the baroreflex system at different levels. The pressure information encoded in the nerve firing rate was transferred to the primary control center in the brain. The primary control center for the baroreceptor reflexes is a diffuse network of highly interconnected neurons in the brainstem medulla called the medulla cardiovascular center [9]. The detail of neural interactions between the diffuse network in the medulla is not clear. The efferent pathways from the medulla cardiovascular center are the sympathetic and parasympathetic nervous system.

The sympathetic and parasympathetic divisions are anatomically, physiologically, and functionally distinct. The nerve fibers of both divisions leave the central nervous system (CNS) at different levels, the sympathetic fibers from the thoracic and lumbar regions of the spinal cord, whereas, the parasympathetic fibers from the brain and sacral portion of the spinal cord. The cell bodies of most sympathetic postganglionic fibers lie close to the spinal cord and the cell bodies of the parasympathetic postganglionic fibers lie within the effector organs. The cell bodies of the sympathetic preganglionic fibers lie within the spinal cord, and the cell bodies of the parasympathetic preganglionic fibers lie within the brainstem. Sympathetic and parasympathetic fibers release different neurotransmitters. The major neurotransmitter release between pre- and postganglionic fibers for both divisions is acetylcholine. In the parasympathetic division, the major

neurotransmitter between the postganglionic fibers and the effector cell is also acetylcholine. In the sympathetic division, the major transmitter between the postganglionic fiber and the effector cell is usually norepinephrine [9]. Corresponding to different neurotransmitters, there are different kinds of receptors. In fact, there are several receptors for each transmitter. For example, most sympathetic receptors in the heart are $\beta 1$-adrenergic receptors whereas most sympathetic receptors in the vascular system are $\alpha 1$-adrenergic receptors. The interaction time between different neurotransmitters and receptors is different, which affects the baroreflex response time, and thus the dynamic features of the baroreflex system.

The baroreflex controlled autonomic nervous system affects blood pressure by changing cardiac output and peripheral vascular resistance. The autonomic nervous system strongly affects the heart by terminating a large number of sympathetic and parasympathetic nerve fibers on the heart. The adrenergic sympathetic fibers terminate at the SA node, conduction system, atria, ventricles and coronary vessels. When active, these sympathetic nerves release norepinephrine (noradrenaline) on cardiac cells. Norepinephrine interacts with beta-adrenergic receptors on cardiac muscle cells to affect the heart activities. Cholinergic parasympathetic fibers travel to the heart via the vagus nerve and innervate the SA node, atrioventricular (AV) node, atria, ventricles and coronary vessels. When active, these parasympathetic nerves release acetylcholine on cardiac muscle cells. Acetylcholine interacts with muscarinic receptors to affect the heart activities. The autonomic nervous system affects the heart activities through three major mechanisms: 1) by altering the slope of the pacemaker potential in the SA node. 2) by altering the speed of the conducting system of the heart. 3) by affecting the contractile force of the heart. Figure 3.1 demonstrates the effects of the autonomic innervation to the

50 │ a,b c are pacemaker potentials:

a = control
b = during sympathetic stimulation
c = during parasympathetic stimulation

Membrane potential (mV)

0

Threshold
potential

b   a   c

−50

Time ⟶
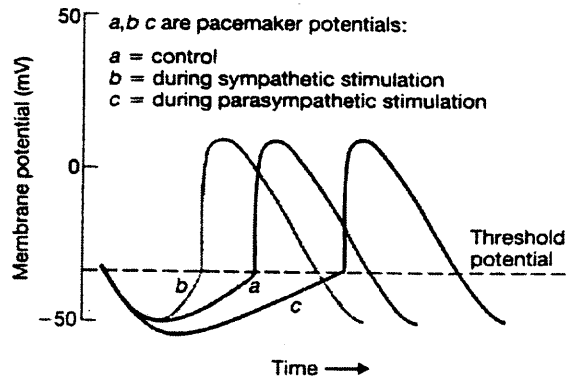
Figure 3.1 Effect of autonomic stimulation on the slope of the pacemaker potential in the SA node (from A. J. Vander, J. H. Sherman, and D. S. Luciano, *Human Physiology*, 1994)

slope of the pacemaker potential. Curve 'a' represents the control situation. Curve 'b' represents the situation when the sympathetic activity is increased. An increase in sympathetic nerve activity increases the slope of the pacemaker potentials, which causes SA pacemaker cells to reach the threshold faster, and therefore increasing the heart rate. Curve 'c' represents the situation when the parasympathetic activity is increased. An increase in parasympathetic nerve activity decreases the slope of the pacemaker potential, which causes pacemaker cells to slowly reach the threshold and decreasing the heart rate. In addition to affect the slope of the pacemaker potential, an increase in sympathetic outflow speeds conduction speed of the action potential throughout the heart and increases the heart contractility, while an increase in parasympathetic outflow slows the conduction speed of the action potential throughout the heart and decreases the heart contractility.

Vascular features are mainly controlled by the sympathetic division. The sympathetic nerve fibers innervate arterioles in all systemic organs. The sympathetic nerves release norepinephrine, which combine with the alpha-adrenergic receptor on

smooth muscle of the arterioles. Norepinephrine, combining with the receptor, causes a decrease in arteriole membrane potential and an increase in the rate of spontaneous action potential generation in arteriole smooth muscle, which results in arteriole contraction.

In a similar manner, the sympathetic neurons innervate the smooth muscle on the venous walls. Stimulation of these neurons releases norepinephrine, which causes contraction of the venous smooth muscle, decreasing the diameter and compliance of the vessels and raising the pressure within them. Increased venous pressure drives more blood out of the veins into the right heart, which will increase the stroke volume.

With but few exceptions--notably the blood vessels supplying the external genitals—there is little important parasympathetic innervation of arterioles. Where such innervation exists, stimulation of the parasympathetic nerves causes vasodilatation [9].

The sympathetic nervous system controls vascular contractility in the following manner. Normally, sympathetic nerves always discharge at a set frequency, thus causing some degree of tonic vessel constriction. When the activity of sympathetic vasoconstrictor nerves is increased above normal, arterioles constrict and cause blood flow in the vessel to fall below normal. On the other hand, when the activity of sympathetic vasoconstrictor nerves is decreased below normal, arterioles dilate and cause an increase in blood flow in the vessel. Therefore, control of the sympathetic constrictor nerves to arteriolar smooth muscle can accomplish either vasodilatation or vasoconstriction [9].

By regulating either or both peripheral vascular resistance and cardiac output through the autonomic nervous system, the baroreceptor reflex maintains blood pressure at a normal level.

3.2 Literature Review

Studies of the baroreflex regulation of the cardiovascular system largely depend on the development of surgical techniques in preparing the baroreceptor regions. In the early stage of baroreflex investigation, most studies concerning the carotid sinus and aortic arch baroreflex systems were done in dogs and rabbits. The primary reason for using these species is their size and therefore ease with which the baroreceptor regions can be isolated. In 1926, Moissejeff developed the first surgical technique to make a blind sac out of the carotid bifurcation of the dog by tying off all the arterial branches [10]. The reflex changes in heart rate and arterial pressure were provoked by putting various static fluid pressures into the sac. Since then, surgical techniques have been gradually modified, improved, simplified and various types of studies have been done to explore the features of the baroreflexes. For example, in 1932, Bronk and Stella [11] established the proportional relationship between the carotid sinus baroreceptor nerve firing rate and distension of the vessel wall; in 1969, Allison, Sagawa, and Kumada [12] made a preparation that allowed an investigation of the effects of stepwise pressure variation in the isolated aortic arch on cardiac pumping and systemic vascular resistance in anesthetized open-chest dogs. They claimed that the aortic arch baroreceptor reflex was in many ways similar to the carotid sinus reflex though there were some quantitative differences; in 1963, Scher and Young [3] produced the first systematic analysis of the dynamic performance of the open-loop carotid sinus reflex in the cat and dog over a reasonable range of frequencies (0.01-0.1 Hz).

3.2.1 Baroreceptor Surgical Preparation in Rats

3.2.1.1 Carotid Sinus Preparation: Since 1970, the rat has emerged as an important subject in the study of cardiovascular regulation, and in recent years, impressive progress has been made in understanding the basic neuroanatomy and synaptic mechanisms of the rat's baroreceptors. For CNS neurophysiology and cellular studies, the rat has the favorable characteristics of stereotaxic standardization, cost and convenient size, and in fact, for electrophysiology, binding studies, or microanatomy, larger animals, such as the dog, have little or no advantage. Also, unlike the dog where the aortic baroreceptor nerves are practically inseparable from the vagus, the rat has distinct aortic depressor nerves (ADN) in the neck, and thus, the four major baroreceptor inputs, the two carotid sinuses and the two ADN's, can be surgically isolated, and selectively stimulated or inactivated. However, in contrast to the extensive and sophisticated dog literature on baroreflex cardiovascular mechanisms, the rat literature is, so far, small and rudimentary. For the most part, studies of baroreflex mechanisms in rats have been either acute experiments in anesthetized subjects, or experiments in minimally instrumented, freely moving rats, in which pharmacological blood pressure manipulation is substituted for direct stimulation of the baroreceptors, and heart rate change is the only index of baroreflex activation. To complement and interpret the accumulating knowledge of central mechanisms, better understanding of the basic cardiovascular properties of the rat baroreflex are needed.

In 1991, Shoukas developed a new simple technique to completely isolate the carotid sinus baroreceptor regions in Long-Evans rats [14]. At the bifurcation of the common carotid artery, the external artery was first ligated at the root of the bifurcation. Then an injector was attached to a catheter in the common carotid artery, and two

cylindrical rubber plugs were introduced into the palentine and internal carotid arteries to

occlude the vessels and form a completely isolated carotid sinus in the baroreceptor

region. The schematic of isolation of the carotid sinus region is shown in Figure 3.2.
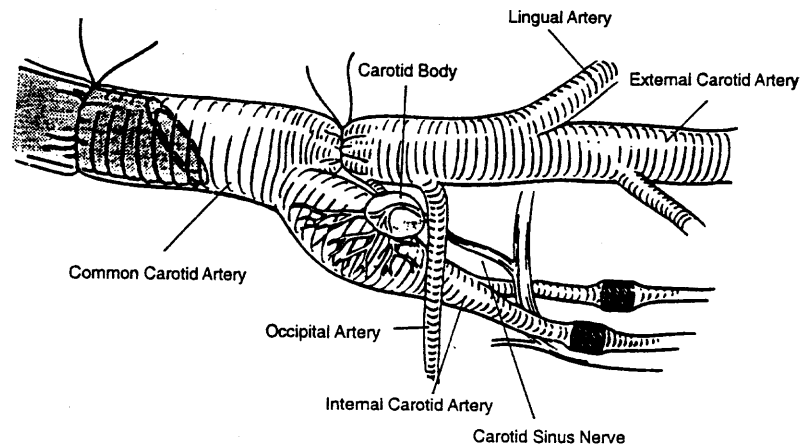
Figure 3.2 Isolation of the carotid sinus region in rat (From A. A. Shoukas, *et al.* "New technique to completely isolate carotid sinus baroreceptor regions in rats," Am. J. Physiol. 260, 1991)

Using the isolation method, McKeown and Shoukas [15] have made observations,

in conscious partially mobile Sprague Dawley and spontaneous hypertensive rats (SHR),

of blood pressure, cardiac output and heart rate. At the early stage of our experiment, we

attempted to adopt Shoukas' technique to investigate the features of the carotid sinus

baroreflex system. During the first one or two days after forming of the cul de sac at the

carotid sinus region, the methods worked satisfactorily. However, at around the third

day, the carotid sinus cul de sac started to leak. In order to investigate the carotid sinus

baroreflexes chronically, based on McKeown and Shoukas' isolation approach, our lab

developed a new method, which substituted a volumetric intra-sinus balloon, for a

barometric open sinus. During the surgery, the external carotid artery was ligated; two 0.025″ (.635mm) 316-stainless steel balls (Salem Specialty Ball, Canton, CT) were injected into the two branches of the internal carotid artery and the carotid sinus was completely isolated; a custom made cylindrical stainless steel silicon balloon was inserted into the isolated sinus. By inflating and deflating the balloon, we distended the vessels at the sinus to different degrees, and thus, stimulated the baroreflex at different levels.

Aside from Shoukas' recent work with an isolated carotid sinus preparation in freely moving rats [14], and Dr. Dworkin's earlier observations incidental to their studies of Pavlovian conditioning of the baroreflex in neuromuscular blocked rats [7], there are no other unanesthetized rat studies that describe the cardiovascular patterns of baroreceptor activation. Also, there are no previous studies that systematically described the sequelae of multiple cardiovascular response recruitment as a function of stimulus magnitude and stimulation mode. In this dissertation, some key effects of direct stimulation of the high pressure baroafferent pathways in unanesthetized rats were described; the pattern of effects mediated by the aortic receptors and those mediated by the carotid receptors were compared.

3.2.1.2 Aortic Arch Preparation: Most studies examining the aortic baroreceptor reflex features were done by electrical stimulation of the ADN. Rat and rabbit are uniquely suited for the ADN stimulation because their aortic nerve runs separately from the vagus nerve in the neck and contains only mechanoreceptor fibers [16]. The electrical stimulation of rats' or rabbits' ADN nerve, therefore, can provide a well controlled, "purely" baroreceptor input to the reflex arc. In contrast, the carotid sinus nerve contains both chemoreceptor and baroreceptor fibers, and thus, responses to the carotid sinus

nerve stimulation are more difficult to interpret. Douglas *et al.*, [17] demonstrated that on the rabbit aortic nerve, as long as the total number of impulses per second was constant, grouped impulses have the same effect as uniformly distributed pulses. The same conclusion was researched by Jonzon *et al.* with dog carotid sinus nerve stimulation [18]. However, Kendrick et al. [19] found that intermittently stimulating the carotid sinus nerve of the cat could cause much greater depression. By electrocardiogram-coupled intermittent stimulation of the rabbit aortic nerve, Stinnet *et al.* obtained a maximum depressor response [20]. Due to the heterogeneous fiber composition of the afferent nerves, the mechanism for the greater effect of intermittent stimulation is not immediately clear.

Recently, Sato *et al.* [1] developed a new technique to isolate the aortic arch baroreflex regions. In the surgery, the innominate artery was ligated at its root. A polyethylene tubing (PE-50) was cannulated into the right common carotid artery with its tip located at the bifurcation of the innominate artery. The polyethylene tube was connected to a fluid-filled transducer and servo-controlled pump system. The subclavian artery was ligated immediately proximal to its first branch, i.e. the vertebral or internal thoracic artery. The schematic illustration of in situ isolation of the baroreceptor region of the right aortic depressor nerve is shown is Figure 3.3. This technique provided us a new possibility to further investigate the aortic arch baroreflex features in rats.
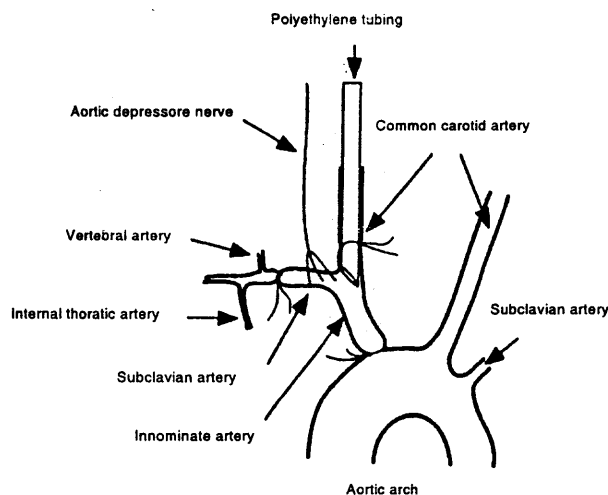
Figure 3.3 Isolation of the baroreceptor region of the right aortic depressor nerve (from T. Sato, *et al.* "New simple methods for isolating baroreceptor regions of carotid sinus and aortic depressor nerves in rats," Am. J. Physiol. 276, 1999)

3.2.2 Steady State Features of the Baroreflex System

With development of the surgical techniques, as well as the data analysis methods, features of the baroreflex system have been uncovered over the years. Since 1931, the steady state stimulus-response curve relating mean systemic blood pressure to mean carotid sinus stimulation pressure has been studied by a great number of authors across species [21-24]. The curve was found to be in a sigmoid shape across species and may be characterized by three input parameters: 1) the pressure at the threshold, 2) the pressure at the saturation level, and 3) the maximum slope of the curve, which represents the maximum baroreflex sensitivity. It was found that, for the carotid sinus baroreceptor stimulation in the dog: threshold pressure is 45-70 mmHg, saturation pressure is 170-200 mmHg, and the pressure at the point of maximal sensitivity is 120-140 mmHg [21, 23, 25]. The pressure levels for cats are comparable to those in dogs [22, 24]. The pressure levels for the rabbit are relatively lower [26]. In the rat, the threshold pressure appears to

be at around 80 mmHg, saturation pressure at 160 mmHg, and the pressure at the point of maximal sensitivity at around 120 mmHg [1, 14]. The stimulus-response relationship between aortic depressor nerve activity and aortic arch pressure stimulation showed that the steady state response of aortic nerve activity appears nearly saturated at 160 mmHg. The pressure threshold for evoking a steady state aortic nerve response appears to be ~80mmHg [1]. Sato's results' demonstrated that the stimulus-response curves were similar for both aortic arch and carotid sinus baroreceptors. Similar results were achieved by DiBona in 1994 [27]. However, other studies reported that the absolute values for threshold pressure, saturation pressure, and the pressure level at maximal sensitivity were higher for the aortic arch baroreceptors than for the carotid sinus baroreceptors [12] [21] [28, 29]. Their different results may due to the variance in their preparation procedures.

In our study, we used electrical stimulation of the ADN and volumetric stimulation of an isolated carotid sinus. Our goal was to document the pattern of activation of several key mechanisms at various levels of carotid and aortic stimulation, and to help answer questions about the interdependence of the response mechanisms. Within each stimulus mode, analysis of the stimulus strength effect is straightforward, but there is an obvious problem in comparing sinus and aortic stimulation effects, because of the difficulty of equating the mechanical and electrical stimulus properties applied at different loci. We have tried to partially resolve this by using the net blood pressure changes as a common measure of reflex activation, and comparing the subsidiary responses at similar levels of blood pressure effect; thus, to provide a rational comparative measure of patterns of activation.

Investigators also have compared different systemic blood pressure responses to pulsatile and non-pulsatile input pressure stimulation. Results showed that the shape of

non-pulsatile stimulus-responses curves is different from that of pulsatile stimulus curves for both carotid sinus and aortic arch baroreceptors. It was demonstrated that when the pulse frequency of the carotid sinus or aortic arch pressure is increased while the pulse pressure and mean pressure are kept constant, systemic blood pressure will decrease [3, 4, 30]. When the carotid or aortic mean pressure is low and carotid or aortic stimulation pulse pressure is high [3, 30, 31], this phenomenon is more distinct. It was also observed that when the carotid sinus or aortic arch stimulation pulse pressure amplitude is increased while the pulse frequency and mean pressure are maintained constant, systemic blood pressure will decrease [3, 4, 30-34]. The pulse-pressure effect is much greater at a low mean pressure in the carotid sinus or aortic arch than at a high mean pressure. It is observed that above a mean pressure of about 150 mmHg alteration of pulse pressure has little or no effect [31]. Similarly the influence of alterations in dP/dt at the carotid sinus or aortic arch is much greater at low than at a high mean pressure level.

The static stimulus-response curves between baroreceptor stimulation and the heart rate also appeared as a sigmoid shape. Recently, Shoukas [35] suggested that stimulation of the aortic arch baroreceptors evoke more heart rate response than stimulation of the carotid sinus baroreceptors. Afferent information from the aortic arch and cardiopulmonary baroreceptors contribute more significantly to the reflex heart rate response than do the carotid sinus baroreceptor. Similar results were observed in our studies. The effects of the carotid sinus and aortic arch stimulation to the systemic vascular resistance responses were reported to be opposite from what was observed in the heart rate response to the carotid sinus and aortic arch stimulation. Angell James and Daly [31] demonstrated that the reflex reduction in systemic vascular resistance produced

by a rise in the mean carotid sinus pressure was significantly greater than that resulting from the same rise of aortic arch pressure. Such results were not observed in our studies.

3.2.3 Effects of Sinoaortic Denervation

It is reported that after SAD, the blood pressure exhibits a substantially increased variability. Such increased variability was reported in rats, rabbits, cats and other animals after baroreflex denervation. Investigators [36-44] reported that the standard deviation of the blood pressure is much higher in sinoaortic denervated rats than that in the baroreflex intact rats. The quantitative increase in variability with SAD is robust, and largely independent of how it is measured. Two groups have explicitly studied the effect of the sampling interval: Alper *et al.* [37] compared 5 second to one minute measurement intervals and found no difference, and Buchholz *et al.* [45] compared one-hour to 24-hour intervals, and also found no difference; In fact, comparing across the studies, there was scarcely any difference over intervals 5 sec and 24 hours. For samples composed of individual observations, this consistency is to be expected, because the number of observations affects only the confidence interval of the standard deviation estimation, not its central tendency. However, in our study, the difference of the means of two consecutive 30 s blood pressure samples (composed of approximately 200 heart beats each), also yielded a similar standard deviation estimate. For completely random data, this is not what is expected: for samples composed of means of n observations each, the standard deviation of the samples should decrease with increasing n. A possible explanation (our predication) of this is that the post-SAD blood pressure, although random, has a non-uniform frequency distribution with greater power in the very low frequencies. Because the blood pressure data are a time series, taking a mean over n

observation is equivalent to convolution of the original data with a rectangular function of height $1/n$ and length nt, where t is the inter-observation interval; this, in turn, amounts to applying a "low-pass" filter with a cut-off frequency of less than $1/(n \cdot t)$ Hz. If the variability is within the pass-band of the filter, the filter (averaging) is without effect, or a little effect. Our predication, regarding the post-SAD blood pressure variability, was tested by calculating the spectrum of the post-SAD blood pressure signal and the filter effects of the consecutive 30 s mean difference. The analysis results agreed with our predication, which is: the post-SAD blood pressure has a great power in the very low frequency range, and the pass-band of the averaging filter overlapped the major power band of the blood pressure variability. The shape of the post-SAD blood pressure spectra is shown in figure 8.3, whereas the filter shape of the 30 s mean difference is shown in section B.1.

Much research has been conducted to explore the mechanisms underling the variability evoked by SAD. The most immediate question is whether the variability observed in SAD rats is due to the hemodynamic alterations associated with movement? Since the skeletal muscle contraction and small variations of body movement may alter vessel contractility, venous return, cardiac output, and therefore cause higher blood pressure variability. Barres et al [46] observed that, during the daytime, when the studies are conducted, the rats are more often resting or sleeping and that marked variations in the arterial blood pressure continued or were even exaggerated in the absence of movement. They concluded that the movement-induced variations in pressure represent infrequency events under the conditions of their experiments and thus would not appear to account for the source of the variability. High blood pressure variability observed after SAD in our unique rats' preparation confirmed their conclusion. In our NMB rats'

preparation, rats were positively ventilated at a constant rate, constant volume, fixed inspiratory, expiratory ratio, and fixed air mixture; no movement was involved either before or after SAD, Therefore, marked increase of blood pressure variability appearing after SAD is definitely not attributable to the muscular movement.

Alper, *et al.* reported that Chlosondamine ganglionic blockade greatly reduced the blood pressure variability after the SAD, but did not return the variability to the control rats' level [37]. Their observation suggested two things: first, the variability was probably neurally mediated in part, and second, the variability was not purely neurally mediated. Because ganglionic blockade did not totally reduced the variability to the control rat's level, other non-neurogenic mechanisms must be involved in generation of the variability. Alper *et al.* [47] reported that when SAD rats were administered Chlosondamine plus either captopril or a vasopressin antagonist, pressure variability was returned to levels seen in the baroreceptor intact rats. This suggested that hormones, by interacting with the nervous system, play an important role in producing and maintaining blood pressure variability. The same study showed that hormones by themselves do not alter the variability; thus, special interaction between hormone and neural components is critical for the variability.

It is reported that effects of muscarinic blockade with atropine or β-receptor blockade with propranolol did not significantly affect the variability of the arterial blood pressure in the rats with electrolytic lesions of the NTS. However, subsequent blockade of α_1-receptors with prazosin resulted in a 38% reduction in the lability of the mean arterial blood pressure in rats with NTS lesions [48]. In 1985, Alper, *et al.* [47] showed that intravenous administration of an α-adrenergic receptor antagonist significantly decreases the variability of mean arterial blood pressure produced by SAD. These two

experiments implied that for the neurogenic part, the baroreflex sympathetic nervous system is directly involved in generation of the variability, whereas the parasympathetic autonomic branch is less involved in generating the variability.

Now, the question is whether the sympathetic system is passively or actively involved in generating and maintaining the blood pressure variability resulting from the denervation.

Alexander showed [49] that after SAD, indices of the sympathetic activity, plasma norepinephrine(NE), epinephrine (Epi), and dopamine-β-hydroxylase (DBH), were increased significantly within 2 days in SAD rats. Afterwards, plasma NE and Epi declined by 3 weeks and thereafter remained close to values of control rats. DBH was increased in the heart, mesenteric blood vessels and adrenal glands of SAD rats up to 6 weeks, then dropped to values of control rats. However, during this time, blood pressure variability remained high. Variability did not decrease to the level of control rats as the sympathetic activity indices declined. Another study [50] showed that the renal sympathetic activity increased during acute SAD, and returned to a normal level in rats after chronic SAD. However, the blood pressure variability persisted in acute and chronic phase of SAD. Furthermore, Barres, et al. [46] showed that arterial pressure variability and renal sympathetic nerve activity are dissociated in SAD rats. Results in their study showed that arterial blood pressure and renal sympathetic activity were negatively correlated in 90% cases in control rats. However, rats with both acute and chronic SAD exhibited only 30% negative and 25% positive correlation. If, as shown in the early study [51], that the overall sympathetic drive to the cardiovascular system is indexed by renal sympathetic activity, the observations in the Barres' study, as well as in the Alexander [49] and Irigoyen's [50] studies mentioned above suggest that the high

variability of the arterial blood pressure after acute and chronic SAD is correlated infrequently with the sympathetic activity. Although the sympathetic nervous system appears to be directly involved in generation of lability, it only plays a passive role in generating and maintaining blood pressure variability after SAD. It is possible that the sympathetic nervous system is simply providing background tone to allow peripheral mechanisms to cause the marked swings in pressure observed after chronic baroreceptor denervation.

Many other studies have been conducted to exploring various possible mechanisms involved in blood pressure variability after SAD. However, so far, the real mechanism involved in maintaining the average mean arterial blood pressure in the absence of baroreflexes and the driving force behind blood pressure variability remains poorly understood.

The pre and post-SAD blood pressure variability were also studied by using power spectrum analysis. Our spectrum results showed that the arterial blood pressure spectra were both quantitatively and qualitatively different between the control and SAD rats. Blood pressure spectra were separated into three frequency bands: a very low frequency band (VLF) 0.00195 to 0.2 Hz, a low frequency band (LF) 0.2 to 0.6 Hz, and a high frequency band (HF) 0.6 to 5 Hz. After SAD, rats exhibited a huge power increase in the VLF band and a power decrease in the LF band. Our results are similar to those reported for ambulatory rats: for example, following SAD Jacob et. al. [52] found a >10 fold increase in 0.005-0.05 Hz power, and Cerutti *et al.* [53] found a >6 fold increase in the 0.02-0.25 Hz band. Although, similar to our results, the post-SAD increases in VLF power were the most prominent result of both studies, the highlighted feature of both was the comparatively small post-SAD decreases in the LF (0.3-0.5 Hz;) region of the

spectrum. Since the effect of SAD on baroreflex variability is large, and substantial variability implies substantial spectral power, this emphasis seems inappropriate. However, LF is the only region that shows a consistent decrement with SAD. Because LF power decreases with SAD, the LF peak might be said to be a "marker" of the baroreflex, but if it is, it is a paradoxical one. A negative feedback element, such as the baroreflex, constrains variability, and so an increase in noise power, not a decrease, is what is expected, when it is removed.

In fact, SAD greatly increases the VLF noise power. It is fundamental that, an element, such as the baroreflex, can oppose and neutralize a disturbance, such as endogenous blood pressure variability, only where the transfer function of the element, and the noise spectrum of the disturbance overlap; it is a corollary, that the spectral change that occurs when an element is removed delineates the element's filter characteristic; thus, the spectral change with SAD predicts the transfer function of the baroreflex will have gain in the VLF region.

It is known that the dog and rabbit baroreflex response curves have corner frequencies at approximately .05 Hz [3, 4, 54]; if the rat is similar, an intact baroreflex would substantially attenuate variability only at approximately <0.1 Hz. Why, then, would the LF peak, at 0.4 Hz, depend on an intact baroreflex? Burgess *et al.* [51, 55] modeled the rat baroreceptor reflex using a combination of transport delays and a first-order linear component, and conclude that the ".4 Hz' peak is a resonance. Their explanation is logical; it suggests that the LF peak is an aberration of the regulator, outside of its normal operating range; however, their lag estimates are calculated by combing closed-loop cross-correlation analyses with data from other species.

CHAPTER 4

METHODOLOGY

Studies in this thesis were conducted on the chronic rat model developed by Dr. Barry

Dworkin at the Department of Behavioral Science at the Pennsylvania State University,

Hershey Medical Center. The protocol was originally approved by the Rockefeller

University animal care committee in 1973, and has been monitored and re-approved by

the Pennsylvania State University College of Medicine for the past 19 years. In this

chapter, only the scope of the experimental preparation is introduced; the detail of each

preparation step is described in Appendix A. The material written in this chapter, as well

as Appendix A, mainly reference the methodology parts of references [2] and [7].

4.1 Scope of the Preparation

250-350g female cesarean derived, barrier sustained (CDBS), viral antigen free (VAF),

Long-Evans female rats (Charles River, Wilmington, MA) were used in the studies. The

rats were received 3-4 weeks prior to the start of an experiment and housed in groups of

4-6 in an isolation cubicle at the Central Animal Facilities. The night before the

experiment, all of the rats in one cage were deprived of food. The total experiment time

for each rat was at least 20 days, with an average of 30-40 days, and one rat survived for

90 days. During surgeries, the rats were under deep (>1.5%) isoflurane anesthesia, and

were positive-pressure ventilated at a rate of 72 breaths/min, with an inspiratory and

expiratory ratio of 1:2, and a minute volume of 180-200cc. Expiratory CO_2 levels were

measured using a Hewlett Packard Capnometer equipped with a modified ultra-low

volume cell located on the stainless steel expiratory tracheal tube.

Two silver wire electrodes were wrapped around two 0-80 screws mounted on the scull to record the electroencephalogram (EEG). Three subcutaneous electrodes (#30 silver wire) were implanted precordially to record the electrocardiogram (ECG). A Teflon catheter (28g) was inserted into the abdominal aorta from the left femoral artery to measure aortic blood pressure (ABP) and a renathane catheter (.040 x .025) was inserted into the inferior vena cava from the left femoral vein to administer drugs and record venous pressure. Transonic V-reflector RB-1 ultrasonic pulse transit time flow probes were applied to the right femoral artery and to the superior mesenteric artery to record blood flows. Skin flow was recorded by applying a transonic right angle type R Laser Doppler flow probe to the right paw. The rat's body temperature was regulated at 36 °C. In some rats, the right cervical vagus nerve and right peroneal nerve were dissected from the surrounding tissues; the nerve signals were acquired by attaching pairs of Teflon coded twisted silver wire (Ag7/40T, Medwire, Mt. Vernon NY) electrodes to the vagus and peroneal nerves. Urine output was monitored each hour. During the surgery, the depth of isoflurane anesthesia was adjusted to maintain the rats' blood pressure and heart rate at normal levels of MAP < 100 mmHg, and HR< 420 bpm, and the EEG was synchronized and was dominated by high voltage slow wave (δ) activity.

The ADN was dissected from the surrounding tissues, and a Ta-Ta$_2$O$_5$ field effect electrode (FEE) constructed in our laboratory was mounted onto the nerve for nerve electrical current stimulations. A silicon balloon constructed in our laboratory was inserted into the sinus from the common carotid artery for sinus pressure stimulation. The negative feedback closed loop baroreflex system was opened by sinoaortic denervation. The completeness of the denervation was assessed by a phenylephrine challenge: a bolus dose of phenylephrine (2-5 ug/kg) sufficient to increase pressure at 30-

50 mmHg was given intravenously. Bradycardia of less than 25 beats/min was used as the criterion for a successful denervation.

Details of the surgery preparation are described in Appendix A.

CHAPTER 5

EXPERIMENT PROTOCOLS

To analyze the features of the baroreflex system, electrical stimulation was applied to the
ADN nerve, and hydraulic stimulation was applied to the carotid sinus in conscious NMB
rats. Since the rat ADN contains only baroreflex axons [56-59], the cardiovascular
responses to the ADN electrical stimulation are 'purely' baroreflex in origin.

The ADN contains two kinds of nerve fibers, myelinated A fibers and
unmyelinated C fibers. These fibers have markedly different discharge characteristics
[10, 56, 57, 60-62]. Myelinated A fibers have a low current intensity threshold but take
high stimulation frequencies to produce a large depressor response, whereas
unmyelinated C fibers have a high threshold but cause a long-lasting and strong depressor
effect at low frequencies. Since the C fiber has a higher threshold than the A fiber,
stimulating the C fiber would cause the A fiber to be stimulated. Recently, a new
technology was developed by Andresen *et al.*, at the Oregon Health Sciences University,
Portland, Oregon, to separately stimulate A and C fibers [75], although no technologies
were available to separately stimulate A and C fibers when our experiments were
conducted. In our experiment, ADN-A, and ADN-A+C fiber baroreceptor reflexes were
studied separately by stimulating the ADN nerve with different current intensities and
frequencies.

There were two major patterns used for electrical and hydraulic stimulations: step
and sinusoid. Figure 5.1 shows the variety of stimulations we used in studying the
baroreflex system.

```
                                                              ┌──► A Fiber
                                            Step Stim.────────┤
                                      ┌─►                     └──► C Fiber
                    ┌─►ADN Stim.    ──┤
                    │                 │                       ┌──► A Fiber
                    │                 └─► Sinusoidal Stim. ───┤
    Baroreflex      │                                         └──► C Fiber
    Stimulation ────┤
                    │
                    │                     ┌──► Step Stim.
                    └─► Sinus Stim.    ───┤
                                          └──► Sinusoidal Stim.
```
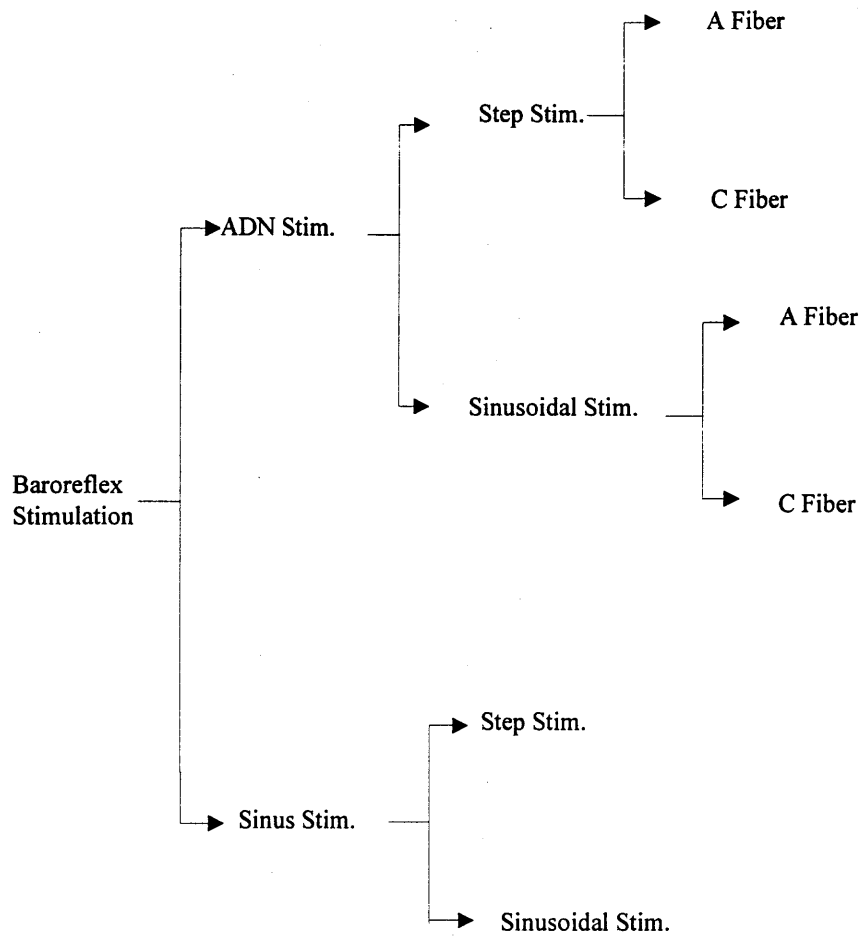
Figure 5.1 Baroreflex stimulation structure

In each hour, a total of 3 ADN-A, ADN-A+C and Sinus stimulation trials were distributed randomly. Each trial lasted for 60 s; during the remaining 57 minutes there was no stimulation (the resting periods). The resting periods were used to allow the rat's physiological state to return to baseline level.

5.1 Determination of the ADN Current Stimulation Intensity

The current intensities for the ADN-A and ADN-A+C fibers were determined by measuring the blood pressure response to test frequencies of 2 Hz and 40 Hz,

respectively. The stimulation current pulse width was fixed as 150 µs for the ADN-A fiber, and 300 µs for the ADN-A+C fiber in all cases. For determination of ADN-A fiber stimulation current intensity, a current, with a frequency of 40 Hz, and pulse width of 150 µs, was applied to the ADN nerve. The current intensity was gradually increased from zero in 10 µA steps, until the depressor response in an ensemble average of 5 trials was ≥10 mmHg. This procedure was repeated until the effect was stable for two replications. The determined current intensity was used through all the ADN-A fiber stimulation cases. The stimulator was then set to 2 Hz, and 300 µs, and the procedure was repeated to establish the ADN-A+C fiber stimulation current intensity. The longer pulse width for the ADN-A+C fiber assured that both current levels would fall within a signal range setting of the analog input of the optical isolator. This permitted fully automated control of the stimulus sequences by the computer and the Master-8 stimulator. The intensity for all the rats was around 50 - 60 µA for the ADN-A fiber stimulation, and 80 – 100 uA for ADN-A+C fiber stimulation.

The stimulation patterns for both aortic arch and carotid sinus baroreceptors were generated by a Master-8 eight channel pulse generator. For the ADN stimulation, the Ta-Ta_2O_5 FEE ADN electrode was driven by the CCIU-8 optical isolator stimulator, which was controlled by the Master-8. For the carotid sinus stimulation, inflation and deflation of the sinus balloon were controlled by a modified HP 7035A sevo X-Y plotter, which was also controlled by the Master-8.

The Master-8 channel 4 was used to drive the CCIU-8 optical isolated current source for the ADN stimulation, because the channel 4 voltage output amplitude could be programmed via the front panel or via the PC. Channel 5 was employed to drive the modified HP7035A servo X-Y plotter for the sinus stimulation. The 'increment or

decrement step mode' in channel 5 was used to set the number of steps per cycle and the value of each individual step.

5.2 Protocol 1. Baseline Blood Pressure Recording

More than 4 hours of undisturbed pre-and post-SAD baseline blood pressure signals were recorded on DAT tapes at 6 KHz sampling rate for analysis. The aim of this recording is to evaluate the effects of SAD on the blood pressure signals.

5.3 Protocol 2. Step Response

5.3.1 ADN Step Stimulation

The ADN-A, ADN-A+C fiber step stimulations were mixed in each hour. Each ADN step stimulation lasted for 60 s. The "magnitude" of the step was determined by the stimulation frequencies. With a fixed pulse duration of 150 μs and a fixed current intensity of 50 ~ 60 μA, ADN-A fibers were stimulated at frequencies of 3, 5, 10, 20, 30, 35, 40, 50 and 60 Hz. For one rat, the stimulation frequency went up to 100 Hz. With a fixed pulse width of 300 μs, current intensity of 80 ~ 100 uA, ADN-A+C fibers were stimulated at frequencies of 1, 2, 3, 5, 7, 9, 10, 11, 12, 15 Hz. ADN-A fiber step stimulations were performed on 5 rats. ADN-A+C fiber step stimulations were performed on 3 rats.

The Master-8 channel 4 controlled current output of the CCIU-8. The current output of the CCIU-8 optical isolated current source was set to 0.1 mA/Vin, which defined the output current range from 10 μA to 1 mA. The Master-8 channel 4 was set in the train mode. After a trigger, channel 4 would deliver a train of pulses. The pattern of this train of pulses determined the pattern of ADN electrical stimulation. Here is an

example of how the Master-8 was programmed to provide a 1 min 10 Hz ADN-A fiber step stimulation (with current intensity of 60 µA, and pulse width of 150 µs). Channel 4 was set in a train mode, with amplitude of 6 volts, pulse width of 150 µs, inter pulse interval of 0.1 s, and total number of pulses of 600 (60 s). After receiving a trigger from the Macsym 350, channel 4 would deliver a train with the above properties to the CCIU-8 current source, which would drive the FEE electrode to stimulate the ADN-A fiber at 10 Hz for one minute.

5.3.2 Sinus Step Stimulation

The carotid sinus baroreceptor was stimulated by inflating the balloon inserted at the sinus to different extensions. Preliminary testing with the sinus balloon determined that the maximum depressor effect was at volume of 3.5 µl, that inflation of > 4 µl could permanently damage the sinus, and that statistically reliable differences in depressor effect could be detected with 0.25 µl volume increments. Depressor effects were not elicited by volumes of less than 1 µl, and for efficiency, volume of < 1 µl were not included in the test series.

Each sinus step stimulation lasted for 60 s. Balloon volume was increased by 1.2, 1.5, 1.75, 2, 2.25, 2.75, 3, 3.25, and 3.5 µl. Inflation and deflation of the balloon were determined by the movement of the plunger of the 10 µl Hamilton gas-tight syringe mounted on the platform of a modified HP7035A servo X-Y plotter. Motion of the plunger was controlled by the Master-8. Two channels, channel 5 and 7, were involved in generating sinus step stimulation. Channel 7 was used to control the Hamilton ultra low volume motorized 3-way valve. Just before balloon inflation, channel 7 output became high, the 3-way valve was closed to the atmosphere and the balloon was

connected to the syringe. Immediately before balloon deflation, the channel 7 output became low, the 3-way valve was opened and the balloon was connected to the atmosphere. Closing and opening the 3-way valve before inflation and deflation of the balloon prevented negative pressure from being generated at the sinus during the syringe movement. Channel 5 was used to provide different sinus stimulation amplitudes by generating different voltage outputs. The syringe plunger movement was calibrated to 1 µl/volt. Channels 5 and 7 were both set in TRIG mode, which means that, following each trigger, the channels would deliver a single pulse.

Here is an example of how the Master-8 was programmed to provide a 1 min 3µl carotid sinus step stimulation. Channels 5 and 7 were set in TRIG mode, with pulse width of 60 s. The output amplitude of channel 5 was set at 3 volts. The delay for channel 5 was set at 1 s. Following a trigger from the Macsym 350, channel 7 would immediately deliver the pulse, with a pulse width of 60 s, to close the 3-way valve to the atmosphere. Delaying about 1 sec, channel 5 output a pulse, with a pulse width of 60 s and amplitude of 3 volts, to inflate the sinus balloon and stimulate the sinus at 3 µl for 1 min. The carotid sinus step stimulations were performed on 3 rats

5.4 Protocol 3. Sinusoidal Stimulation

5.4.1 ADN Sinusoidal Stimulation

Due to the difficulty of varying ADN electrical stimulation sinusoidally, an intermittent burst train, with fifty-percent duty cycle, was used to simulate the sinusoidal stimulation. The intermittent burst train was generated by switching current stimuli on and off, with equal time interval, at modulation frequencies between 0.02 to 0.4 Hz. For example, if the switch frequency was at 0.025 Hz, then the current stimuli would be delivered for 20

s (one burst), then 20 s of no stimuli, another 20 s of stimuli (another burst) and another 20 s of no stimuli, etc. Within bursts, current pulses contained fixed intensity (50~60 μA for the ADN-A fiber, 80~100 μA for the ADN-A+C fiber), pulse width (150 μs for the ADN-A fiber, 300 μs for the ADN-A+C fiber), and frequency (30 Hz for ADN-A fiber, and 5 Hz for ADN-A+C fiber). The current intensity, frequency and pulse width of the intermittent burst were all in the ADN linear response region (Details about linear region estimation were introduced in Chapter 7). Each sinusoidal ADN stimulation trial lasted for 120 s.

Two channels (including channel 4) of the Master-8 were employed to generate intermittent burst trains. Channel 4 was used to drive the CCIU-8 optical isolator. For example, if a 0.025 Hz sinusoidal stimulation was applied to an ADN-A+C fiber, one channel (other than channel 4) was set in free run mode, with inter pulse interval of 40 s (0.025 Hz). In free run mode, the channel delivers pulses continuously. Channel 4 was set in train mode, with inter pulse interval of 0.2 s (5 Hz), pulse width of 300 μs, and total pulse number of 100 (20 s). Channel 4 was set to be triggered by the free run channel. Following each pulse from the free run channel, channel 4 would deliver a train of pulses with the above properties. Since the inter pulse interval was 40 s for the free run channel, after each trigger pulse, at the output of channel 4, following 20 s of stimuli, there would be 20 s of no stimuli. The extra current pulses after 120 s were cut. The current output of the CCIU-8 optical isolated current source was set to the 0.1 mA/Vin range. The voltage amplitude of channel 4 was set at 5 volts. The ADN A+C fiber sinusoidal stimulations were performed on 1 rat, whereas, the ADN A fiber sinusoidal stimulations were performed on 3 rats.

5.4.2 Carotid Sinus Sinusoidal Stimulation

For sinusoidal stimulation, the hydraulic pressures applied to the carotid sinus were varied sinusoidally. The series stimulation signals contained a fixed mean (2.45 µl), a fixed amplitude (p-p, 1.5 µl) and different frequencies between 0.02 to 0.4 Hz. The mean and amplitude were all chosen carefully, so that the variation of the sinusoidal waves was in the linear region of the carotid sinus baroreflex system (Details about linear region estimation were introduced in Chapter 7). Three channels, channel 4, 5,and 7, were used to sinusoidally inflate and deflate the sinus balloon. Among three channels, channel 5 was used to drive the modified HP 7035A plotter. The other two channels could be interchanged with other channels. Channel 7 was used to control the Hamilton ultra low volume motorized 3-way valve. Just before balloon inflation, channel 7 output became high, and the 3-way valve was closed to the atmosphere and the balloon was connected to the syringe. Immediately before deflation, channel 7 output became low, and the 3-way valve was opened and the balloon was connected to the atmosphere. The purpose of closing and opening the 3-way valve before inflation and deflation of the balloon was to prevent negative pressure from generating at the sinus during the syringe movement. Channel 4 was set in train mode. The inter pulse intervals of channel 4 were set as the periods of the modulation cycle. The total length of the pulse train was set at 120 s. Channel 5 was set in 'increment and decrement step' mode. With the 'increment and decrement step' mode, each individual step, as well as the number of steps per cycle can be set. Channel 5 was triggered by channel 4. Following each pulse from channel 4, 10 voltage values, representing 10 steps, were delivered from channel 5 to the HP7035 plotter to drive the syringe. Each voltage value lasted for one-tenth of the period. The 10 values were calculated according to the equation

$$V = A * \sin(2 * pi * f * t - pi / 2) + m \qquad (5.1)$$

where $V = V_1, V_2 \ldots V_{10}$ are the voltage outputs.

A is the modulation amplitude.

m is the mean of the sinusoidal stimulation.

f is the modulation frequency.

The syringe plunger movement was calibrated to 1 µl/volt, so that with every 1 volt output from channel 5, the plunger moved forward 1 µl. Here is an example of generating a 120 s sinus sinusoidal stimulation wave, with mean of 2.45 µl, peak-to-peak value of 1.5 µl, and frequency of 0.025 Hz. Channel 7 was set in TRIG mode, with pulse width of 120 s. Channel 4 was set in train mode, with inter pulse interval of 40 s, total pulse number of 3, and delay of 1 s. Channel 5 was set as 'increment and decrement step' mode, with 10 steps, and step width of 4 s. The values for the 10 steps were set as 1.7, 1.887, 2.361, 2.9, 3.2, 3.2, 2.9, 2.361, 1.887, and 1.7 volts, sequentially. Receiving a trigger from the Macsym 350, channel 7 immediately delivered a pulse with width of 120 s. Delaying about 1 sec, channel 4 delivered pulses to trigger channel 5. Following each pulse from channel 4, channel 5 continuously output 10 voltages with the above values. Each step lasted for 4 s, and the time for 10 step outputs was 40 s (0.025 Hz). In this example, channel 5 received 3 trigger pulses from channel 4, and repeated the 10 step pattern 3 times, which would be total 120 s. The sinus sinusoidal stimulations were performed on 2 rats.

CHAPTER 6

DATA ACQUISITION

For each experiment, the acquired data included the electrocardiogram (ECG), arterial blood pressure (ABP), venous blood pressure (VBP), ultrasonic abdominal and femoral blood flow, laser-Doppler skin flow, peroneal and vagus nerve firing rates and raw neurograms, electroencephalogram (EEG): α, β, θ, δ power levels, intratracheal pressure (PIP), urine output, expired CO_2, and core, heater-skin interface, and ambient (air) temperatures. Urine was analyzed, daily, for specific gravity, hemoglobin, pH, glucose, protein, nitrogen, bacteria and yeast. In each of the first four days of the experiment and when necessary thereafter, 150 µl of blood was drawn from the arterial cannula and analyzed for pO2, pCO2, pH, Na+, K+, glucose, hematocrit, total protein, prothrombin time and WBD.

Three data acquisition systems, Macsym 350, HP 3852A and Teac RD-145T tape recorder, were employed in the study. The three systems contain different features and are suitable for different kinds of analysis.

The Macsym 350 acquired data based on cardiac-respiratory cycles. The data acquisition cycle was triggered 100 ms before each inspiratory peak by a hall-effect device on the respirator shaft. The first sample was taken at the first systolic blood pressure maximum, the second sample at the diastolic minimum, the third at the first systolic maximum after the start of expiration, and the fourth at the next diastolic minimum. A new cycle was initiated 2.5 sec after the start of the previous cycle. 55 physiological variables were continuously acquired by the Macsym 350 during the entire

experiment procedure. The Macsym provided us the best opportunity to monitor the interaction of the most variables in the physiological system.

The HP 3852A acquired data based on cardiac cycles. The data acquisition cycle was triggered by TTL pulses generated by the window discriminator (FHC Brunswick, ME 04011, USA) at EKG R wave positions. In every cardiac cycle, two samples were taken from each physiological variable. The first sample was taken at the systolic blood pressure maximum and the second sample was at the diastolic minimum. 23 physiological variables were continuously acquired during the entire experiment period. Compared with the Macsym 350 system, the HP 3852A acquired data at higher resolution but fewer variables.

The Teac RD-145T is a 16-channel high-density multiplex PCM data recorder. The sampling rate was 6000 samples/second per channel, which contains the highest sampling rate among the three data acquisition systems. The Teac tape recorder was only used to acquire data during certain event periods. Table 6.1 summarizes the sampling rates for each of the three data acquisition systems.

Table 6.1 Sampling rate of the data acquisition systems

Acquisition System	Sampling Period (s)
Macsym 350	2.5
HP 3852A	Cardiac Cycle
Teac RD-145T	1/6000

In the following sections, first, the general structure of the entire data acquisition system is presented, then, each of the three acquisition system is introduced. Since the HP 3852A configuration is part of the dissertation work, it is described in detail.

6.1 Structure of the Entire Data Acquisition System

Figure 6.1 demonstrates the general structure of the entire data acquisition arrangement. From top to bottom, left to right, the rats' vagus and peroneal nerve signals were first fed into the Xcell-3x4 4-channel microelectrode amplifier. There, according to the experimental situation, nerve signals were amplified 1000~5000 times. The amplified nerve signals were then split into two branches (shown in the figure). One branch was directly fed into the TEAC tape recorder to be acquired. Another branch was fed into FHC Window Discriminator. The time base for the two nerve channels in the Window Discriminators was set as 20 ms. The trigger levels for the nerve counters were set by maximizing the amplitude of the pulse synchronous component of the ensemble averaged firing rate (because the raw nerve data were all on tape, they could be reanalyzed with different criteria). The TTL pulse outputs, corresponding to nerve spikes, were fed into the Counter/Totalizers of both the HP 3852A and the Macsym 350 acquisition systems to be recorded. Each channel in the Window Discriminator also contained a digital-to-analog (DAC) converter. The Discriminator passed nerve pulses to the DAC in the Discriminator, which proportionally converted nerve rate information into voltage outputs, which was called as analog nerve activity. The analog nerve activity was then fed to the voltmeters of both the HP 3852A and the Macsym 350 to be recorded. The analog nerve signal paths are not shown in the figure.
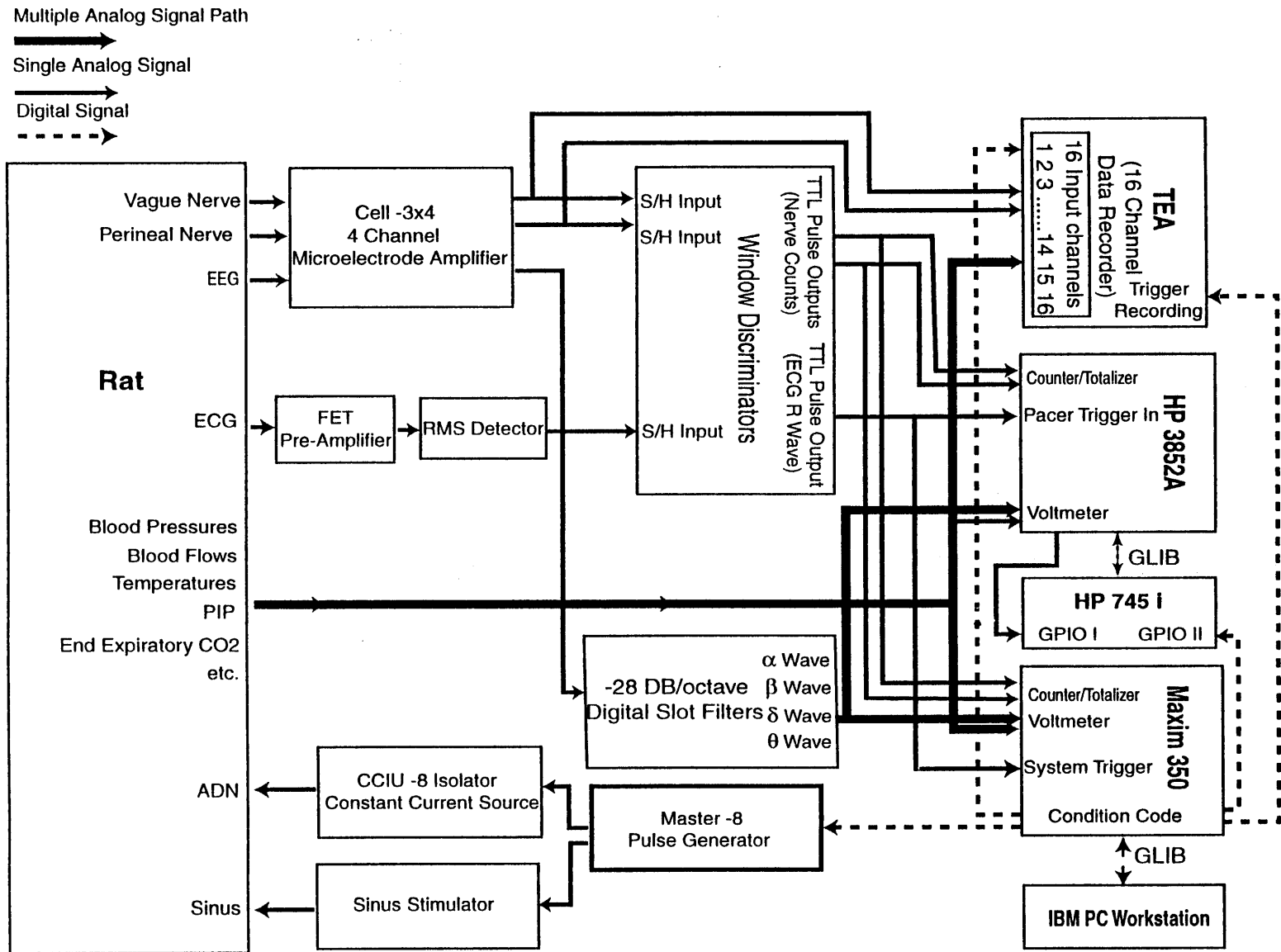
Figure 6.1 General structure of the entire data acquisition system

The EEG signal was first fed into the Xcell-3x4 4-channel microelectrode amplifier, and the amplified EEG was then fed into $-28DB$/octave digital slot filters, where the signal was separated into 4 wave bands, δ (0.5-3 Hz), θ (6.6-7.5 Hz), α (8.5-18 Hz) and β (20-45 Hz). The 4 wave band signals were then sent to the voltmeter of both the HP 3252A and Macsym 350 systems to be recorded.

The three lead ECG signal was first fed into a dual field effect transistor amplifier. The amplified ECG signal was sent into a RMS detector, whose output was sent to the FHC Window Discriminator. The TTL pulse outputs, corresponding to the R wave in the ECG signal, were used as triggers for the HP 3852A data acquisition system. Following each R wave TTL pulse trigger, the HP 3852A system pacer sent out a train of pulses (6 pulses), which synchronized the whole HP 3852A acquisition system. The scheme of the HP 3852A data acquisition system is described in detail in Section 6.2. The R wave TTL pulses were also fed into the Counter/Totalizers of both the HP 3852A and Macsym 350 system, where the inter beat intervals were calculated and recorded.

Through Baxter 43-600 uniflow disposable pressure transducer (Irvine, CA), the femoral arterial and venous pressures were amplified and fed to the voltmeters of the HP 3852A and Macsym 350 to be recorded. Similarly, through a temperature transducer, rats' temperature was amplified and recorded by the HP 3852A and Macsym 350 systems.

Through transonic and Doppler flow meters, the mesenteric, femoral and the skin blood flows were directly sent to the voltmeters of the HP3862A and Macsym 350 systems.

Expiratory CO_2 levels were measured using a HP 47210A Capnometer equipped with a modified ultra-low volume cell located on the stainless steel expiratory tracheal

tube. The output of the Capnometer was directly fed into both the HP 3852A and Macsym 350 acquisition systems.

Experimental schedules were controlled by the Macsym 350. Before each experiment, stimulation schedules and stimulation patterns were loaded into the Macsym 350 and Master-8, eight-channel pulse generator, respectively. A total of 8 paradigms could be programmed in the Master-8. According to the time schedule, the Macsym 350 selectively activated the paradigms in the Master-8. The output of the Master-8 drove the CCIU-8 isolator constant current source, or the 10 μl Hamilton gas-tight syringe mounted on the bed of the HP 7035A servo X-Y Recorder, to stimulate the ADN and carotid sinus, respectively.

6.2 HP 3582A Data Acquisition System

The HP 3852A data acquisition system employed a mainframe and six different kinds of plug-in accessories. The six plug-in accessories are the HP 44704A high-speed voltmeter, HP 44711B 24 channel high-speed FET multiplexers, HP 44715A 5 channel counter/totalizer, HP 44733A 4-Bridge 350 Ohm dynamic strain gage FET multiplexers, HP 44721A 16 channel digital input board and HP 44724 digital output board. The HP 3852A data acquisition system is controlled by the HP VEE program running on a HP UNIX workstation.

Sequentially, the HP VEE acquisition program performs three major steps, 1) System configuration, 2) Data transferring, and 3) Data saving. Figure 6.2 is the flow chart of the general structure of the acquisition system.

```
┌─────────────────┐
│     Start       │
└─────────────────┘
         │
         ▼
┌─────────────────┐
│ System Configuration │
└─────────────────┘
         │
         ▼
┌─────────────────┐
│ Data Transferring │
└─────────────────┘
         │
         ▼
┌─────────────────┐
│  Data Saving    │
└─────────────────┘
         │
         ▼
┌─────────────────┐
│      End        │
└─────────────────┘
```
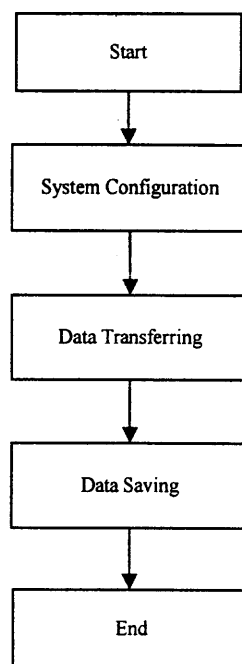
Figure 6.2 Outline of the data flow in the HP 3852A system

At the beginning of each experiment, the acquisition system was initiated, the HP 3852A main frame and six different accessories were configured individually. After initiation, data were continuously acquired. The acquired data were transferred from the HP 3852A to the HP UNIX workstation at every cardiac cycle. At the end of each hour, data were saved into the HP UNIX hard disk. At the end of two or three days, data on the HP UNIX hard disk were transferred to a CD disk for permanent storage, thus, hard disk spaces was freed up for further data acquisition.

In the following sections, the major features of the HP 3852A main frame and six different plug-in accessories are first briefly introduced, then the detailed mechanism employed in the data acquisition system is described.

6.2.1 Characteristics of HP 3852A Mainframe and Six Plug in Accessories

6.2.1.1 The HP 3852A Main Frame: The HP 3852A is an updated Hewlett-Packard

data acquisition and control unit. It could measure temperature, strain, voltage,

resistance, analog input and digital input, and any other physical/electrical properties.

The HP 3852A could sample data up to 150,000 readings per second (digital), and

100,000 readings per second (analog). With its own MC 68000 processor, the HP 3852A

can download subprograms and other tasks from the host computer, saving its resources

for high-level tasks. To function as a data acquisition unit, the HP 3852A depends on its

plug-in accessories. Every HP 3852A mainframe could hold 7 accessories and carry 6

HP 3852A extenders, while every extender could hold 9 accessories.

The system pacer contained in the HP 3852A mainframe can be used to regulate

the speed of the backplane scan, or it may be used to trigger functions within the HP

3852A or in external devices. When activated, the pacer of the HP 3852A can output 1 to

65535, or a continuous stream of negative-going pulses. The pulse width can be set to

either 0.5 µs or 5.0 µs. These pulses are capable of driving CMOS/HCMOS, TTL and

LSTTL loads.

Interrupts could be generated from the HP 3852A plug in accessories, and

handled either with the mainframe or with the controller.

6.2.1.2 The HP 44704A High-Speed Voltmeter: The HP 44704A is a 16 bit high-speed

voltmeter. For the ribbon cable measurement, which was configured in our acquisition

system, the scan rate for the measurement could reach 100,000 readings/second in

channel to channel operation.

The voltmeter has an on-board microprocessor, which accepts commands from the mainframe. With ribbon cable operation the voltmeter is capable of operating independently. That is, the voltmeter is configured by commands issued from the mainframe and can then operate independently via the ribbon cable to take and store measurements.

6.2.1.3 The HP 44711A 24 Channel High-Speed FET Multiplexer: The HP 44711A is a 24 channel high-speed FET multiplexer. With ribbon cable operation, the multiplexer operates independently of the mainframe. The maximum switch rate for the ribbon cable operation is 100,000 channels/sec. Each channel on a HP 44711A can be configured independently, so multiple functions can be measured on the same accessory.

6.2.1.4 The HP 44733A Dynamic Strain Gage FET Multiplexer Accessory: The HP 44733A is a 4-channel dynamic strain gage FET multiplexer. Each individual channel can have a gain of 1, 10, or 100. Each channel can perform filtering, track/hold, positive peak detection, negative peak detection, or the signal can be directly sent to a multiplexer channel. In this study, the HP 44733A was set in peak detection mode for detecting blood pressure peaks.

Figure 6.3 shows the basic structure of the relationship between the high-speed voltmeter, high speed FET multiplexer and computer in our data acquisition system.
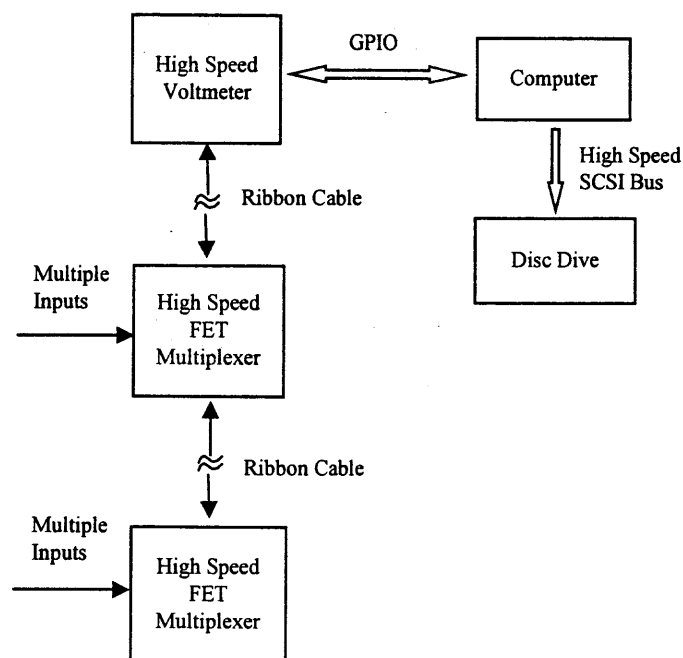
Figure 6.3 Relationship between the high-speed voltmeter, FET multiplexer and computer

6.2.1.5 The HP 44715A 5 Channel Counter/Totalizer: The HP 44715A is a 5 channel counter/totalizer, which contains two types of functions: counting and measuring. The counting functions include totalize counts, up/down counts, and count with direction control, while the measuring functions include ratio measurement, period measurement, and frequency measurement. The counting speed of the totalizer could reach 200 kHz. On counter overflow or measurement complete conditions, an interrupt can be generated from the HP 44715A.

Two HP 44715A accessories were used in this study, one was set as period measurement to measure the cardiac cycle period. The other one was set as totalize counts for counting the nerve firing rate.

6.2.1.6 The HP 44721A 16 Channel Digital Input Accessory: The HP 44721A is a 16 channel digital input accessory, which can be used to detect the state of an input, count input state changes (edges), and generate interrupts on state changes and counter overflow conditions.

In our system, it was used to count state changes of the pulse signal generated by the mainframe pacer, and generate interrupts on the overflow conditions.

6.2.1.7 The HP 44724A Digital Output Accessory: The HP 44724A is a 16-channel digital output accessory. Each channel on the accessory acts as an ON-OFF switch to control low-voltage DC devices, or to drive logic levels. The digital output accessory can be used to switch devices on or off at rates up to 1 kHz. In our system, the HP 44724A was configured to start and stop the HP 44715A (counter/totalizer) counting operation.

6.2.2 Physiological Signals and Their Accessories

For the purpose of clarity, before describing the algorithm of the HP 3852A acquisition system, we first present Table 6.2, in which the HP 3852A accessories and their relating input physiological signals are listed.

The HP 3852A acquires 23 physiological variables. In order to acquire as much of the important information to the existing amount of disc space as possible, a large amount of unnecessary data in the signals were filtered out at pre-processing stages using different HP 3852A plug-in accessories. For instance, the blood pressure signals, since the systolic and diastolic pressures were the only values we planned to record, both femoral arterial and venous blood pressure signals were fed into the HP 44733A strain gage multiplexer. The HP 44733A strain gage multiplexer was set in peak detection

Table 6.2 Signals and their corresponding accessories

Accessories	Physiological Signals
HP44733A; HP 44704A	Femoral Arterial Blood Pressure; Femoral Venous Blood Pressure
HP 44715A (1)	Vagus Nerve Activity; Peroneal Nerve Activity
HP 44715 A (2)	R-R Intervals (IBI)
HP 44711A; HP 44704A	Left Femoral Arterial Blood Flow; Mesenteric Blood Flow, Right, Left Peripheral Vasoconstriction; Cerebral Blood Flow; EEG $\alpha,\beta,\delta,\gamma$ Wave Power; R Wave Amplitude; Respiration; Expiratory CO_2; Positive Inspiratory Pressure; Caudal Temperature; Ambient Temperature; Plate Temperature; and Time Code
HP 44721A	R Wave Pulse Number; Pacer Pulse Number

mode. For each cardiac cycle, systolic and diastolic values of the femoral arterial and venous blood pressures were detected by the HP 44733A, and only those two values of each blood pressure signal were transferred to computer disc for storage. In this way, the HP 44733A discarded a large amount of blood pressure data, which are unnecessary to the experiment.

Similarly, for the EKG signal, the periods of R to R intervals in the EKG signal were measured by feeding the EKG signal into the HP 44715A counter/totalizer accessory. The counter/totalizer EKG channel was set in period measurement mode. For each cardiac cycle, only one value, which was the interbeat interval, was acquired and stored by the HP 44715A for the EKG signal.

Nerve activities were represented by the total number of spikes generated within each cardiac cycle. The number of TTL pulses, corresponding to the total number of nerve spikes for each cardiac cycle, generated by a window discriminator (FHC Brunswick, ME) were counted by the HP 44715A counter/totalizer and stored in the system disc.

In the system, the HP 44711A 24 channel FET multiplexer was used to collect most of the signals (Table 6.2). It collects signals at a rate of 2 points per cardiac cycle, one point at the cardiac systolic position, and one point at the cardiac diastolic position for each signal.

6.2.3 HP 3852A Data Acquisition Algorithm

In this section, the logic sequence of the HP 3852A data acquisition system, shown in figure 6.4, is explained. The description follows top to bottom, left to right order.

First, it has to be emphasized that the HP 3852A data acquisition system was triggered by the TTL pulses generated at the ECG R wave positions by the Window Discriminator (FCH, Brunswick, ME), missing R wave pulses for several cardiac cycles would cause the HP 3852A data acquisition system to hang.

Following each TTL R wave pulse, three events were triggered to occur in the HP 3852A system. 1) The system pacer in the HP 3852A main frame was externally triggered to generate a train of pulses. The pacer train contained 6 pulses, and the inter pulse interval was 15 msec. 2) The HP 44721A digital input board was externally
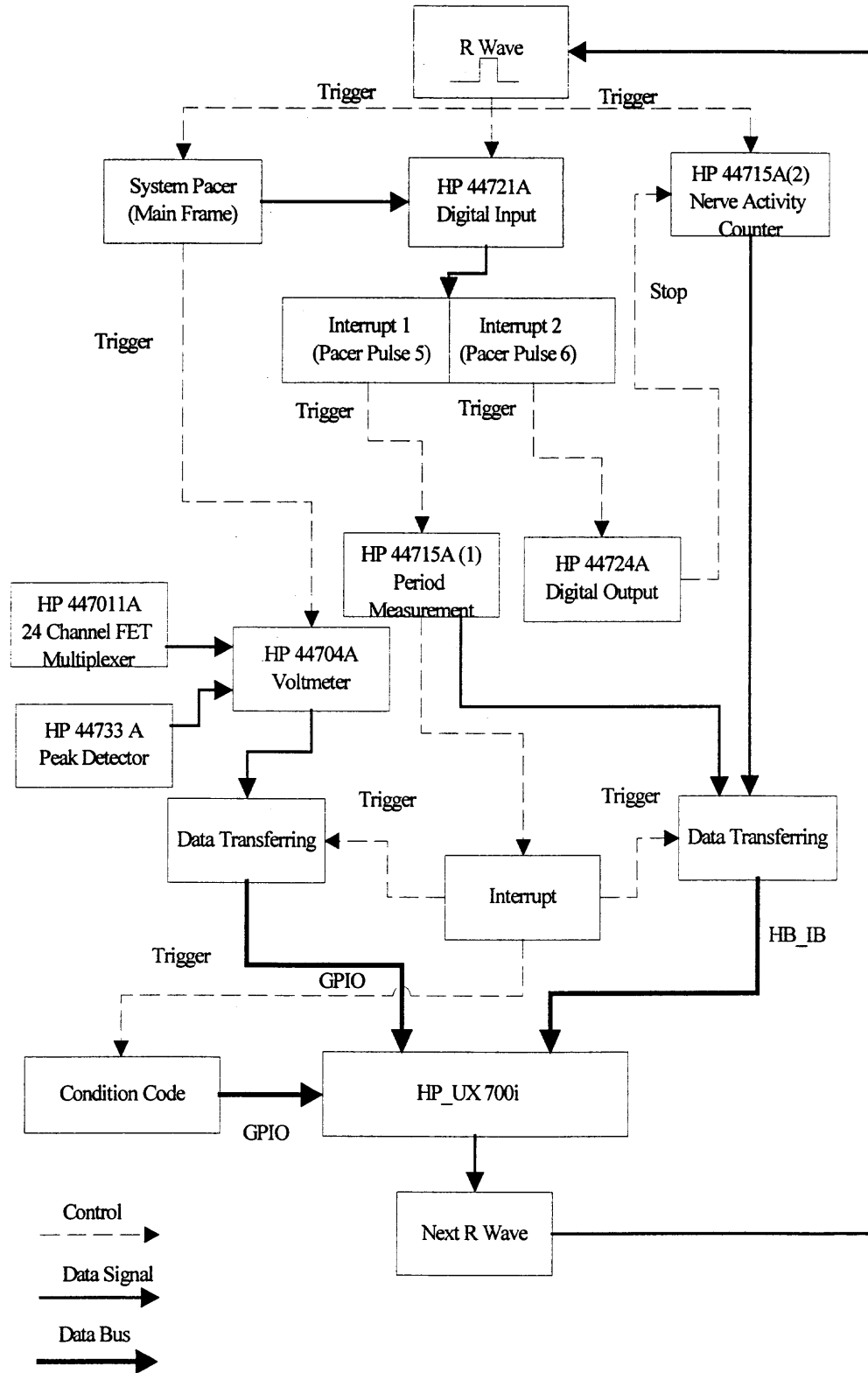
Figure 6.4 Logic sequence of the HP 3852A data acquisition system

triggered to count the pulses of the input signal, which was the system pacer train. 3) The

counter/totalizer (2), HP 44715A (2), was externally triggered to count nerve activities.

Nerve activity was represented by the number of TTL pulses generated at nerve spikes by

the Window Discriminators. Two nerve signals were fed into the HP 44712A (2) board.

The system pacer train played an important role in synchronizing the acquisition

process. The pace pulses performed two major functions: first, they served as external

scan triggers for the HP44704A voltmeter. On each trigger (pulse), the voltmeter

scanned the list of channels connected to the HP 44711A multiplexer. The channels in

the scan list included three blood flow signals, two blood pressure signals, EEG σ, θ, α,

and β waves, R wave amplitude, positive inspiratory pressure, two analog nerve signals,

expiratory CO_2, positive inspiratory pressure, caudal temperature, ambient temperature,

plate temperature, and time code. The scanned in data were temporally stored in the

voltmeter memory, at the end of each cardiac cycle, data were transferred to the HP UX

workstation via GPIO bus. Second, the pacer pulses were counted by the HP 44721A

digital input board, which generated two interrupts on the 5th and 6th pulses of the pacer

train. The interrupt generated on the 5th pulse triggered HP 44715A(1) to start a period

measurement on the heart rate signal. The period measurement measured the time

between the 6th pacer pulse and the 1st pacer pulse of the next pacer train. The interbeat

interval was derived by adding 75 ms (The time between the 1st pulse and the 6th pulse in

the first pacer train) to the time measured between the 6th and the 1st pulses. The interrupt

generated on the 6th pulse triggered the HP 44724A digital output board to stop the HP

44715A (2) from counting the nerve activities. The measured nerve activities (during the

75ms of the systole cardiac period) and heart rate period (measured afterwards) were

stored in a system array in the HP 3852A main frame. During this period, the system

reset the HP 7721A digital input board, and HP 44715A (2) counter/totalizer, so that these boards could be ready for the next cycle. The pacer trigger was also reset, so that it could generate a pacer train when the next R wave occurred. After finishing the period measurement, the HP 44715A (1) generated an interrupt, which triggered to start data transferring. Data in the output buffer of the HP 3852A, collected by the voltmeter, were transferred to the HP-UX via the GPIO bus, the condition code was transferred to the HP-UX via another GPIO bus, whereas, the data array in the HP 3852A memory was transferred to the HP-UX via the HP-IB bus.

In the acquisition, data was acquired in 64-bit real format; however, in order to save storage space, data were saved as 16-bit integer format. In order to avoid quantization errors, data in each channel were scaled before the storage.

In scaling, first, data, in each channel was rectified, then the maximum value of the rectified data was calculated and a factor b was derived by the formula:

$$b = floor(\log 32767.9 / m) \qquad (6.1)$$

where m is the maximum value of the rectified data in each channel. 32768 is the maximum value that a 16-bit integer data could represent. b is the factor to be derived. *floor* is a matlab function. *floor(x)* rounds the elements of x to the nearest integers towards minus infinity.

After b value was available, data in each channel was scaled according to the formula:

$$Scaledata = 10^b * data \qquad (6.2)$$

where *Scaledata* was the data after being scaled, *data* was the original data in each channel. After being scaled, the data value in each channel filled up all quantization levels that a 16-bit integer could provide, and thus, quantization error was avoided. Of course, during the data analysis stage, data had to be re-mapped to the original values.

6.3 Macsym 350

The Macsym 350 is the earliest data acquisition system developed in Dr. Dworkin's lab at Pennsylvania State University, Hershey Medical Center. It did not have a very high sampling rate, only 2.5 second per sample. However, its acquisition cycle was synchronized with cardio-respiratory cycles. Each acquisition cycle was triggered 100 ms before the inspiratory peak by a magnet sensor positioned on the respirator shaft. The first sample was during the first systolic blood pressure maximum, the second sample during the following diastolic minimum, the third during the first systolic maximum after the beginning of expiration, and the fourth during the following diastolic minimum. Each of these 4 cardio-respiratory coordinated samples included 55 variables. Data were in an industry standard binary data format (HP-BDAT) [7]

This acquisition system also provided trigger signals for the Teac and HP 3852A acquisition systems.

6.4 Teac RD-145T

The Teac RD-145T (Teac America, Inc. Methuen MA) is a high-density multiplex PCM data recorder utilizing helical scanning recording techniques on standard DAT tape. It contains 16 selectable data channels, which acquired condition code, EKG, aortic blood pressure, EEG, raw peroneal nerve activity, raw vagus nerve activity, nerve stimulation

current, positive inspiratory pressure, integrated peroneal nerve activity, integrated vagus

nerve activity, CO_2 level, carotid sinus hydraulic pressure stimulation signal, venous

pressure, cerebral brain blood flow, mesenteric blood flow and right femoral blood flow.

The sampling rate for each channel was set at 6000 samples/second.

CHAPTER 7

DATA ANALYSIS

In order to have a relatively complete understanding of the baroreflex system, extensive analyses were performed on the experimental data. First, the effects of the SAD on the blood pressure signal was investigated, and a comparison was made between the power spectra of the baseline blood pressure signal from the baroreflex intact rats and spectra of the baseline blood pressure signal from the SAD rats. Second, the steady state features of the baroreflex system were investigated, and the linear response region of the baroreflex system was estimated. Third, the dynamic features of the baroreflex system were estimated by three system analysis techniques: 1) Step response, 2) Spectrum analysis, and 3) Sinusoidal fit. In the following sections, details of each analysis method are described.

7.1 Spectral Analysis of Arterial Pressure Lability in Rats with SAD

Data used in this analysis were the baseline blood pressure data from the pre- and post-SAD periods. Data were acquired according to protocol 1 described in section 5.2. The blood pressure signals used for analysis were extracted from Teac tapes. There are two major reasons for using the Teac data, but not the Macsym 350, and HP 3852A data. For the Macsym 350, with a sampling rate of 0.4 Hz, it is only suitable for investigating data whose maximum frequency is less than, or equal to 0.2 Hz. In our case, the blood pressure contains frequency of more than 1 Hz. For the HP 3852A system, although its sampling rate is high enough to avoid the aliasing problem, the system was not engaged

during the most the pre-SAD period (except for rat EH), and data was missed during the acquisition stage for the pre-SAD period.

The blood pressure traces were extracted from the tape with QuickVu-RD software, version 1.04, developed by the Teac Company (TEAC America, Inc. Methuen MA 01844). Data on the tape was located according to the data ID and COUNTs information recorded on the logbook during the acquisition stage. 100 segments of baseline data were randomly chosen and downloaded from tapes. 50 of them were from pre- and 50 of them were from post-SAD periods. Each segment was 1.5 min. The major steps used for deriving the spectra are shown in figure 7.1.

In the spectral analysis, the systolic peaks were first detected: data was low pass filtered and detrended. A horizontal window, with a length of about one cardiac cycle, was used to discriminate against false detections. A threshold determines a vertical window below which peaks were ignored. The threshold was chosen as 15% of the maximum value of the entire blood pressure trace plus 30% of the maximum value of the blood pressure in the window range. Since the threshold values depend on the window's local positions, it varies with the baseline level. Within each window, the maximum value (the peak), above the threshold was detected. The horizontal window was moved in such a way that the beginning of the next window is at the previous peak position. The detected peaks were stored in a vector.

Due to noisy blood pressure as well as the presence of dichrotic notches, some false detections may occur during the peak detection. The accuracy was checked by plotting the detected peak values on top of the blood pressure signals. If the false detections were severe, then the peak detection had to be reprocessed. During the
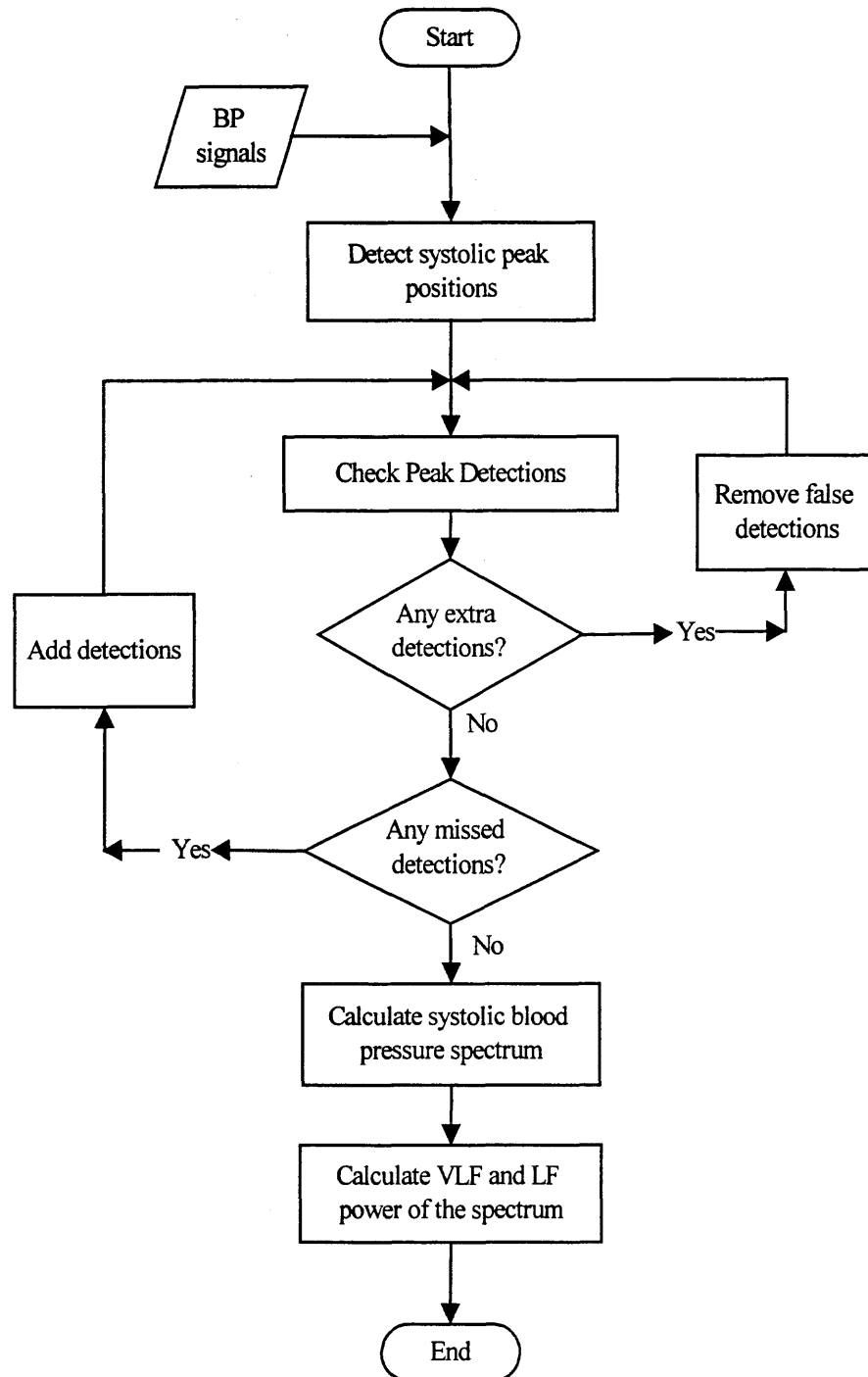
Figure 7.1 Flowchart of the blood pressure spectrum analysis

reprocessing, the horizontal window size and threshold had to be re-chosen. For the non-severe false detection cases, missed detected peaks could be manually added, and double detected peaks could be manually deleted. The adding peak processing contained two steps: 1) Locate missed peak positions. 2) Add missed peak wave into peak vector. The deleting peak processing also contained two steps: 1) Locate double detected peak positions. 2) Delete double detected positions from the peak vector.

Since the detected peaks were not equally spaced alone the time axis, the signal was interpolated using the backward step function. The backward step interpolation assumed that no new information about the direction of the time series was available until the next heartbeat occurred. The amplitude of all of the interpolated systolic blood pressure valued between a beat at time T_{n-1} and the beat at T_n were set equal to the amplitude of the systolic value at the beat at T_{n-1} The spectrum was calculated on the interpolated systolic blood pressure signal.

The spectrum was calculated by first Hanning windowing the entire data sequence, then, a 16384 point FFT was performed on the windowed sequence. The power was calculated as the magnitude squared of the FFT. The corresponding frequency vector of the spectrum was created according to:

$$f = Fs * (0 : nfft / 2) / nfft \tag{7.1}$$

where Fs is the data sampling frequency, and nfft is the length of the FFT. A flowchart of this program is shown in figure 7.2.
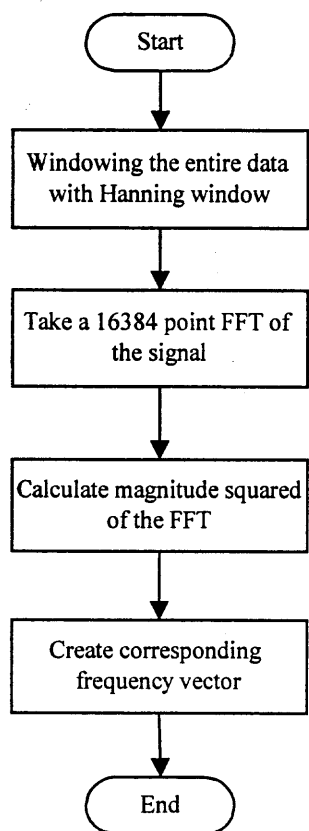
Figure 7.2 Flowchart of the spectrum calculation

The VLF and LF powers in the systolic blood pressure spectrum were derived by calculating the areas under the power spectral density curve at frequencies between 0.000195-0.2 Hz and 0.2-0.6 Hz, respectively. This was achieved by summing all the power spectrum density values in each of the frequency ranges. A Paired t-test was performed to compare the results obtained in control and the SAD rats. Results are presented in section 8.2.

7.2 The Steady State Responses
of the ADN and the Carotid Sinus Baroreflex Systems

The steady state features of the carotid and aortic baroreflex systems were investigated on

the heart rate, blood pressure, mesenteric vascular conductance, and femoral vascular

conductance. Data were acquired according to protocol 2, which was described in

section 5.3. For a single stimulation trial, the response effects were calculated as 30 s

mean difference, which was the difference in mean individual component response

between a 30 s pre- stimulation baseline and the initial 30 s of the stimulation period in

the step stimulation trials. Each component contained an average of 15 trials for each

stimulation level. The final responses of each stimulation level for each component were

represented as Mean±SD. The stimulus–response curves were generated by plotting

responses versus their corresponding stimulation levels. The results are presented in

figure 8.11-8.13.

7.3 Comparison of the Sinus
and Aortic Stimulation Effects and the Linear Range Estimation

Although the analysis presented in section 7.2 revealed the general features of the steady

state responses of the sinus and aortic baroreflex system, the obvious problem in that

analysis is the comparison of the sinus and aortic stimulation effects, because of the

difficulty of equating the mechanical and electrical stimulus properties applied at

different loci. We have tried to partially resolve this by using the net blood pressure

change as a common measure of reflex activation, and comparing the subsidiary

responses at similar levels of blood pressure effect; thus, to provide a rational

comparative measure of patterns of activation. Data used in this analysis were the step

responses acquired in protocol 2. Of the 5 rats in this protocol; DU, EF, and EH had both

responses acquired in protocol 2. Of the 5 rats in this protocol; DU, EF, and EH had both sinus balloons and ADN electrodes that were adequate for extensive data collection; of these, the experiments with DU were completed prior to Fan and Andressen's [57] analysis of the fiber types in the rat ADN. Therefore, data for all three stimulus modes were only obtained for EF and EH. For DU, complete data was obtained for the Sinus, and ADN-A modes. The other two rats, EC and EG had only ADN electrodes; for EG complete data were obtained for both ADN-A and ADN-A+C fibers; for EC the only complete data were for ADN-A fibers.

For each of the five rats, and for all of the completed stimulus sets, we determined the linear range of the blood pressure effect, mapped the stimulus domain corresponding to this range onto a standard scale, and used the scale to systematically compare the maximum size and linearity of the individual component responses. The linear range was determined as follows: the stimulus-response data were least-squares fit with first, second, and third order polynomial functions, shown as figure 7.3; the ANOVA model-corrected regression coefficients for these expressions were calculated, and the order-of-fit that yielded the largest model-corrected squared coefficient was determined. For all of the Sinus data, probably because of combined stimulus and receptor mechanical factors, the best fit was obtained with a cubic; for the ADN data in all cases, a quadratic fit was the best. The obtained regression equations were differentiated, set to zero, and solved. For the Sinus, the two roots were taken as the minimum and maximum extent of the linear range; for the ADN, the minimum was defined as a stimulus of zero strength, and the maximum as the signal root.
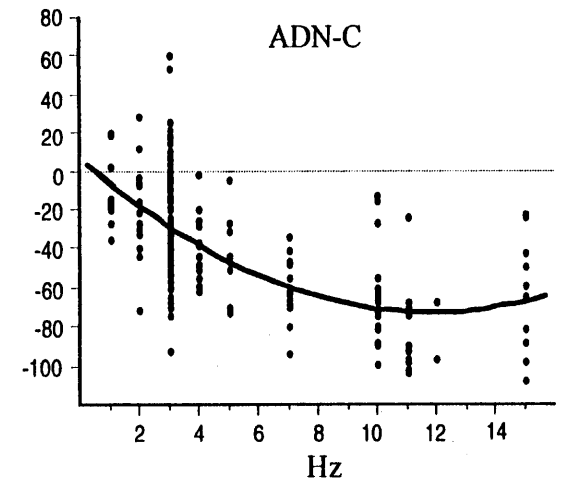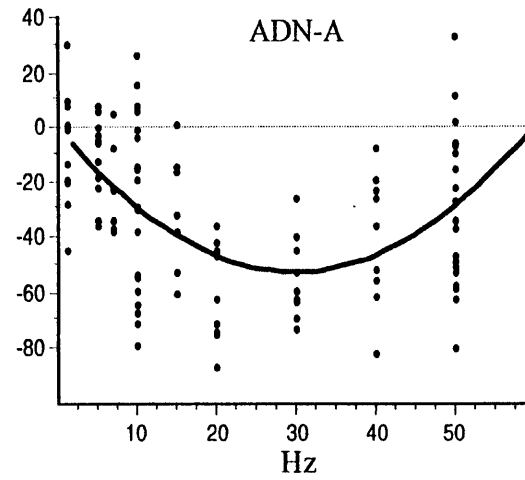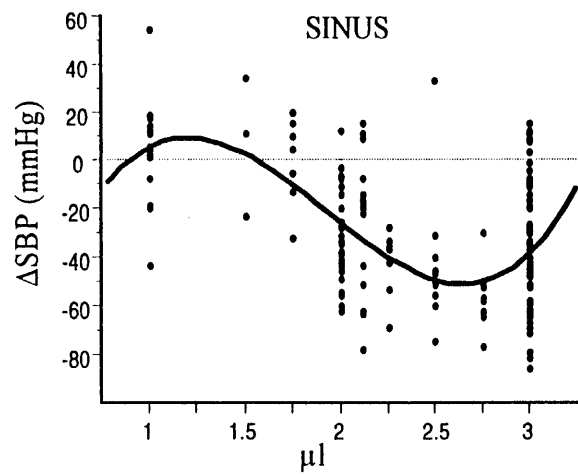
Figure 7.3 Linear range estimation

EF Sinus

$Y = -188.626 + 386.293 * X - 233.236 * X^2 + 40.386 * X^3; R^2 = .318$

EF A Fiber

$Y = -.044 - 3.498 * X + .058 * X^2; R^2 = .287$

EF C Fiber

$Y = 6.568 - 13.415 * X + .567 * X^2; R^2 = .41$

To estimate the linearity and comparative sensitivity of the component response effects, for each rat and each stimulus mode, the minimum stimulus strength within the previously defined linear blood pressure range was assigned a value of zero and the maximum a value of 100. Each response, including blood pressure, itself, was linear fit with respect to this standard "% of blood pressure linear range" scale, and the slope, R^2, and the reliability of the ANOVA were entered in Table 8.1.

7.4 Transfer Function Estimation

7.4.1 Step Response Approach

Data used in this approach were acquired in protocol 2. Transfer functions were derived for the Sinus, ADN-A and ADN-A+C modes for the blood pressure, heart rate, mesenteric vascular conductance (low abdominal vascular conductance for EH), and femoral vascular conductance baroreflex responses. The ADN-A fiber baroreflex transfer functions for all the components were derived from rats EH, EF, EC, EG, and DU, whereas, the ADN-A+C fiber baroreflex transfer functions were derived from rats EH, EF and EG, and the Sinus baroreflex transfer functions were derived from rats EH, EF, and DU. Data used were in HP-VEE format.

In this section, blood pressure is used as an example to describe the procedures employed in deriving the transfer functions from the step responses. For each rat, for the ADN-A, AND-A+C fibers and Sinus, 20 SBP responses to the step stimulation at each of 2-4 levels within the linear range were ensemble averaged. Using the difference between SBP during the stimulation period and mean of the 12 second pre-stimulation baseline, the initial 20 seconds of the response was iteratively least square fit with an exponential curve of form $y(t) = k_1(1 - e^{-k_2 t})$. The transfer function was derived by the formula:

$$H(s) = \frac{Y(s)}{X(s)}; \text{ where } Y(s) = k_1(\frac{1}{s} - \frac{1}{k_2 + s}) \text{ is the Laplace transform of } y(t), \text{ and}$$

$X(s) = 1/s$, the Laplace transform of the step input. The amplitude transfer function

plots were constructed from the poles and zeros of $H(s)$ and normalized. For each kind of

stimulation, a representative transfer function was calculated by averaging over all

stimuli; the corner frequency defined at −3dB from the maximum.

7.4.2 Sinusoidal Fit

Linear system theory states that, for a sinusoid input signal, whose frequency is ω_0, the

output of a linear time-invariant system is still a sinusoid signal with the same frequency

ω_0, but different amplitude and phase. The amplitude and phase of the output are

determined by the dynamic features of the system. The system amplitude attenuation

characteristics at frequency ω_0 could be directly estimated by calculating the output to

input amplitude ratio at frequency ω_0.

Data used in the sine fit analysis were acquired from protocol 3 described in

section 5.4. Data used were in HP-VEE format. Sine fit analysis was only performed on

the blood pressure signal. Data for all three modes were obtained for EH; for EF, data

was obtained for the Sinus mode; and for EC and DU, data were obtained for ADN-A

fibers.

The blood pressure responses were first ensemble averaged. An exponential

curve, with a form of $y(t) = k_1 + k_2 \cdot \exp(-k_3 \cdot t)$, was least square fit on the initial period

of the responses. The system is assumed to reach steady state after 5 time constants,

where the time constant $\tau = \frac{1}{k_3}$. At the steady state region, the average trace was least

square fit with a sinusoidal signal at the test frequency. Figure 7.4 shows an example of an ensemble averaged blood pressure trace with a sine fit signal overlying it during the steady state period. The fitting results are presented in Table 8.6. The fitting processes were done in the Igor Pro program (WaveMetric, Lake Oswego, Oregon, USA).

The amplitude transfer functions were generated by plotting the amplitude of the fit sine wave against its fit frequency. The functions were normalized and the corner frequency defined at −3dB from the maximum.

7.4.3 Spectrum Analysis

The data sources for the spectrum analysis were the same as those for the sine fit analysis. Spectrum analysis was also only implemented on the blood pressure signals. Usually, the spectrum analysis provides similar information as the sine fit analysis. However, in this case, the spectrum analysis was not only used to confirm the results derived from the sine fit analysis, but, in addition, it provided us with a clear picture of the relative relationship between the modulated blood pressure power and the noise blood pressure powers at each modulation frequency.

For each rat, stimulus mode, and test frequency, 5 to 27 spectra were averaged (Table 8.7). The algorithms used to derive the spectrum were similar to what was described in section 7.1. Briefly, the spectrum was obtained by performing 16384 point FFT on the 120 second interpolated, Hanning windowed blood pressure responses. The power of the output blood pressure spectrum at the modulation frequency was derived by calculating the area of the power spectral density curve at the modulation frequency. The amplitude transfer function was obtained from the normalized square root power values. The corner frequency defined at −3dB from the maximum.
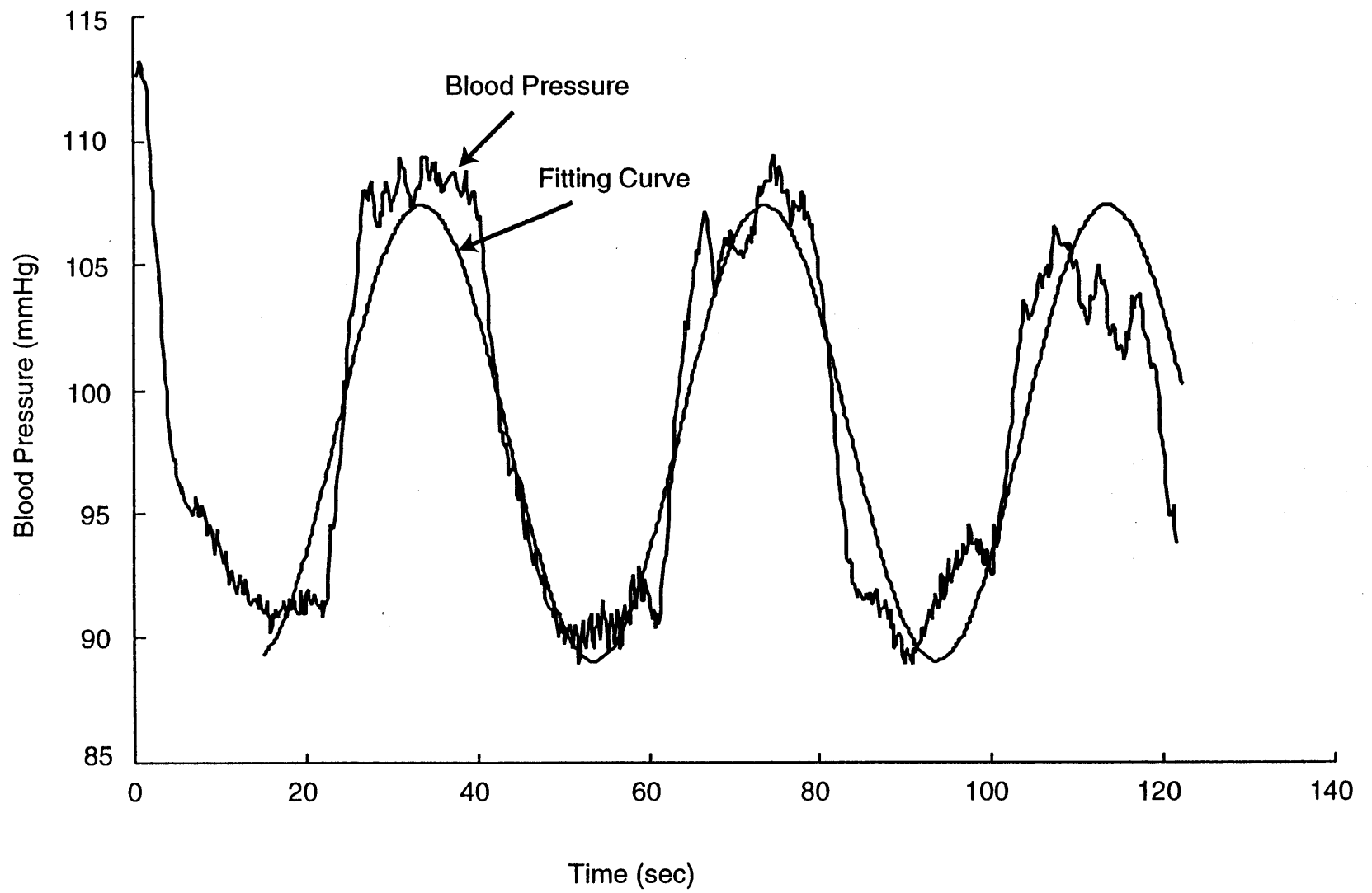
Figure 7.4 An example of the least square sinusoidal fit to the BP sinusoidal resposne

7.5 Transportation Lag Estimation

Before a baroreceptor stimulation has an effect on the blood pressure, it must travel through the baroreflex afferent nerve, central nervous system, and the baroreflex efferent nerve branches. The fixed delay between step input and the initiation of the blood pressure response is the transportation lag. The transportation lag affects the baroreflex possible oscillation frequency range.

7.5.1 Total Transportation Lag - Exponential Fit of the Step Response

The open-loop transportation lags of the baroreflex system were derived from both ADN and Sinus modes. Data were in HP_VEE format, and acquired according to protocol 2.

Each data set was composed of 50 Pre-stimulus and 80 stimulus-on cardiac cycles. Data was interpolated to 1 sample/msec resolution. The stimulation onset time was set as 0; a straight line was least square fit to the pre-stimulation periods, and an exponential to the stimulation period. The equations were set equal, and solved to calculate the intersection. The time between the intersection and the stimulus onset was taken as the transportation lag. Figure 7.5 demonstrates an example of the line and exponential fits and the transportation lag. In the figure, t_0 is the stimulation onset time, which was set as 0, t_{lag} is the intersection point, which is the system transportation lag. It is clear that the blood pressure did not decrease until t_{lag}, which provided solid evidence that the baroreflex contained a pure time lag.

The baroreflex transportation lags were determined for five rats for the Sinus, ADN-A and ADN-A+C modes. Except for rat EG A fiber (3 analyses), and rat DU Sinus (12 analyses), the results are means of >20 independent analyses, the detailed results are presented in Table 8.8.
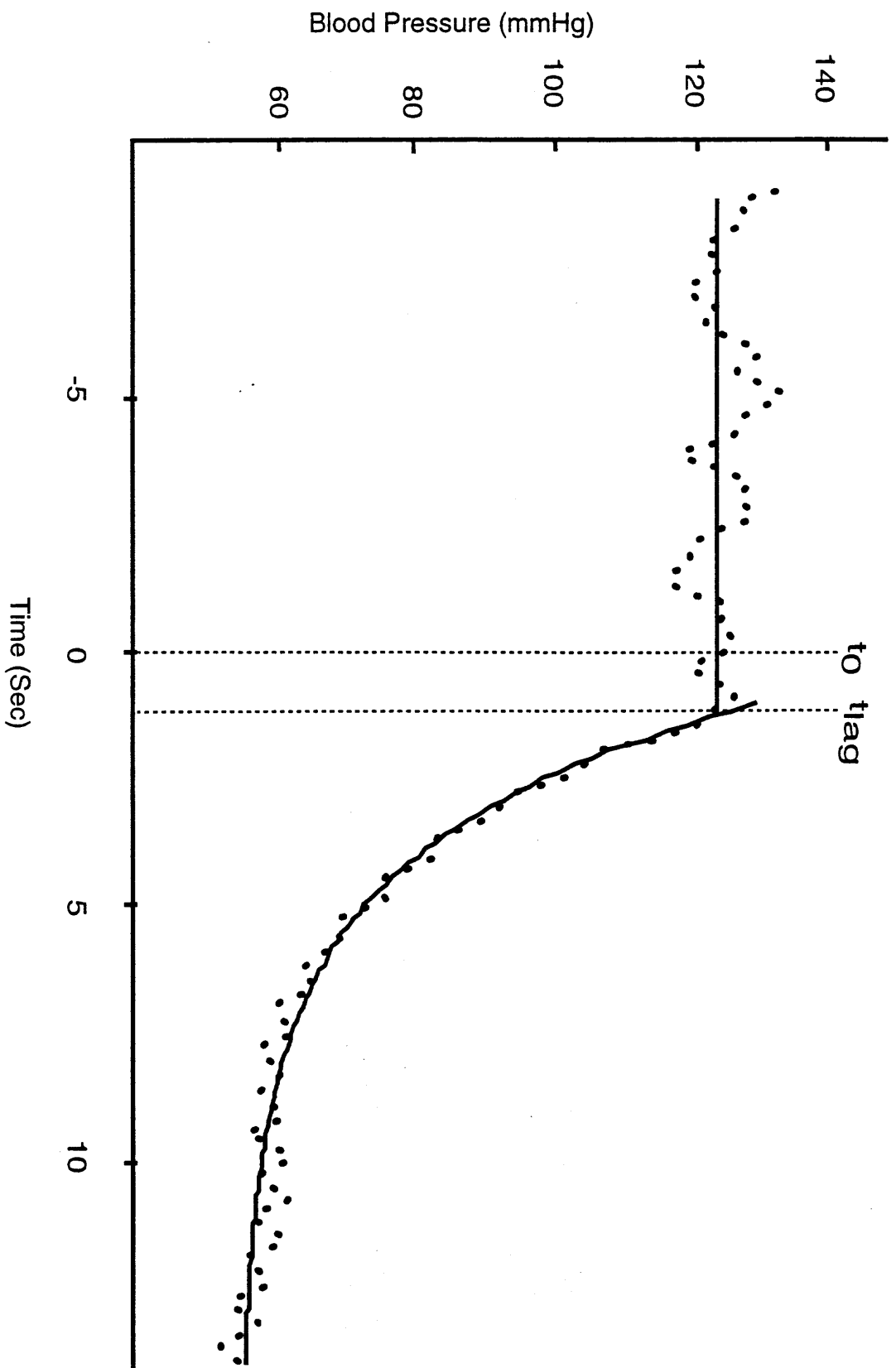
Figure 7.5 Transportation lag estimation

7.5.2 Central Nervous System Lag

The time from stimulus onset to the beginning of increased vagus and decreased peroneal activity is an upper estimate of the central lag. Electrical ADN stimulation artifacts in the vagus recording limited the analysis to the Sinus (hydraulic) stimuli: 15 3.0 μl Sinus step stimulations, extracted from 6 kHz DAT tapes, were used in the analysis. The Analysis was performed using Igor Pro software, Version 3.1.3.0 (WaveMetric, Lake Oswego, Oregon, USA)

During the processing, the EKG signal was rectified and smoothed, the R waves were detected on the smoothed EKG signal by using WindowDiscr function existing in the Igor Pro. WindowDiscr function acts much like a hardware window discriminator, with several additional features. By setting two threshold window levels t1, and t2, peaks (R wave) occurring between t1 and t2 were detected. The detected R waves were represented as instantaneous frequencies, which was the reciprocal of the time difference between two adjacent R waves.

The absolute value of the vagus, peroneal neurograms, heart rate, and balloon volume for each stimulation were ensemble averaged, and the vagus, peroneal and heart rate averages were smoothed by a 10 point second-order Savitzky-Golay algorithm. Because balloon volume is a ramp, and the baroreceptor are rate sensitive, the stimulus onset was defined at the peak volume rate of change. The vagus and peroneal response onsets were defined at 3 standard deviation above the mean of the 30s pre-stimulation baseline. The time relationships between the peroneal nerve, vagus, heart rate responses and the balloon volume changes were demonstrated in figure 8.24.

CHAPTER 8

EXPERIMENTAL RESULTS

8.1 The SAD Effects on the Blood Pressure Signal

Our experimental results suggest that the SAD greatly increase the blood pressure variability. The SAD effects on the blood pressure signal found in this study were similar to those published by other groups. Figure 8.1, column B demonstrates typical examples of both the pre- and post-SAD arterial blood pressure traces from a NMB rat. Column A shows the arterial blood pressure recordings in ambulatory rats after control and SAD surgery. Data in column A were published by Brody's group in 1987 [37]. Traces in the upper panel of both columns were from the pre-SAD rats, whereas traces in the bottom panel were from the post-SAD rats. The total length of each trace was about 6 min. In both columns, the pre-SAD blood pressure traces were more stable than those from the post-SAD rats; the post-SAD blood pressure traces showed much more variability. The mean blood pressures were similar during the pre-and post-SAD periods in both columns.

Figure 8.2 shows the effects of the SAD on the blood pressure variability for EC, EF, DY, EH, and EG 5 NMB rats. The effects were calculated as standard deviation of 30 s mean difference. The 30 s mean difference is the difference in mean systolic blood pressure between a 30 s pre-stimulation baseline and the initial 30 s of the stimulation period in the sham or null "trials". In the figure, the X-axis represents the rats' two different stages: the pre-SAD stage (Pre), and the post-SAD stage (Post); the Y-axis represents the standard deviation of the 30s mean differences.

A

Pulse Pressure (mmHg)

B
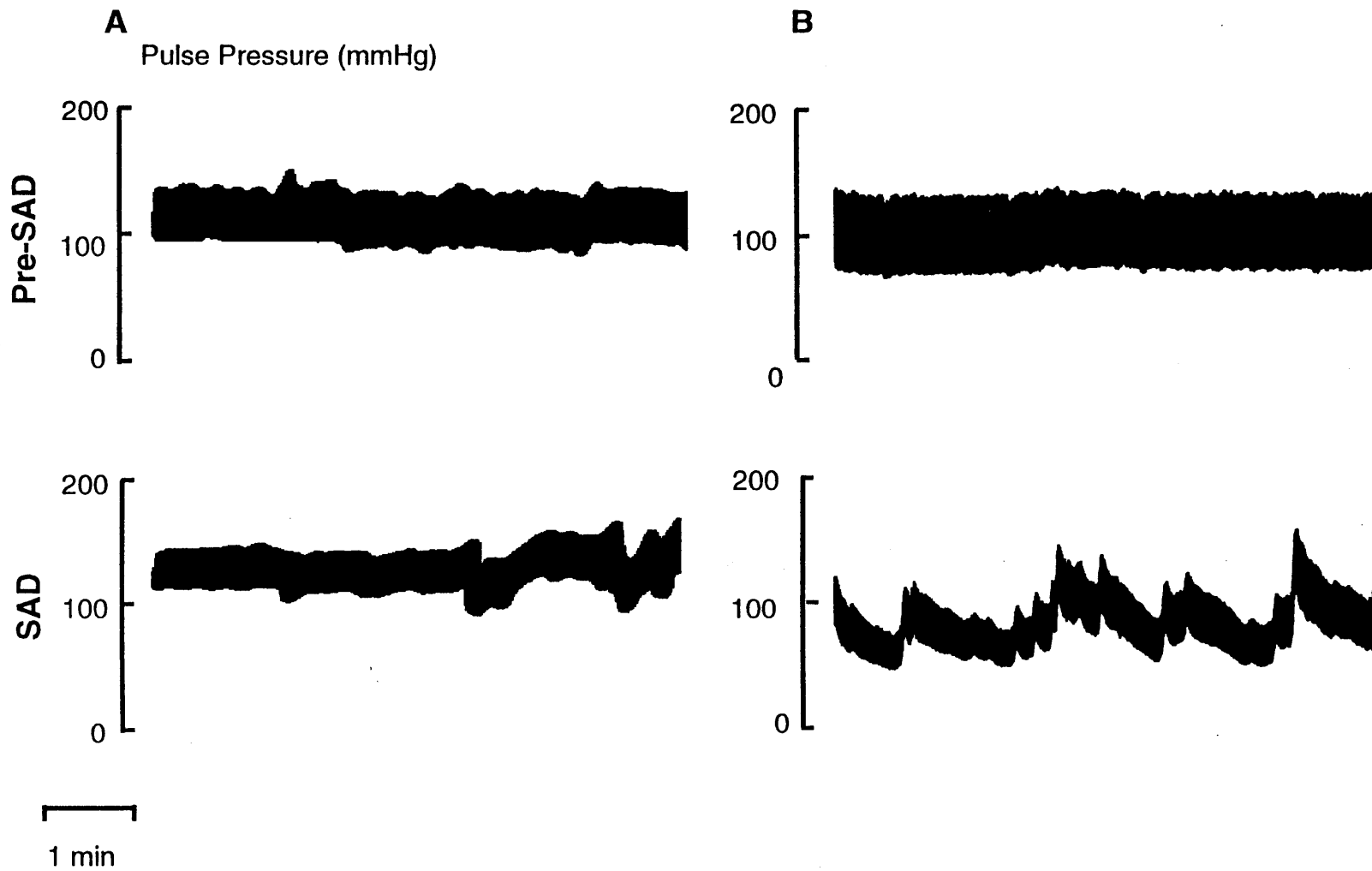
Figure 8.1 Pre- and post- SAD blood pressure traces. **A:** Data from Brody's group; **B:** Data from the present study
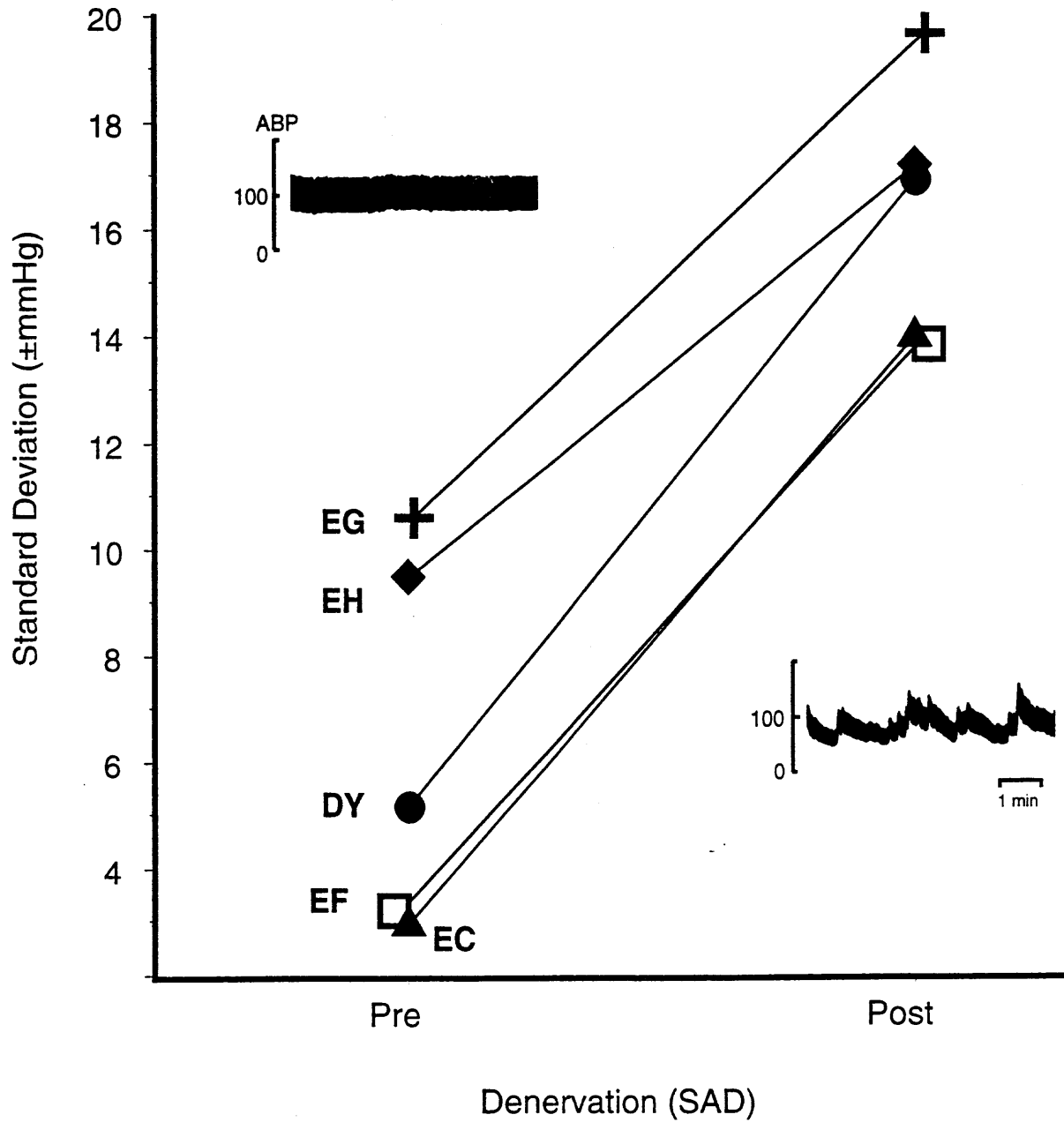
Figure 8.2 Effects of the SAD on the arterial blood pressure variability

Because these observations were made several hours after completion of all

procedures on the first and second surgery days, to assure that there was no residual

incision pain, the rats were maintained at 0.15% isoflurane. At 0.15% isoflurane,

undisturbed rats have normal EEG and baseline heart rate and blood pressure levels, but

heart rate and blood pressure increase, and EEG desynchronizes to loud noise or the light

touch. The power spectral analysis (section 8.2) showed that 0.15% isoflurane does not

affect the features of the blood pressure signal. Data in figure 8.2 show that, in each rat,

the standard deviation of the blood pressure increased by approximately 10 mmHg

following the SAD: the mean blood pressure standard deviation before SAD was 6.3±3.5

and after SAD was 16.3±2.4 mmHg (t=-13.9; df=4, p< 0.0002).

8.2 Power Spectra of Blood Pressure Variability

Comparing the changes of the blood pressure variability before and after the SAD, we

found that the standard deviation of the blood pressure increased by approximately 10

mmHg following the SAD. Although the standard deviation provided us information

about the blood pressure variance around the mean, it did not reveal any temporal and

frequency information contained in the signal. To further understand the features in the

blood pressure variability, we investigated the frequency features of the variability

signals, by calculating the power spectrum of the systolic blood pressure during pre- and

post-SAD periods. The detail of the power spectrum calculation was described in section

7.1. Figure 8.3 demonstrates an example of the mean blood pressure spectra from the 50

pre- and 50 post-SAD trials. Each trial lasted for 1.5 min, and was randomly selected

from the pre- and post-SAD periods (the experimental protocol was presented in section

5.2). The solid line represents the mean spectrum from the pre-denervation trials,
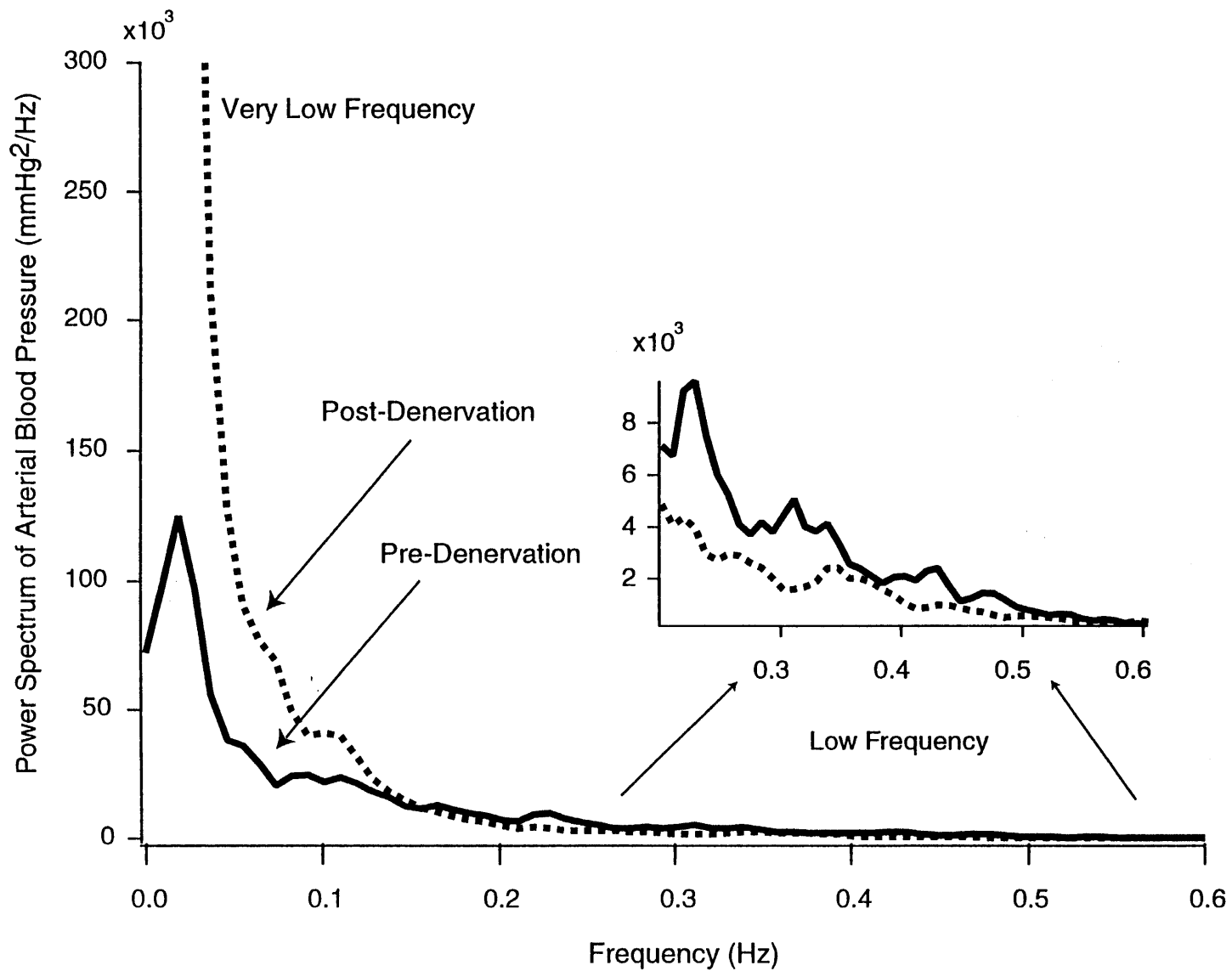
Figure 8.3 Blood pressure power spectra in the pre- and post-SAD periods

whereas the dash line represents the mean spectrum from the post-denervation trials. The extended scale of the center inset displays the full height of the low frequency region. Compared to the pre-SAD spectrum, the post-SAD spectrum shows a huge increase of power at the very low frequency range (VLF) (0.00195 –0.2 Hz) and a decrease of power at the low frequency range (LF) (0.2 – 0.6 Hz). The post SAD blood pressure spectra were not simple proportional increases of the pre SAD spectra. The different features of the pre- and post-denervation spectra imply that the higher variability in SAD rats is not simply the exaggeration of the variability in the baroreflex intact rats. Both spectra in Figure 8.3 were with 0.15% isoflurane analgesia. Figure 8.4 compares the post-denervation spectrum in Figure 8.3 (with 0.15% isoflurane analgesia) to one (the mean blood pressure spectra of 50, 1.5 min, baseline blood pressure traces) from the same rat, without isoflurane, but with otherwise identical procedures, 3 weeks later. It shows that 0.15% isoflurane had minimal effect on the spectrum. The regression slope between the spectra is 0.995, with r^2=0.946 and p<0.0001. (K-S: χ^2=1.4; p>0.999). In figure 8.4, the solid line represents the mean spectra with 0.15% Isoflurane, whereas the dash line represents the mean spectra without Isoflurane.

Figure 8.5 shows the statistical results of LF and VLF power changes calculated from 50 pre- and 50 post-SAD trials in one rat. The black bars represent the results from the pre-SAD trials, whereas the gray bars represent results from the post-SAD trials. A t-test showed that SAD rat contained significantly higher power (ΔPSD=1.247x10^6, df=49, t=3.65; p<0.001) in the VLF range, but significantly lower power (ΔPSD=1.4228x10^4, df=49, t=-2.02; p<0.05) in the LF range than the Pre-SAD rats. The power increases in the VLF range were much more dominant than the power decreases in the LF range.
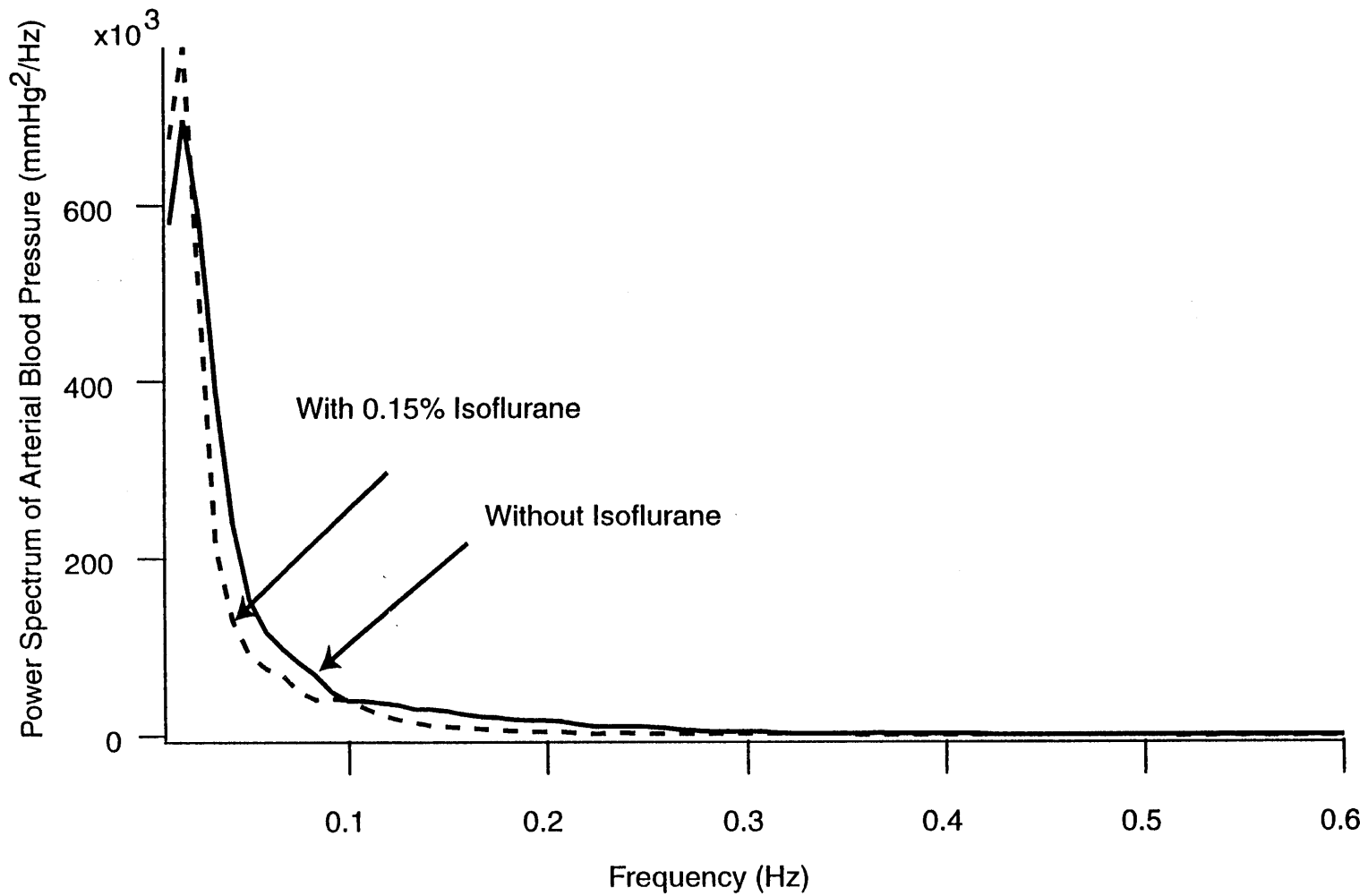
Figure 8.4 Blood pressure spectra with and without Isoflurane
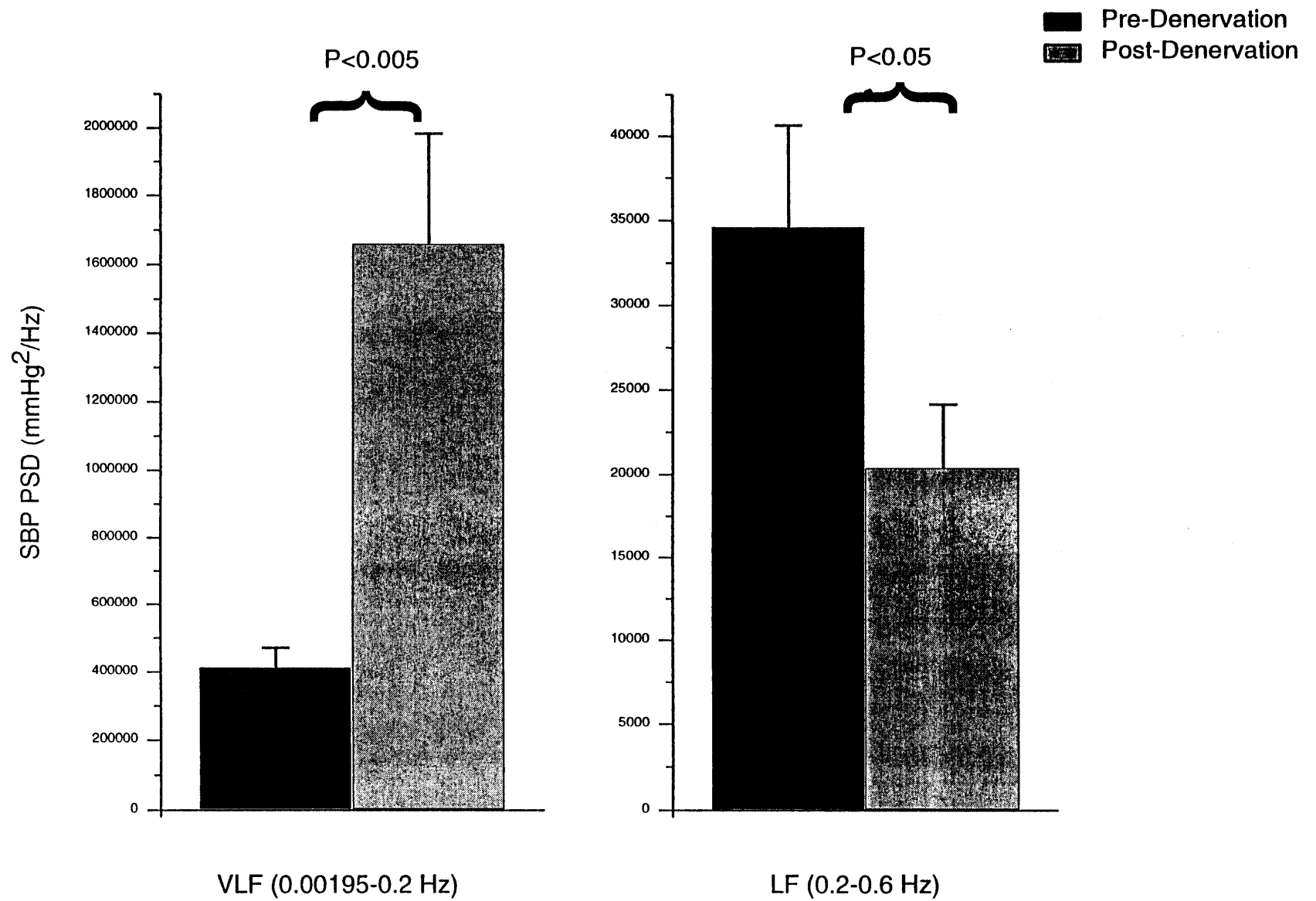
Figure 8.5 Comparison of the VLF, LF power during the pre- and post- SAD periods

Our spectrum results are consistent with what have been reported for ambulatory rats. For example, following SAD, Jacob's group [52] found a >10 fold increase of power in 0.005-0.05 Hz band, and Cerutti's group [53] found a >6 fold increase of power in the 0.02-0.25 Hz band. Both groups found decreases in LF power. Although the post-SAD increase in VLF power was the most prominent results of both groups, the highlighted feature of both groups was the comparatively small post-SAD decrease in the LF (0 3-0.5 Hz) region of the spectrum. Since the effect of SAD on baroreflex variability is large, and substantial variability implies substantial spectral power, their emphasis seems inappropriate. However, the LF is the only region that shows consistent decrement with SAD. Because LF decreases with SAD, the LF peak might be said to be a "marker" of the baroreflex, but if it is, it is a paradoxical one. A negative feedback element, such as the baroreflex, constrains variability, so an increase in noise power, not a decrease, is what is expected, when it is removed. In fact, SAD greatly increased the VLF noise power. Based on the VLF observation, we predict that the major baroreflex function area is around the VLF region.

To verify our predication, we used two sets of experiments to derive the transfer functions of the open-loop baroreflex system. In one set of experiments, we stimulated the aortic arch and carotid sinus baroreceptors using a set of step stimulations (detail of the protocol was described in section 5.3, protocol 2). In another set, we stimulated both areas with a set of sinusoidal stimulations (detail of the protocol was described in section 5.4, protocol 3). The transfer functions derived from the two sets of experiments were consistent.

Since the SAD caused huge increases in the blood pressure variability, before deriving the baroreflex transfer functions, it is important to first evaluate the stability of the baroreflex responses.

8.3 Stability and Variability of the Baroreflex Responses

It was demonstrated that the SAD caused a huge increase in the blood pressure variability, but how would this increased variability affect the BP responses to the ADN and Sinus baroreflex stimulations?

To assess the long-term stability and variability of the electrically elicited BP response, we repeatedly stimulated the ADNs in 2 NMB rats over extended time. To optimize sensitivity to changes in the threshold and response magnitude, the current strengths and frequencies of the test stimuli were set below saturation; but, to assure a more stringent test of fatigue of long term damage, higher frequency stimuli were intermixed with the test stimuli. For the first rat (CP) the stimulation parameters were, for the test stimuli 4 Hz (the stimulation current pulse frequency), 40 μA (the stimulation current pulse intensity), 1 msec (the stimulation current pulse width); 120 sec (the total current stimulation time) train, and for the saturation stimuli 100 Hz, 40 μA, 1 msec, 180 sec train; with 370 of each stimulus distributed over 109 contiguous hours, or somewhat more than 4 days. The ADN thus received 1110 min or > 18 h of 100 Hz stimulation, in addition to the 740 min, or >12 h, of 4 Hz test stimulation. The response measure was the difference in mean SBP between a 30 s pre-stimulation baseline and the initial 30 s of stimulation: Taken over all 109 h, the 4 Hz test stimulus produced a mean BP change of − 4.8±11.9, and the stronger, near maximal stimulus, -39.0±14.7 mmHg. An ANOVA for linear regression determined that, for the 4 Hz stimulus, the slope of the SBP changes

was -0.009 mmHg/h; $r^2 = 0.001$, ns, and for the 100 Hz stimulus, 0.014 mmHg/h;

$r^2=0.001$,ns. These results confirm the stability of the mean response.

We also interleaved a series of control or null "trials" with the actual stimulation.

The null trials standard deviation was found to be 11.8 mmHg, which was almost

identical with the 11.9 for 4 Hz stimulus. A comparable procedure in a second rat,

yielded a similar result, and is illustrated in Figures 8.6 and 8.7. The SBP changes to 100

μA, 300 μs, 20 Hz stimuli are shown in Figure 8.6. In this experiment, there were a 496

test stimulations of this strength and 294 stimulations at 100 Hz during 173 hours or > 7

days; during this time, the average effect of the ADN stimulation changed by 0.2 mm Hg,

from –9.9 to –9.7 mm Hg (linear ANOVA: 0.001 mmHg/h; $r^2=.000$, ns). Again, the near

perfect stability of the mean effect contrasted sharply with a large inter-trial variance of

±8.7, and again using a control trial procedure, shown in Figure 8.7, the standard

deviation of the difference score was determined at ±10.9 mmHg.

For both rats, the lack of any appreciable increment in standard deviation between

the baseline and the actual test stimuli indicates that the large variability in the difference

score is most likely not due to an erratic stimulus, but due to intrinsic variability of the

blood pressure baseline.

Test of the mean stability of sinus balloon stimulation have not been as

systematic, extended or intensive as those with the ADN; however, even when separated

by hundreds of inflations, bouts of stimulations at fixed volume have yielded consistent

average responses. For example, using a 3.5 μl test stimulus in rat DU, the initial mean

systolic blood pressure response was –43.2±20.07 mmHg; following 225 h of two 1.5-3.5

μl (p-p), 5 min duration, sinusoidal inflations per hour (total 550 min), the response to the

test stimulus was still –41.8±23.9 mmHg; (linear ANOVA: 0.007 mmHg/h, $r^2=.000$; ns).

The standard deviation of the sinus elicited responses, as in fact, somewhat more than double that of the ADN; whereas, the baseline, control trial, standard deviation was similar (-0.45±8.98); thus, unlike the ADN, the sinus stimulus appears to substantially contribute to the net response variance.

After extensively evaluating the stability and variability of the baroreflex responses, we concluded that the baroreflex system contains the near perfect stability of the mean effect contrasted sharply with a large inter-trial variance. The stable mean effect provides us a great opportunity to investigate the system schematically. In the following sections, we will sequentially present various important features of the baroreflex system derived from the mean responses.

8.4 The Steady State Features of the Open-Loop Baroreflex System

8.4.1 Average Step Responses of the Baroreflex Stimulation

Figures 8.8-8.10 demonstrate a set of mean blood pressure, inter-beat intervals (IBI), mesenteric vascular conductance, and femoral vascular conductance response traces to the ADN-A, ADN-A+C, and Sinus step stimulations. The 'Stim. Markers' on the top of each figure represent the stimulation onset periods. Each stimulation was about 60 sec; the stimulation levels were at 20Hz, 30Hz, and 40Hz for the ADN-A fiber, 9Hz, 10Hz, and 11Hz for the ADN-A+C fiber and 2.25µl, 2.75µl, and 3 µl for the Sinus. Without exception, all step stimulations of the ADN-A, ADN-A+C, and Sinus caused decreases in the blood pressure, and heart rate, and increases in the mesenteric and femoral vascular conductance. The response patterns for the step stimulations were: for both ADN-A, and ADN-A+C fiber stimulation, the blood pressure first exponentially decreased (exponentially increased for mesenteric and femoral vascular conductance), then stayed

down (up for the mesenteric and femoral vascular conductance) for most the stimulation period, at the end of the stimulation, the responses showed a little adaptation. The situation was a little complicated for the heart rate responses. It is noticed that during the relatively low stimulation cases, e.g. 20Hz for the A fiber, and 9Hz, 10Hz for the A+C fiber, the IBI signals exponentially increased, and stayed up for the most stimulation period, whereas for strong stimulation cases, e.g. A fiber 40 Hz, and C fiber 11Hz, there was a huge IBI increase (surge) at the stimulation onset time, then quickly decreased to a lower level (higher than the baseline level), and stayed at that level for the most of the stimulation period. The high frequency component (the surge) at the beginning of the stimulation onset time may be due to fast response of the heart to the parasympathetic activity, while the slower sympathetic reaction may cause the decreases in IBI afterwards. The Sinus step responses showed different patterns from the ADN-A, and ADN-A+C fiber stimulations. Compared to the ADN-A, and ADN-A+C fiber stimulation cases, the response levels for the Sinus were substantially smaller, and the adaptation speed was faster. Of course, at this sage, since we did not equate the mechanical and electrical stimulus properties applied at the two baroreceptor loci, we could not perform a reasonable comparison between the electrical and hydraulic stimulation effects. The information regarding the comparison is going to be provided in section 8.4.3.
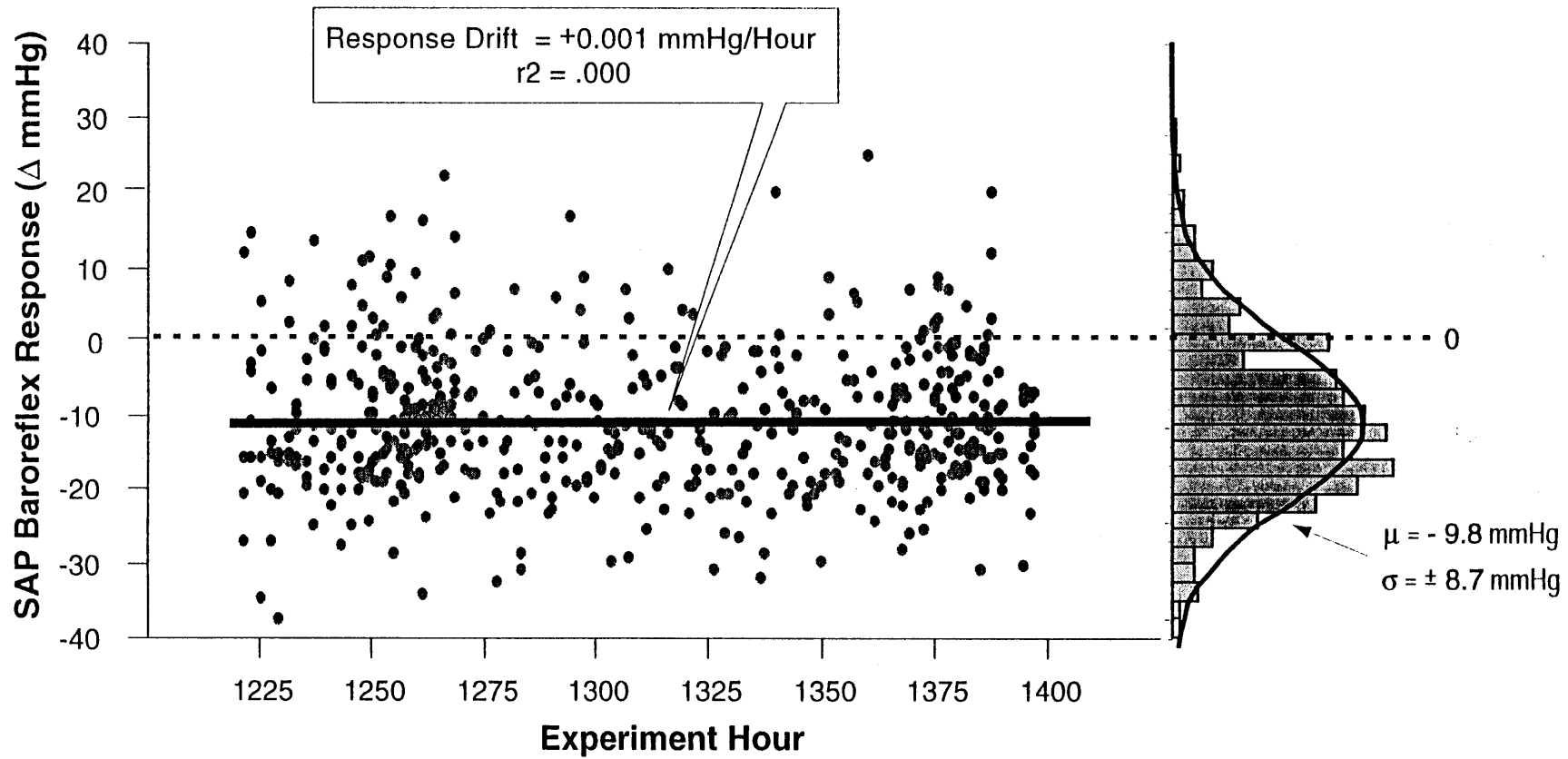
Figure 8.6 The stability test of the responses to the high level ADN stimulations
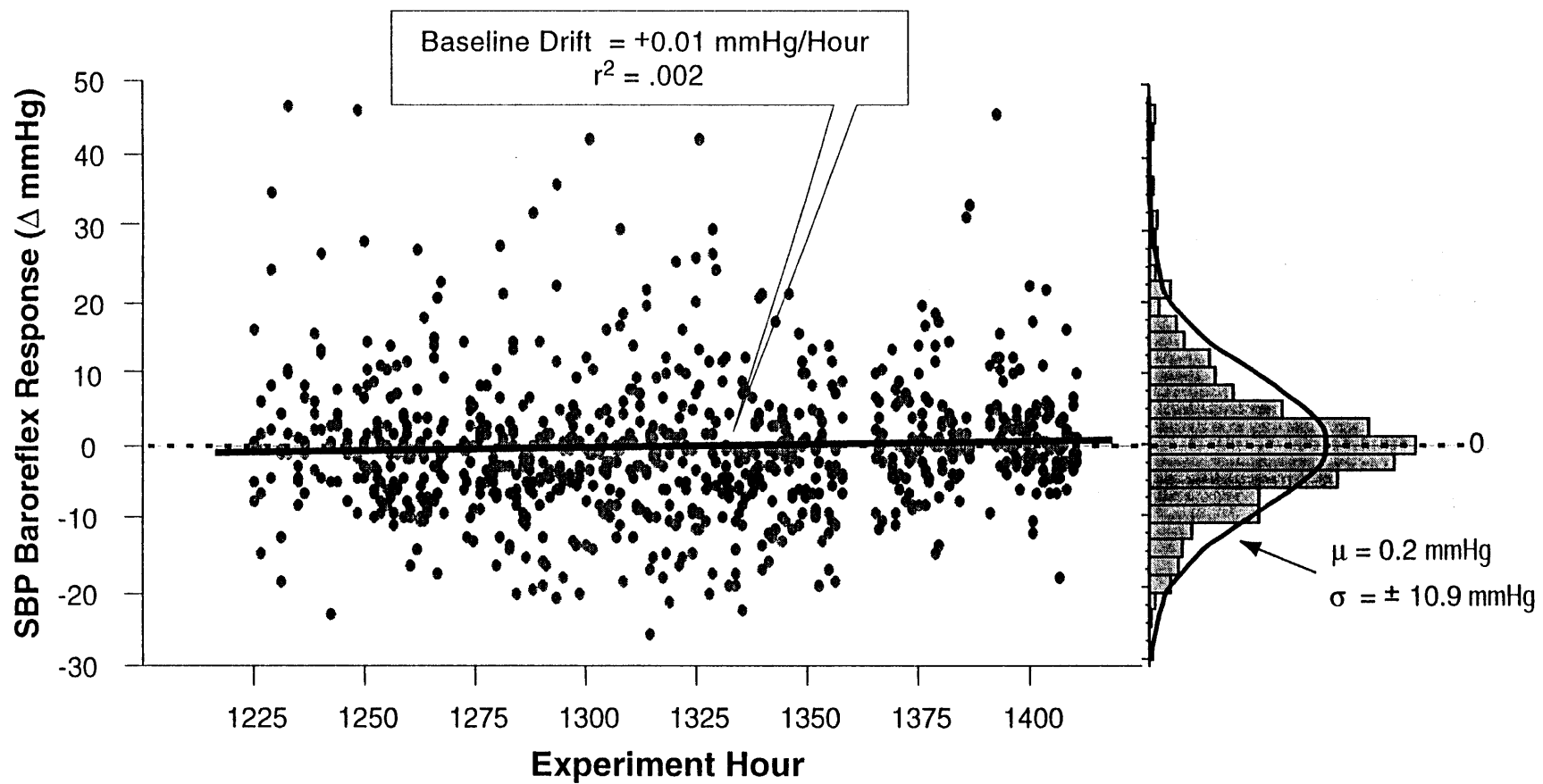
Figure 8.7 The stability test of the responses to the low level ADN stimulations
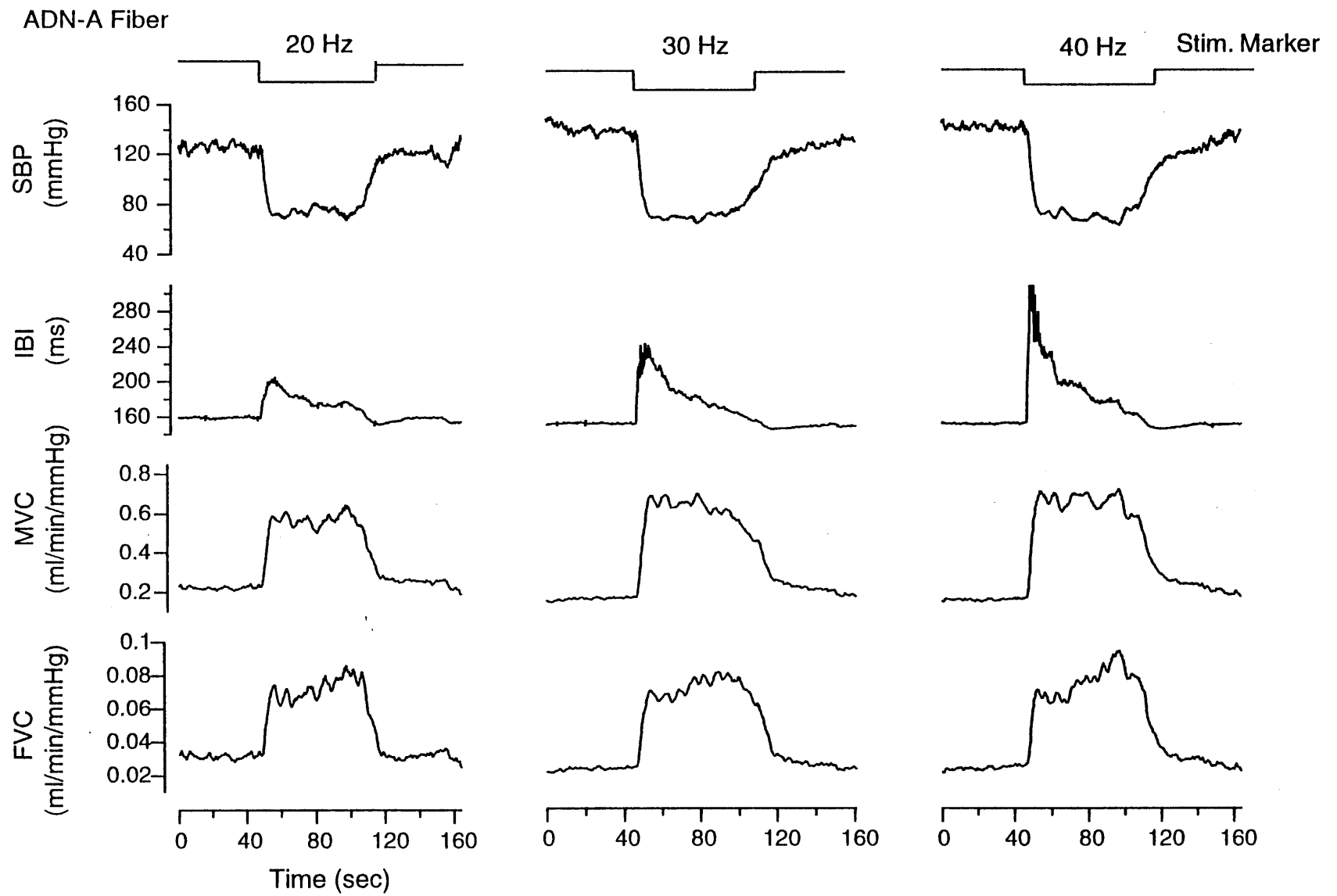
Figure 8.8 Individual cardiovascular responses to the ADN-A fiber step stimulations
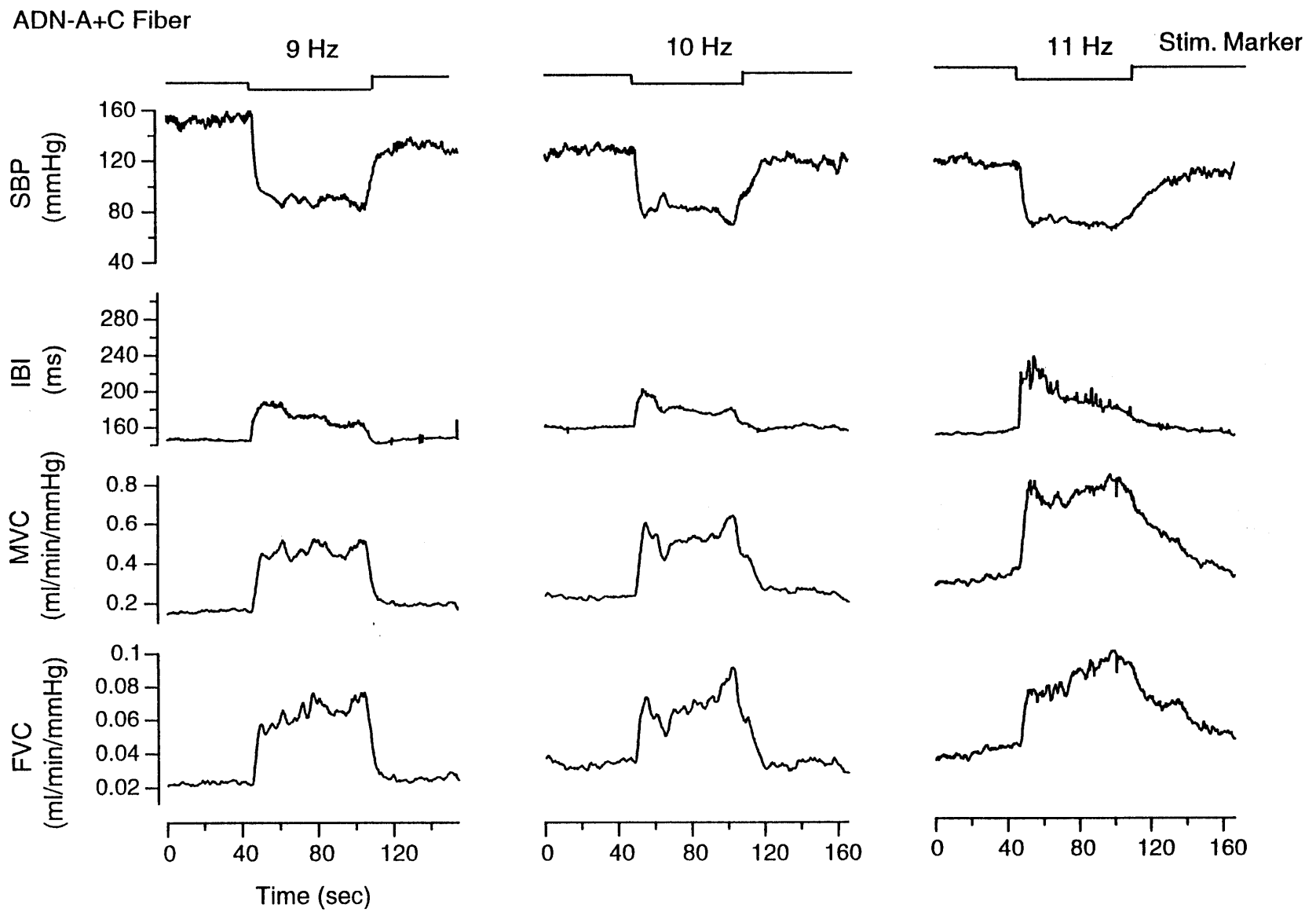
Figure 8.9 Individual cardiovascular responses to the ADN-A+C fiber step stimulations
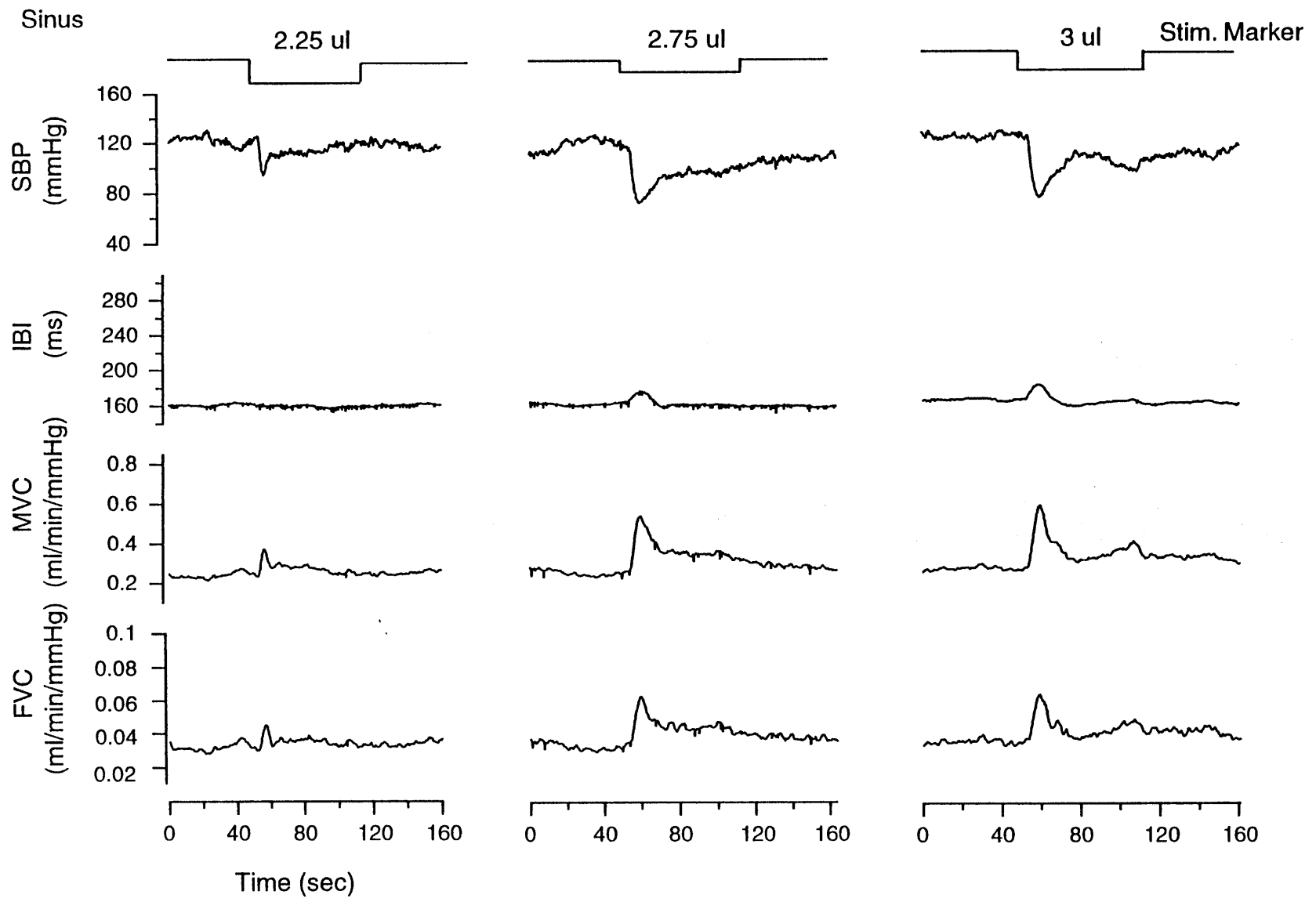
Figure 8.10 Individual cardiovascular responses to the Sinus step responses

8.4.2 The Steady State Features of the Open-Loop Baroreflex System

The steady state feature of the open-loop baroreflex system was obtained by raising the baroreflex step stimulation levels from a subthreshold level (e.g. 60 μA, 150 μs at 3 Hz for A fiber; 100 μA, 300 μs at 1 Hz for C fiber; 1 μl for Sinus) to a saturation level (e.g. 60 μA, 150 μs at 60 Hz for A fiber; 100 μA, 300 μs at 15 Hz for C fiber; 3.5 μl for Sinus) in multiple steps. The corresponding protocols and data analysis procedures were described in section 5.3 and 7.2, respectively. The response was calculated as the 30 s mean difference. Figures 8.11-8.13 demonstrate typical examples (from EH) of the steady state responses of the open-loop ADN-A, ADN-A+C and Sinus baroreceptor reflex. In the figures, the six individual cardiovascular responses are the arterial blood pressure response (ΔSBP), heart rate response (ΔHR), femoral venous pressure response (ΔVBP), low abdominal vascular conductance response (ΔMVC), femoral vascular conductance response (ΔFVC), and skin vascular conductance response (ΔSVC). The X-axis represents stimulation levels, whereas, the Y-axis represents the response levels. The responses are represented as Mean±SE. Each cardiovascular response in the figure was least square fit with a Gussian curve. Except for the skin vascular conductance, the responses of the other five cardiovascular components increased with the increase of stimulation levels and reached their plateau at around the same place, which were at about 40Hz for the ADN-A fiber, 12Hz for the ADN-A+C fiber and 3μl for the Sinus. The skin static responses showed a different pattern, which may be due to complicated local influences to the vascular beds. All of the Sinus response curves appear as sigmoid shapes, whereas, the ADN response curves appear as quadratic shapes. Compared to the ADN stimulation, the heart rate (ΔHR) showed very little response to the Sinus stimulation.
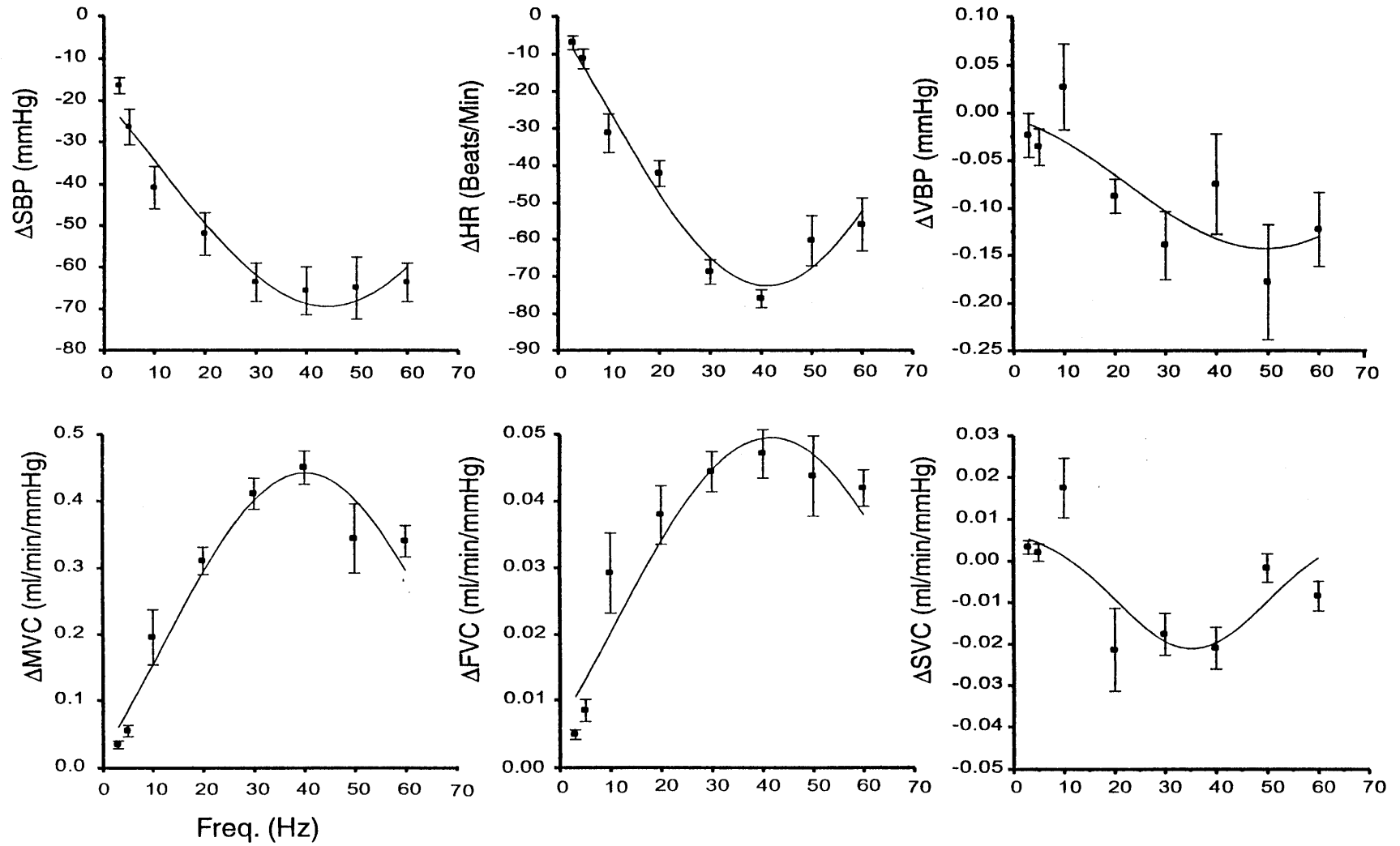
Figure 8.11 Steady state features of the baroreflex ADN-A fiber stimulations

ADN C Fiber Step Response
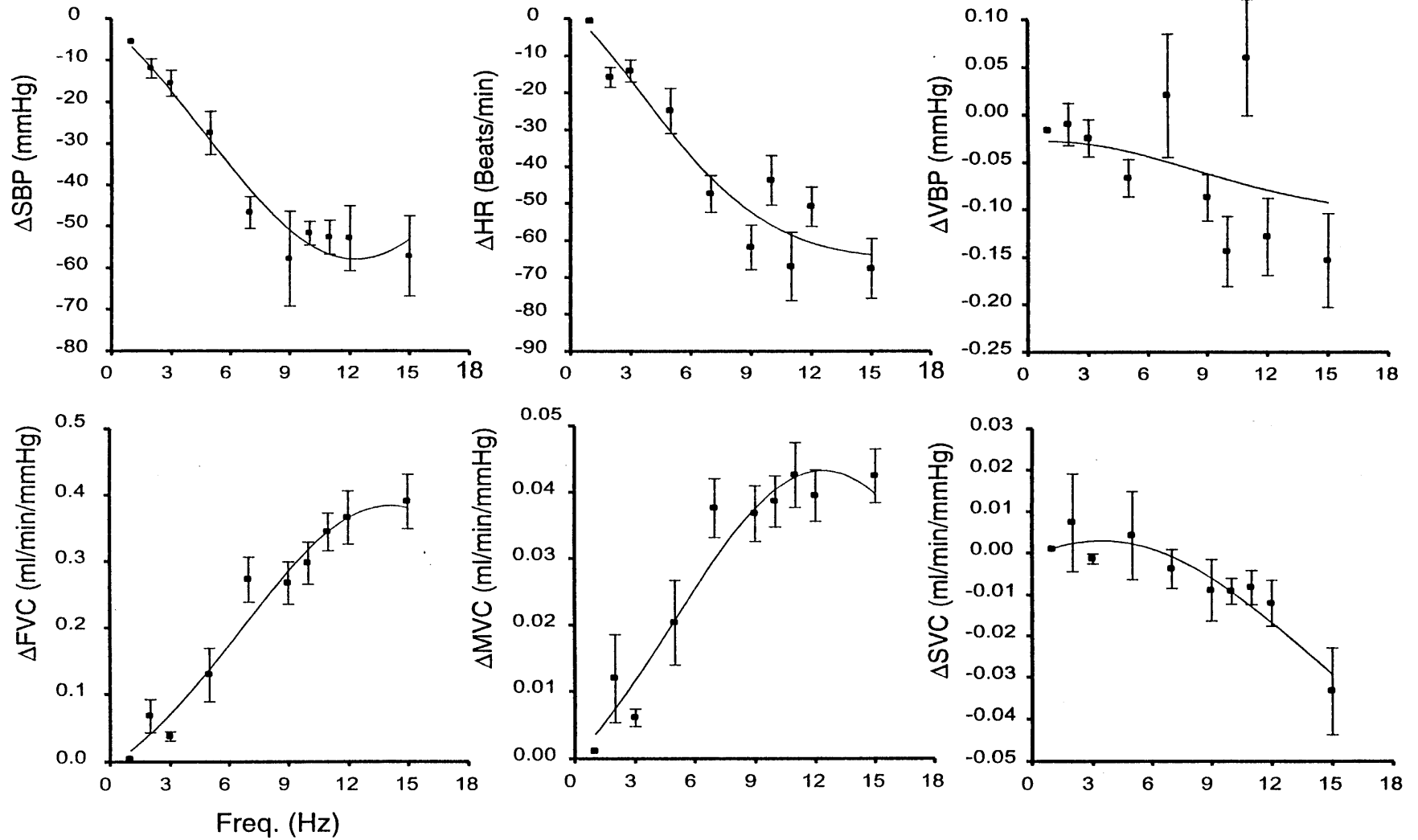
Figure 8.12 Steady state features of the baroreflex ADN-A+C fiber stimulations

Carotid Sinus Step Response
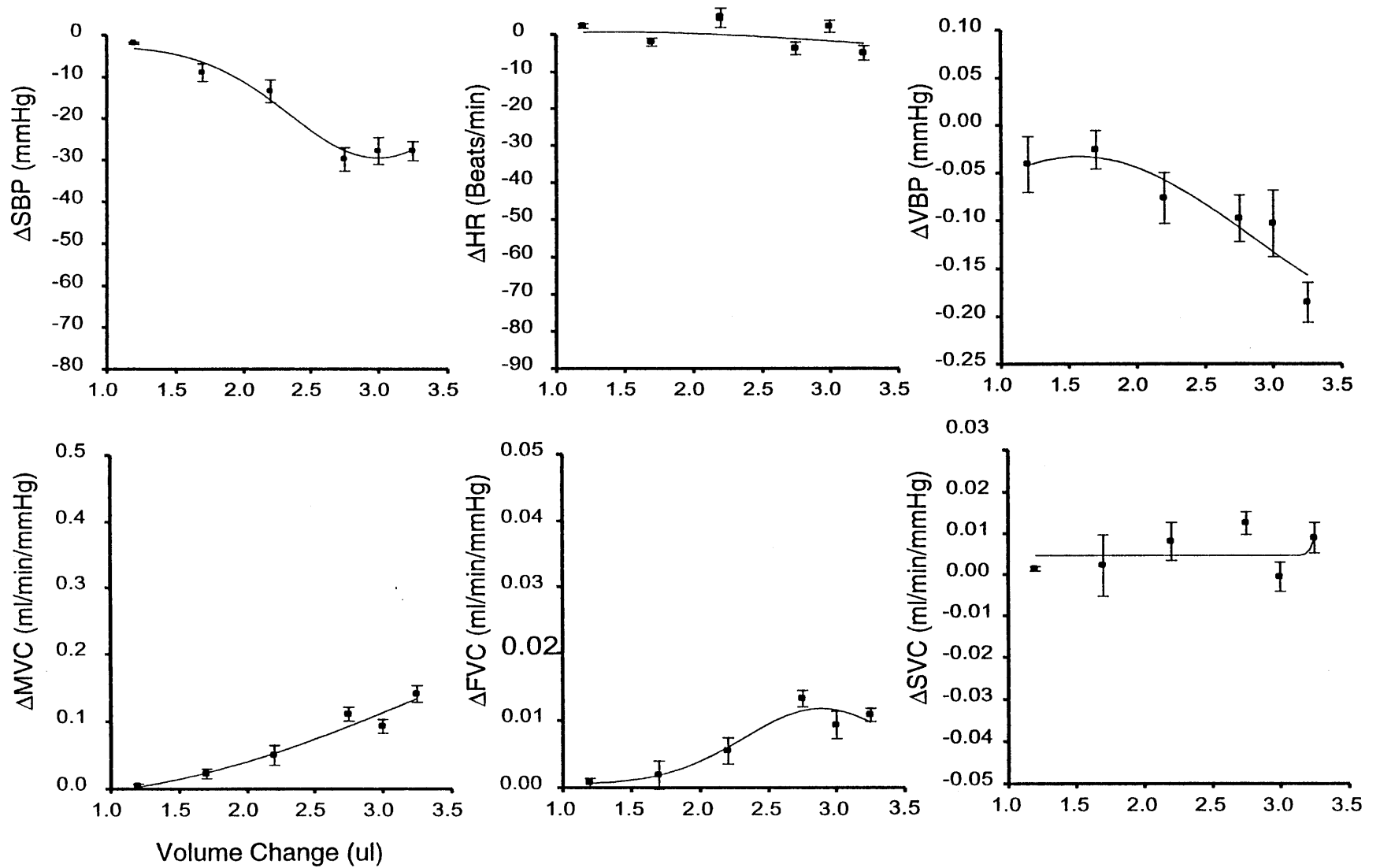
Figure 8.13 Steady state features of the baroreflex Sinus stimulations

8.4.3 Comparison of the Sinus and Aortic Stimulation Effects

How important is a particular vascular or cardiac mechanism in the net "depressor" effect, and how does the relative importance compare for the Sinus, ADN-A, and ADN-A+C stimulus modes?

Table 8.1 demonstrates the linearity and comparative sensitivity of the individual component response effects. Five rats were included in the table; data for all three modes were obtained for rat EF and EH. For DU, complete data was obtained for the Sinus and ADN-A modes. The other two rats, EC and EG had only ADN electrodes. For EG complete data were obtained for both A and A+C fibers, and for EC, the only complete data were for A fibers.

The maximum responses of each rat are listed in the last column of the section for each individual rat, the average of the maximum responses over all rats are listed in the last two columns of the entire table. For all three Sinus and ADN rats (rat EF, EH and DU), the maximum ADN stimulus was substantially more effective than the maximum Sinus stimulus in producing blood pressure decreases; the individual component responses, with the exception of ΔIBI, generally reflected the magnitude of the blood pressure effect (see the Mean-Max column of the Table). For ΔIBI, the ADN-A maximum response was on average 5 times that of the Sinus, and for rat EF, the ADN-A+C ΔIBI was nearly a factor of 40 times the maximal Sinus ΔIBI. Overall, although at maximal Sinus stimulus strength, a measurable heart effect was evident in all rats, it was probably too small to be of regulatory significance.

Because of ceiling effects, testing with a maximal stimulus can distort the normal quantitative relationship among response mechanisms; thus, an appropriate comparison across stimulation modes requires equating the strengths of the physically diverse stimuli

Table 8.1 The linearity and comparative sensitivity of the individual component response effects (Step responses)

Component Response	Stimulus Mode	DU				EC				EF				EG				EH				All Rats		
		Slope	R^2	p<	Max	Slope	R^2	p<	Max	Slope	R^2	p<	Max	Slope	R^2	p<	Max	Slope	R^2	p<	Max	N	Mean Slope	Mean Max
Systolic Blood Pressure (mmHg)	SINUS	-.55	.98	.01	-41.8					-.80	.88	.005	-42.2					-.46	.96	.002	-35.7	511	-.60	-39.9
	ADN-A	-.51	.90	.05	-60.1	-.72	.68	.01	-72.9	-.58	.88	.005	-58.0	-.36	.58	.05	-50.2	-.97	.96	.0001	-89.4	483	-.62	-66.1
	ADN-A+C									-.83	.96	.0001	-83.4	-.43	.92	.01	-41.1	-1.02	.91	.0001	-81.1	303	-.76	-68.5
Interbeat Interval (msec)	SINUS	.12	.92	.02	9.1					.01	.04	.70	2.0					.02	.15	.51	2.4	511	.05	4.5
	ADN-A	.21	.98	.005	23.0	.17	.64	.02	14.0	.13	.75	.005	15.0	.14	.78	.01	16.0	.54	.99	.0001	50.0	483	.24	23.6
	ADN-A+C									.66	.76	.002	78.0	.16	.67	.1	17.0	.42	.93	.0001	33.0	303	.41	42.7
Central Venous Pressure (cmH2O)	SINUS	-.027	.92	.02	-3.02					-.0500	.77	.02	-2.87					-.017	.74	.05	-1.80	511	-.031	-2.56
	ADN-A	-.010	.22	.53	-1.01	-.020	.89	.0005	-1.69	-.0300	.66	.01	-3.76	-.0140	.75	.01	-1.53	-.029	.66	.05	-3.12	483	-.021	-2.22
	ADN-A+C									-.0570	.83	.0005	-4.98	-.011	.60	.1	-1.06	-.039	.68	.003	-3.69	303	-.036	-3.24
Mesenteric Conductance (µl/min/mmHg)	SINUS	.91	.98	.01	69					.73	.83	.01	46									388	.82	92
	ADN-A	1.1	.93	.02	121	.50	.78	.005	43	.88	.86	.001	88	.62	.71	.02	76					400	.79	82
	ADN-A+C									1.9	.96	.0001	189	1.1	.83	.02	105					212	1.5	147
Caudal Aortic Conductance (µl/min/mmHg)	SINUS																	2.5	.91	.01	208	123	2.5	208
	ADN-A																	8.7	.97	.0001	768	83	8.7	768
	ADN-A+C																	8.0	.94	.0001	679	91	8.0	679
Femoral Conductance (µl/min/mmHg)	SINUS	1.4	.99	.001	55	.40	.53	.05	39	.38	.68	.05	23					.10	.97	.002	88	511	.62	55
	ADN-A	.52	.84	.16	65					.19	.81	.002	21	.19	.28	.22	41	.57	.94	.0005	50	483	.37	43
	ADN-A+C									.10	.22	.23	15	.25	.42	.24	32	.65	.90	.0001	50	303	.33	32
Skin Flow (tpu)	SINUS	-.0025	.97	.01	-.169	-.005	.70	.01	-.49	-.0039	.70	.05	-.273					-.0011	.87	.02	-.069	511	-.0025	-.17
	ADN-A	-.0025	.96	.02	-.269					-.0052	.84	.001	-.540	-.0027	.70	.02	-.315	-.0027	.88	.002	-.241	483	-.0036	-.37
	ADN-A+C									-.0088	.95	.0001	-.771	-.0032	.86	.02	-.306	-.0021	.70	.002	-.244	303	-.0047	-.44
Mesenteric Flow (ml/min)	SINUS	.0447	.93	.02	.95	-.002	.03	.66	.258	-.0060	.04	.71	1.02									388	.0226	.98
	ADN-A	.0167	.14	.63	1.22					.0175	.76	.005	1.71	-.0251	.75	.01	-2.81					400	.0153	-.79
	ADN-A+C									.0057	.09	.41	1.42	-.0285	.67	.01	-2.63					212	.0142	-.60
Femoral Flow (ml/min)	SINUS	.0122	.77	.12	.858					.0057	.11	.52	.824					-.0012	.06	.67	.0322	511	.0063	.571
	ADN-A	-.0150	.57	.24	1.11					.0011	.06	.55	.488	-.0055	.04	.65	1.96	.0033	.35	.16	.581	483	.0053	.986
	ADN-A+C									-.017	.57	.02	1.085	-.0021	.03	.92	2.18	.0180	.44	.05	2.26	303	.0067	1.84
Caudal Aortic Flow (ml/min)	SINUS																	.062	.92	.001	4.35	123	.062	4.35
	ADN-A																	.23	.97	.0001	21.85	83	.23	21.85
	ADN-A+C																	.27	.84	.0002	22.65	91	.27	22.65
Stimulations (total)		300				160				454				86				297				1297		
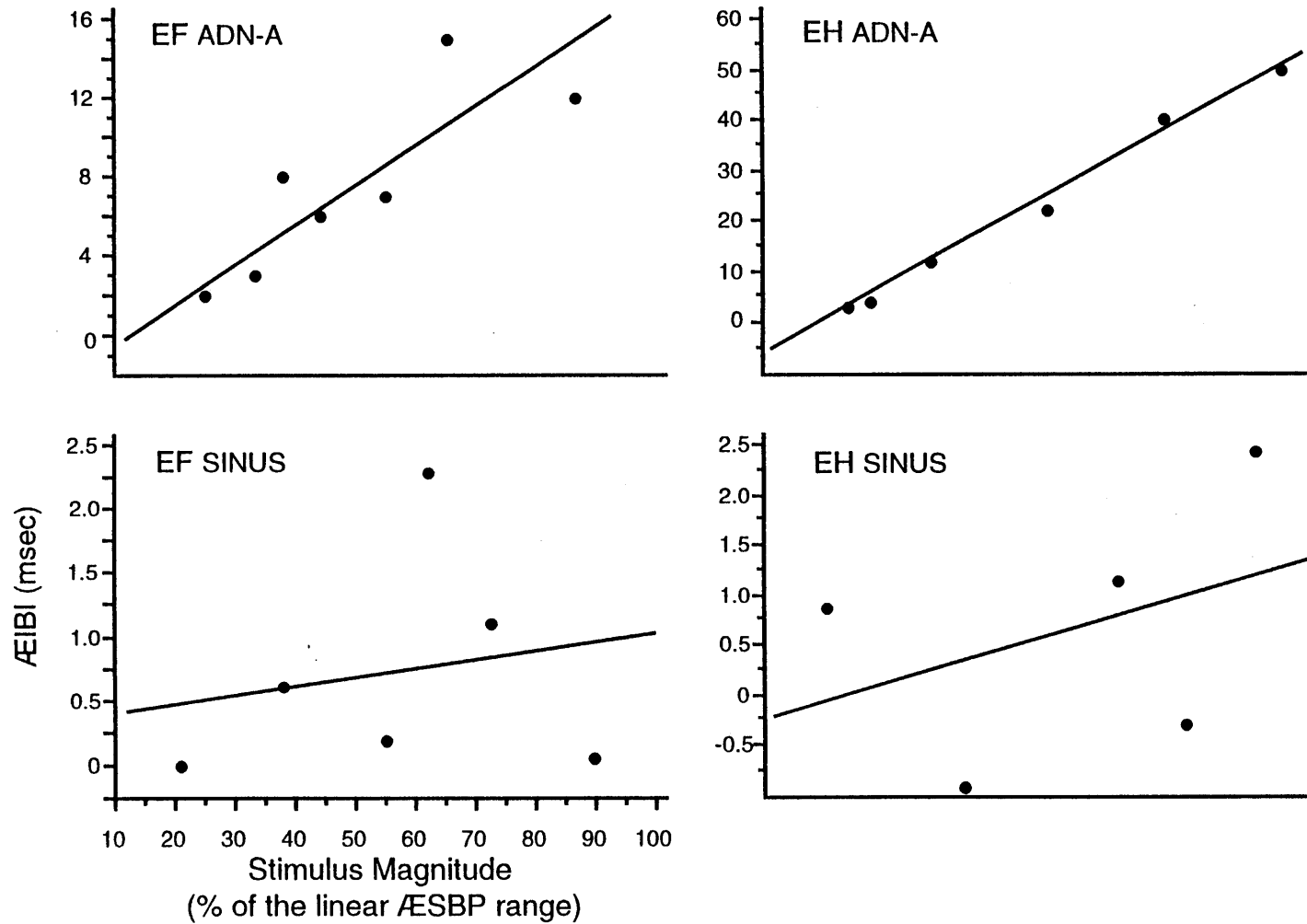
Figure 8.14 IBI change for ADN-A and Sinus stimulation in rats EF and EH, plotted on the corresponding standardized stimulus scale

and also restricting the strength to physiologically realistic values. To do this, for each of the five rats, and for all of the completed stimulus sets, we determined the linear range of the blood pressure effect; mapped the stimulus domain corresponding to this range onto a standard scale, and used the scale to systematically compare the maximum size and linearity of the individual component responses. The detail of linear range determination and scaling procedures were described in section 7.3. The results are included in Table 8.1.

For blood pressure, the slope chiefly reflects the size of the maximum blood pressure effect within the linear range; for example, the larger slope for the ADN-A+C blood pressure corresponds to the larger ADN-A+C maximum effect. For the other component responses, the slope is a function of the minimum and maximum responses to stimuli that are within the range of proportional blood pressure effects.

The slope is a basis for comparing the efficacy with which different stimulus modes activate particular component responses. Although the maximum effect size conveys similar information, the maximum effect could be at a stimulus level above what would bring the blood pressure change to saturation; the standardized regression slope is more stable and realistic estimate of relative sensitivity. Additionally, the statistics of the regression analysis provide information about the consistency of the effect. The percentage transformation of the stimulus scale is linear; thus, the coefficient of linear regression measures the degree to which a particular response is proportional to stimulus magnitude within the threshold-saturation limits of the blood pressure. This is illustrated in the graphs of Figure 8.14, which are the IBI change for ADN-A and Sinus stimulation in rats EF and EH, plotted on the corresponding standardized stimulus scale. The ranges of the ordinate scales, alone, reveal that the sinus effect is smaller; but the graph, in its

entirety, conveys additionally, that compared to the ADN-A effect, the sinus effect is poorly related to stimulus strength. The tabular equivalent of this information, for these and other responses and rats, is in the R^2 and the ANOVA reliability values in Table 8.1. Low R^2 and the ANOVA reliability value represent that the effect is poorly related to the stimulus strength.

8.5 The Dynamic Features of the Open-Loop Baroreflex System --Transfer Function Estimation

8.5.1 The Baroreflex Transfer Functions Derived from the Step Responses

In the linear range of the baroreflex system, the dynamic features of the baroreflex system were first derived using the step responses. Figures 8.15 and 8.16 demonstrate the normalized ADN-A, ADN-A+C fibers and Sinus baroreflex amplitude transfer functions (effective gains) obtained from transient blood pressure, heart rate, mesenteric vascular conductance (low abdominal vascular conductance for EH), and femoral vascular conductance responses to the step stimulations. In each figure, the dashed thin lines represent the results from an individual rat, whereas the thick solid lines are the mean curves for each mode. For each individual component, the effective gains of ADN-A fiber baroreflex were derived from rats EH, EF, EC, EG and DU, those of the ADN-A+C fiber baroreflex were from rats EH, EF, and EG, and the effective gains of the carotid sinus baroreflex were from EH, EF, and DU. Comparing the –3dB cutoff frequency of each component, it is noticed that the heart rate response contained the highest –3dB cutoff frequency value, the cutoff frequency for the blood pressure response was between that of the heart rate and mesenteric vascular responses, and the cutoff frequency for the femoral conductance was slightly higher than that of the mesenteric

conductance. The fast heart rate response may be due to predominant cholinergic fiber innervation to the heart. Since the blood pressure was the net effect of the cardiac output and peripheral vascular response, the blood pressure reaction time was between those for the heart rate and peripheral vessels. Therefore, the cutoff frequency for the blood pressure was between that of the heart rate and mesenteric vascular conductance. The higher cutoff frequency for the femoral vascular conductance than for the mesenteric vascular conductance may be due to innervation of the cholinergic vessel dilation fibers to the femoral vessels.

Section 7.4.1 described the step response approach to derive the effective gain of the baroreflex system. Tables 8.2-8.5 show important parameters related to the exponential fitting and the effective gains of each cardiovascular component. The presented parameters, in the tables, include the fitting plateau, time constant, time constant confidence intervals, $-3dB$ cutoff frequency, -3dB cutoff frequency confidence interval, $-20dB$ frequency and effective gain of the system at 0.4 Hz frequency for the ADN-A, ADN-A+C and Sinus modes.
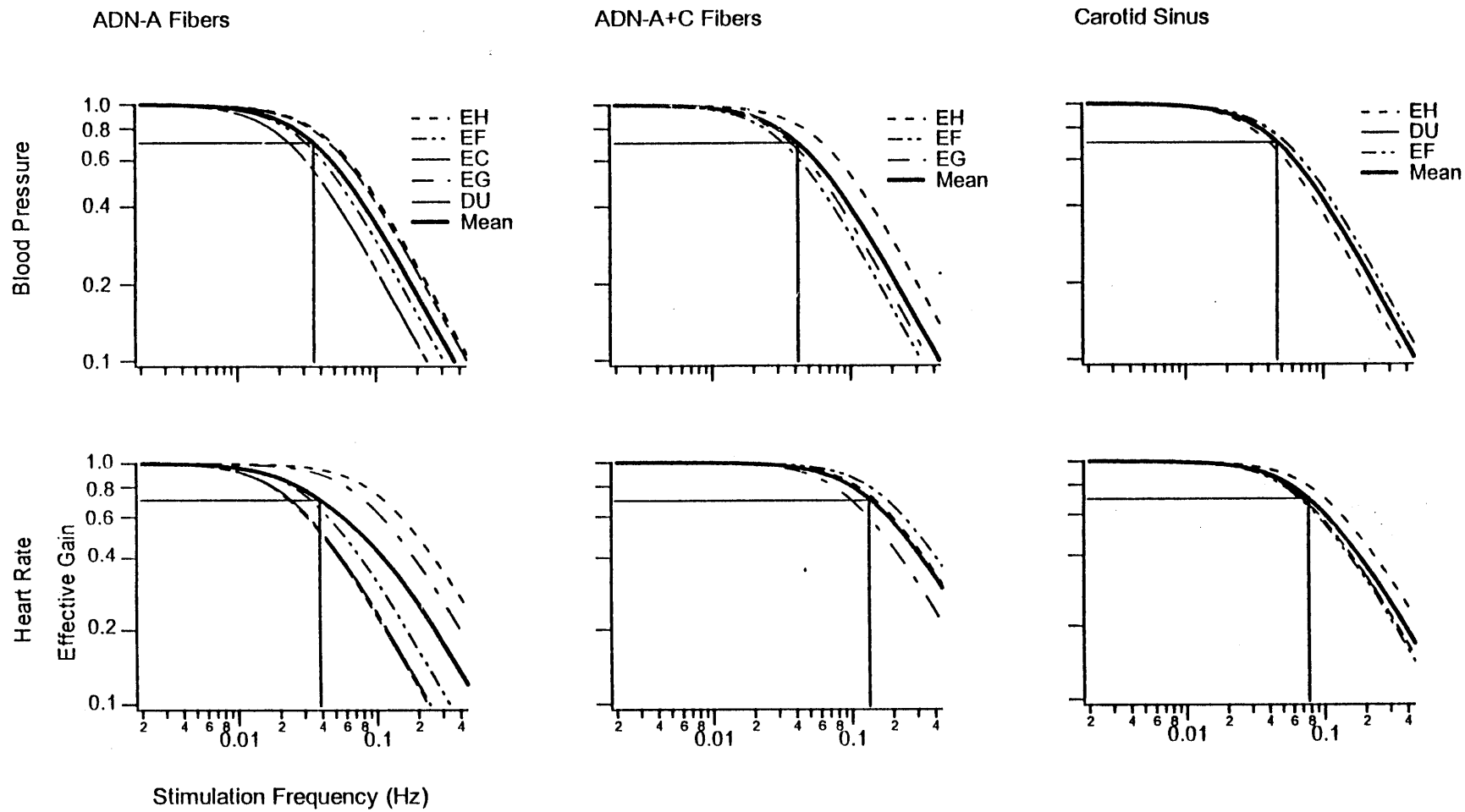
Figure 8.15 Effective gains of the baroreflex system derived from the step responses (I)
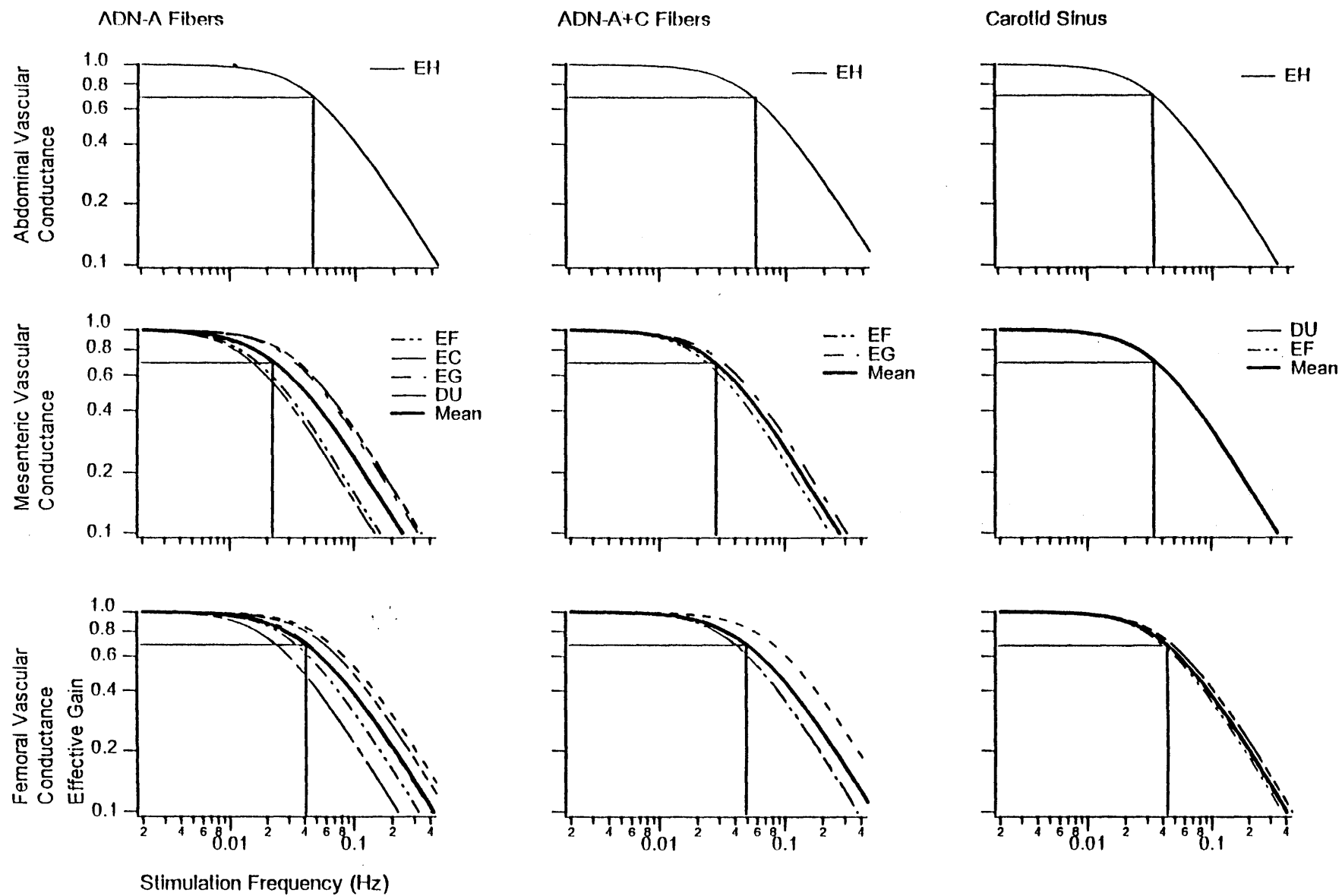
Figure 8.16 Effective gains of the baroreflex system derived from the step responses (II)

Table 8.2 The transient responses and dynamic features of the baroreflexes I: The blood pressure responses

	BLOOD PRESSURE																				
	ADN-A							ADN-A+C							SINUS						
Rat	Hz	N	Asympt ±SD	Time Const ± SD	3DB (Hz)	20DB (Hz)	.4Hz Amp	Hz	N	Asympt ±SD	TimeConst ±SD	3DB (Hz)	20DB (Hz)	.4Hz Amp	µl	N	Asympt ±SD	TimeCon ±SD	3DB (Hz)	20DB (Hz)	.4Hz Amp
EH	20	8	-52.6±1.4	3.21 ±0.32	.050±.005	.448	.123	7	11	-45.3±2.4	2.57±0.42	.062±.010	.500	.142	2.75	11	-43.54±1.9	2.19±0.38	.073±.013	.5	.18
	30	12	-69.3±1.5	3.39 ±0.28	.047±.004	.448	.116	9	5	-65.8±2.2	2.53±0.27	.063±.007	.500	.144	3.00	11	-43.1±2.5	2.42±0.58	.066±.015	.5	.17
	40	11	-68.8±1.5	3.24 ±0.32	.049±.005	.448	.121	10	8	-49.3±2.2	2.39±0.39	.067±.011	.500	.152							
	50	5	-69.4±1.1	3.37 ±0.19	.047±.003	.448	.117	11	11	-48.3±1.9	2.81±0.39	.057±.008	.500	.130							
								12	4	-55.9±1.5	2.51±0.24	.063±.006	.500	.145							
EF	20	9	-57.1±2.9	6.72 ±0.66	.024±.002	.232	.059	7	12	-53.7±2.8	5.18±0.56	.031±.003	.279	.071	2.25	6	-45.0±1.7	2.62±0.41	.061±.010	.500	.150
	30	9	-58.6±2.6	4.66 ±0.51	.034±.004	.323	.085	10	20	-63.4±3.8	4.70±0.62	.034±.005	.323	.078	2.50	10	-54.7±1.7	3.62±0.38	.044±.005	.400	.109
	40	9	-35.3±1.6	4.69 ±0.55	.034±.004	.323	.084	11	7	-85.8±3.2	5.31±0.46	.030±.003	.279	.069							
	50	20	-42.0±2.3	4.94 ±0.66	.032 ±004	.289	.080	12	4	-76.7±1.5	4.45±0.28	.036±.002	.323	.082							
EC	20	11	-72.1±4.5	6.09 ±0.78	.026±.003	.259	.065														
	30	11	-89.0±6.6	7.13 ±0.99	.022±.003	.208	.055														
	40	12	-78.2±4.9	6.77 ±0.81	.023±.003	.232	.058														
	50	12	-80.2±5.9	7.26 ±1.01	.022±.003	.208	.054														
EG	30	22	-32.8±3.2	4.38 ±1.01	.036±.008	.360	.090	3	22	-16.2±2.4	3.09±1.12	.051±.019	.500	.118							
	40	10	-35.6±6.9	6.70 ±2.34	.024±.008	.232	.059	4	4	-35.6±2.1	3.41±0.46	.047±.006	.432	.107							
	50	4	-36.4±3.3	3.28 ±1.01	.049±.015	.448	.120	5	22	-36.4±4.6	5.91±1.27	.027±.006	.241	.062							
DU	10	19	-26.4±1.4	4.28 ±0.59	.037±.005	.360	.092								3.00	9	-24.6±2.4	2.87±0.79	.055±.015	.500	.137
	50	18	-40.8±1.6	2.93 ±0.43	.054±.008	.500	.134								3.50	10	-38.4±3.3	4.26±0.80	.037±.007	.359	.093

Table 8.3 The transient responses and dynamic features of the baroreflexes II: The heart rate responses

	INTERBEAT INTERVAL																				
	ADN-A							ADN-A+C							SINUS						
Rat	Hz	N	Asympt ±SD	TimeConst ±SD	3DB(Hz)	20DB	.4Hz Amp	Hz	N	Asympt ±SD	TimeConst ±SD	3DB (Hz)	20DB Hz	.4Hz Amp	μl	N	Asympt ±SD	TimeConst ±SD	3DB (Hz)	20D (Hz)	.4Hz Amp
EH	20	8	38.45±2.0	2.54±0.35	.063±.009	.500	.154	7	11	25.86±.86	1.68±0.21	.095±.012	.500	.23	2.75	11	16.52±.712	1.26±0.25	.126±.025	.500	.300
	30	12	72.27±3.7	0.92±0.25	.173±.048	.500	.396	9	5	38.60±1.1	2.17±0.20	.073±.007	.500	.18	3.00	11	14.68±.8	1.62±0.36	.098±.023	.500	.24
	50	5	60.45±3.7	1.53±0.36	.104±.025	.500	.251	10	8	34.68±1.1	1.57±0.21	.101±.014	.500	.245							
								11	11	61.25±3.4	1.51±0.45	.105±.035	.500	.2							
								12	4	45.29±1.35	2.04±0.29	.078±.01	.500	.18							
EF	20	9	22.59±1.2	11.07±1.22	.014±.002	.132	.036	10	20	27.74±.64	0.46±0.16	.345±.119	.500	.652	2.25	6	3.86±.206	2.27±0.43	.07±.013	.500	.172
	30	9	21.11±0.9	7.96±0.92	.020±.002	.185	.500	11	7	109.95±7.90	4.74±1.64	.034±.012	.321	.083	2.50	10	5.64±.482	2.67±0.74	.059±.017	.500	.147
	40	9	16.98±0.7	2.34±0.61	.068±.018	.500	.167	12	4	184.89±12.8	1.03±0.92	.154±.137	.500	.358							
	50	20	11.63±0.2	4.99±0.39	.032±.003	.287	.079														
EC	20	11	18.78±1.1	5.14±0.68	.031±.004	.287	.077														
	30	11	28.65±1.3	6.57±0.58	.024±.002	.230	.060														
	40	12	33.20±2.5	8.36±1.07	.019±.002	.185	.047														
	50	12	30.50±1.6	6.98±0.71	.023±.002	.206	.057														
EG	30	22	05.19±0.1	2.90±0.22	.055±.004	.500	.136	3	22	3.81±.16	1.81±0.39	.088±.019	.500	.214							
	50	4	35.70±3.0	1.46±0.76	.109±.057	.500	.262	4	4	8.20±.34	1.73±0.37	.092±.020	.500	.224							
								5	22	10.66±.19	1.79±0.17	.089±.008	.500	.216							
								7	5	16.82±.59	1.29±0.29	.123±.028	.500	.294							
DU	10	19	07.88±0.3	7.22±0.63	.022±.002	.206	.055								3.00	10	7.80±.364	2.05±0.47	.077±.018	.500	.190
	50	18	36.25±0.5	6.42±0.25	.025±.001	.230	.062								3.50	10	10.94±.627	2.73±0.67	.058±.015	.500	.144

Table 8.4 The transient responses and dynamic features of the baroreflexes III: The mesenteric vascular conductance responses

	ADN-A							ADN-A+C							SINUS						
Rat	Hz	N	Asymp ±SD	TimeConst ±SD	3DB (Hz)	20DB (Hz)	.4Hz Amp	Hz	N	Asymp ±SD	TimeConst ±SD	3DB (Hz)	20DB (Hz)	.4Hz Amp	μ1	N	Asymp ±SD	TimeConst ±SD	3DB (Hz)	20DB (Hz)	.4Hz Amp
EH	20	8	.384±.015	3.79±0.49	.042±.006	.402	.104	7	11	.303±.027	3.22±0.78	.049±.012	.447	.122	2.75	11	.175±0.01	4.16±1.73	.038±.017	.36	.10
	30	12	.530±.018	3.79±0.45	.042±.005	.402	.104	9	5	.314±.022	3.52±0.66	.045±.008	.447	.112	3.00	11	.16±0.01	3.77±1.99	.042±.02	.37	.11
	40	11	.517±.013	2.62±0.33	.060±.008	.500	.149	10	8	.346±.026	2.95±0.70	.054±.013	.500	.134							
	50	5	.554±.021	4.71±0.53	.034±.004	.323	.084	11	11	.403±.018	2.30±0.42	.069±.013	.500	.170							
								12	4	.415±.026	3.38±0.60	.047±.008	.447	.117							
EF	20	9	.116±.018	16.39±3.46	.010±.002	.087	.024	7	12	.073±.006	6.34±1.13	.025±.004	.230	.063	2.25	6	.054±.003	4.31±0.72	.037±.006	.359	.092
	30	9	.110±.020	12.96±3.38	.012±.003	.121	.031	10	20	.091±.004	5.59±0.54	.028±.003	.257	.071	2.50	10	.065±.004	4.95±0.83	.032±.005	.287	.080
	40	9	.080±.005	6.33±0.93	.025±.004	.232	.062	11	7	.196±.011	10.2±1.04	.016±.002	.148	.039							
	50	20	.074±.009	9.04±1.92	.018±.004	.167	.044	12	4	.212±.010	6.96±0.94	.023±.003	.206	.057							
EC	20	11	.041±.003	8.70±1.11	.018±.002	.167	.045														
	30	11	.071±.015	17.11±4.74	.009±.003	.087	.023														
	40	12	.052±.005	10.5±1.42	.015±.002	.150	.038														
	50	12	.045±.004	10.17±1.37	.016±.002	.150	.039														
EG	30	22	.072±.008	6.55±1.41	.024±.005	.232	.060	3	22	.024±.005	4.72±2.22	.034±.016	.321	.084							
	40	10	.094±.024	11.09±4.09	.014±.005	.135	.036	4	4	.072±.004	3.64±0.58	.044±.007	.400	.108							
	50	4	.114±.010	2.74±0.91	.058±.019	.500	.143	5	22	.062±.013	7.54±2.77	.021±.008	.206	.053							
								7	5	.135±.011	6.12±1.03	.026±.004	.257	.065							
DU	10	19	.163±.016	7.29±1.38	.022±.004	.208	.054								3.00	9	.087±.007	3.23±0.76	.049±.012	.447	.122
	50	18	.221±.012	3.39±0.62	.047±.009	.448	.116								3.50	10	.219±.050	9.40±3.39	.017±.006	.165	.042

Table 8.5 The transient responses and dynamic features of the baroreflexes IV: The femoral vascular conductane responses

FEMORAL CONDUCTANCE

Rat	ADN-A							ADN-A+C							SINUS						
	Hz	N	Asympt ±SD	TimeConst ±SD	3DB (Hz)	20DB (Hz)	.4Hz Amp	Hz	N	Asympt ±SD	TimeConst ±SD	3DB (Hz)	20DB (Hz)	.4Hz Amp	µl	N	Asympt ±SD	TimeConst ±SD	3DB (Hz)	20DB (Hz)	.4Hz Amp
EH	20	8	.037±.002	2.57±0.46	.062±.011	.050	.153	7	11	.034±.002	2.10±0.47	.076 ±.017	.050	.185	2.75	11	.029±.005	3.80±1.39	.042±.015	.400	.104
	30	12	.044±.001	2.87±0.32	.055±.006	.050	.137	9	5	.036±.001	2.48±0.33	.064 ±.009	.050	.158	3.00	11	.030±.005	4.25±1.46	.037±.013	.359	.093
	40	11	.041±.001	1.97±0.30	.081±.012	.050	.197	10	8	.030±.002	1.61±0.48	.099 ±.030	.050	.239							
	50	5	.048±.002	2.90±0.55	.055±.010	.050	.135	11	11	.033±.001	2.20±0.28	.072 ±.009	.050	.178							
								12	4	.037±.001	2.19±0.36	.073 ±.012	.050	.178							
EF	20	9	.029±.001	5.12±0.58	.031±.004	.287	.077	7	12	.027±.001	4.75±0.68	.033 ±.005	.321	.083	2.25	6	.034±.002	3.58±0.67	.044±.008	.400	.110
	30	9	.030±.002	4.78±0.84	.033±.006	.321	.083	10	20	.027±.001	3.53±0.64	.045 ±.008	.447	.112	2.50	10	.055±.004	5.28±0.79	.030±.005	.287	.075
	40	9	.013±.003	5.65±2.79	.028±.014	.257	.070	11	7	.034±.001	4.12±0.54	.039 ±.005	.359	.096							
	50	20	.026±.002	4.22±0.74	.038±.007	.359	.094	12	4	.041±.001	4.67±0.34	.034 ±.003	.321	.085							
EC	20	11	.062±.003	5.85±0.76	.027±.004	.257	.068														
	30	11	.074±.005	8.14±0.99	.020±.002	.185	.049														
	40	12	.073±.004	7.22±0.87	.022±.003	.206	.055														
	50	12	.063±.004	7.77±0.92	.020±.002	.185	.051														
EG	30	22	.044±.005	4.48±1.10	.036±.009	.321	.088	3	22	.014±.001	3.96±0.77	.040 ±.008	.359	.100							
	40	10	.070±.009	5.34±1.45	.030±.008	.287	.074	4	4	.037±.003	4.31±0.83	.037 ±.007	.359	.092							
	50	4	.062±.005	2.74±0.86	.058±.018	.050	.143	5	22	.040±.002	4.24±0.63	.038 ±.006	.359	.093							
								7	5	.053±.002	4.12±0.42	.039 ±.004	.359	.096							
DU	10	19	.038±.002	3.82±0.61	.042±.007	.040	.103								3.00	9	.022 ±.003	3.49±1.0	.046±.013	.447	.113
	50	18	.067±.004	2.30±0.58	.069±.017	.050	.170								3.50	10	.036 ±.004	3.54±0.99	.045±.013	.400	.112

8.5.2 The Baroreflex Transfer Functions Derived from the Sinusoidal Responses

Figure 8.17 shows typical examples of the raw blood pressure, abdominal blood flow and femoral blood flow responses to the sinusoidal hydraulic stimulation of the carotid sinus. Data were retrieved from a Teac tape.

Figures 8.18-8.20 demonstrate the ensemble average traces of the individual cardiovascular responses to the ADN-A, ADN-A+C fibers and Sinus sinusoidal baroreflex stimulations. The individual components include systolic femoral arterial blood pressure, inter-beat intervals, systolic mesenteric vascular conductance, systolic femoral vascular conductance and systolic femoral venous pressure. The demonstrated sinusoidal modulation frequencies were at 0.025, 0.0375, 0.05, 0.1 and 0.4 Hz. The total time length presented for each trace is 80 sec. For each individual component, at low modulation frequencies, the responses show a clearly sinusoidal pattern with high amplitudes. As the modulation frequency increases, the response curves were gradually out of the pattern, and amplitude of the output responses became smaller.

Table 8.6 provides detail information of the sine fit results. Data in the 'AMPL±SD' column are the normalized mean amplitude values of the sine fit at each frequency, and their corresponding standard deviations. 'Output Freq' column provides the output sine fit frequencies. The frequencies of the output sine fit similar to the input stimulation frequencies, which confirms our linear system assumption. Data in the '-3dB(Hz)' row are the system $-3dB$ cutoff frequencies derived from the sine fit algorithm.

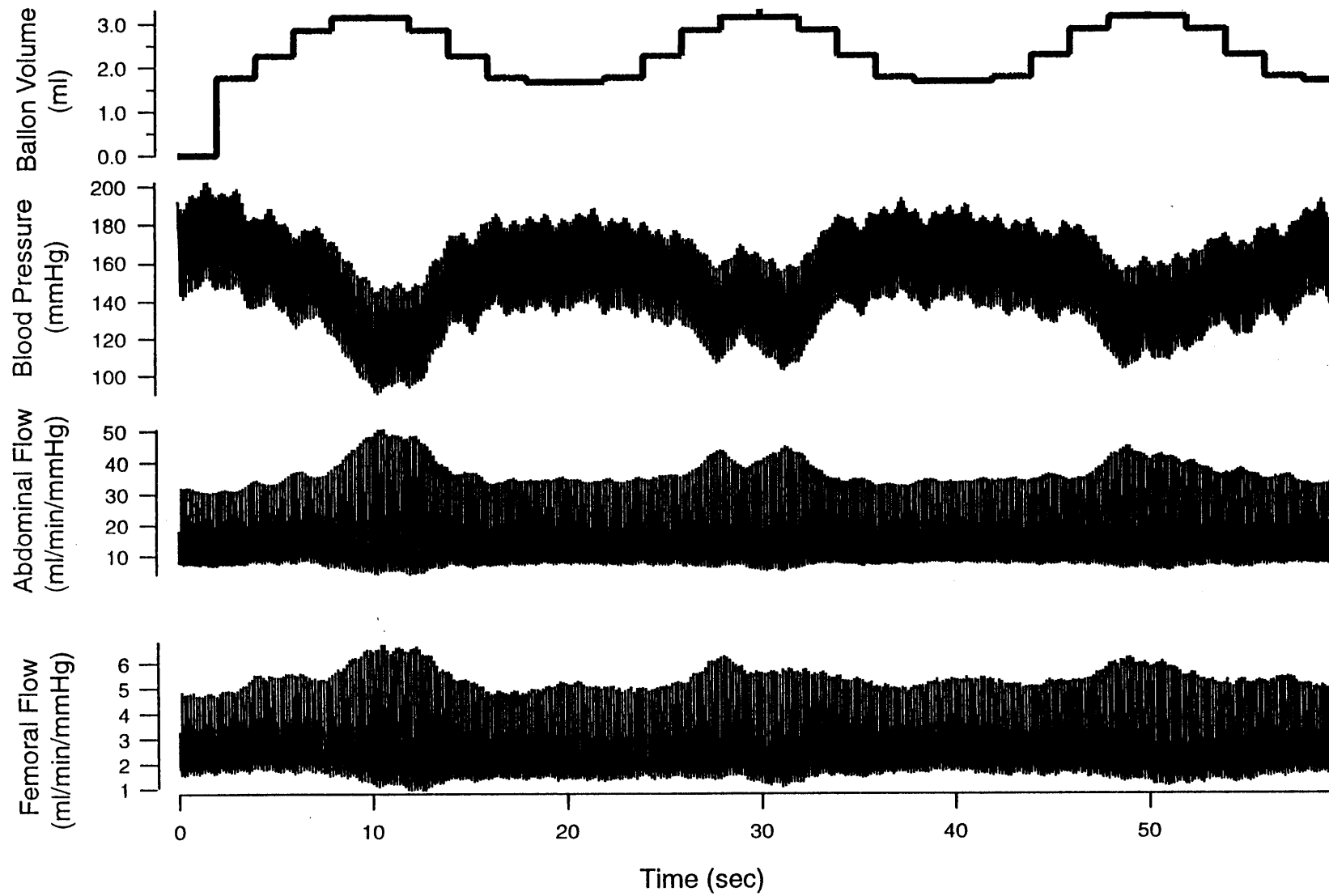**Figure 8.17** Raw blood pressure, abdominal blood flow and femoral blood flow responses to a sinusoidal stimulation
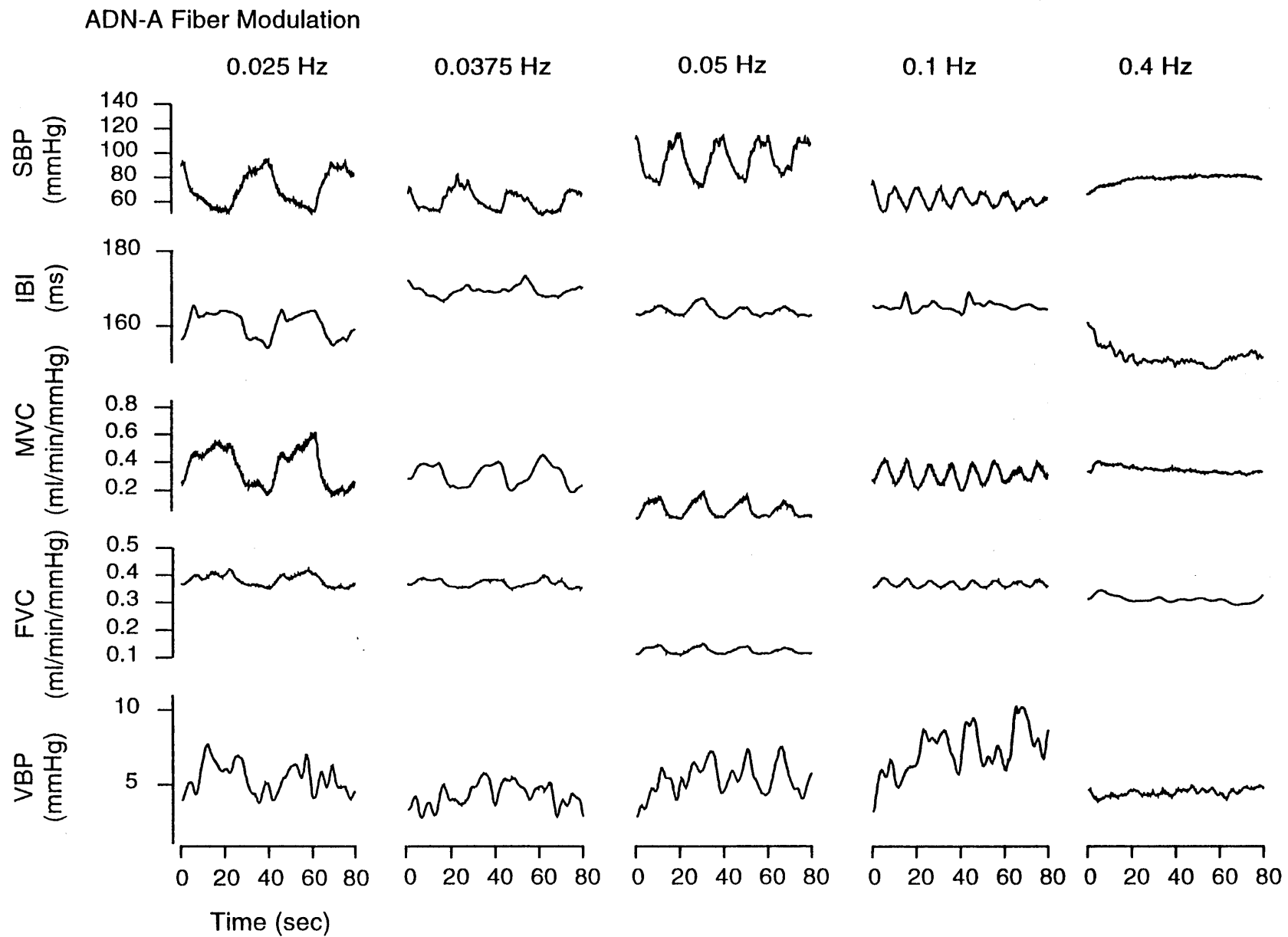
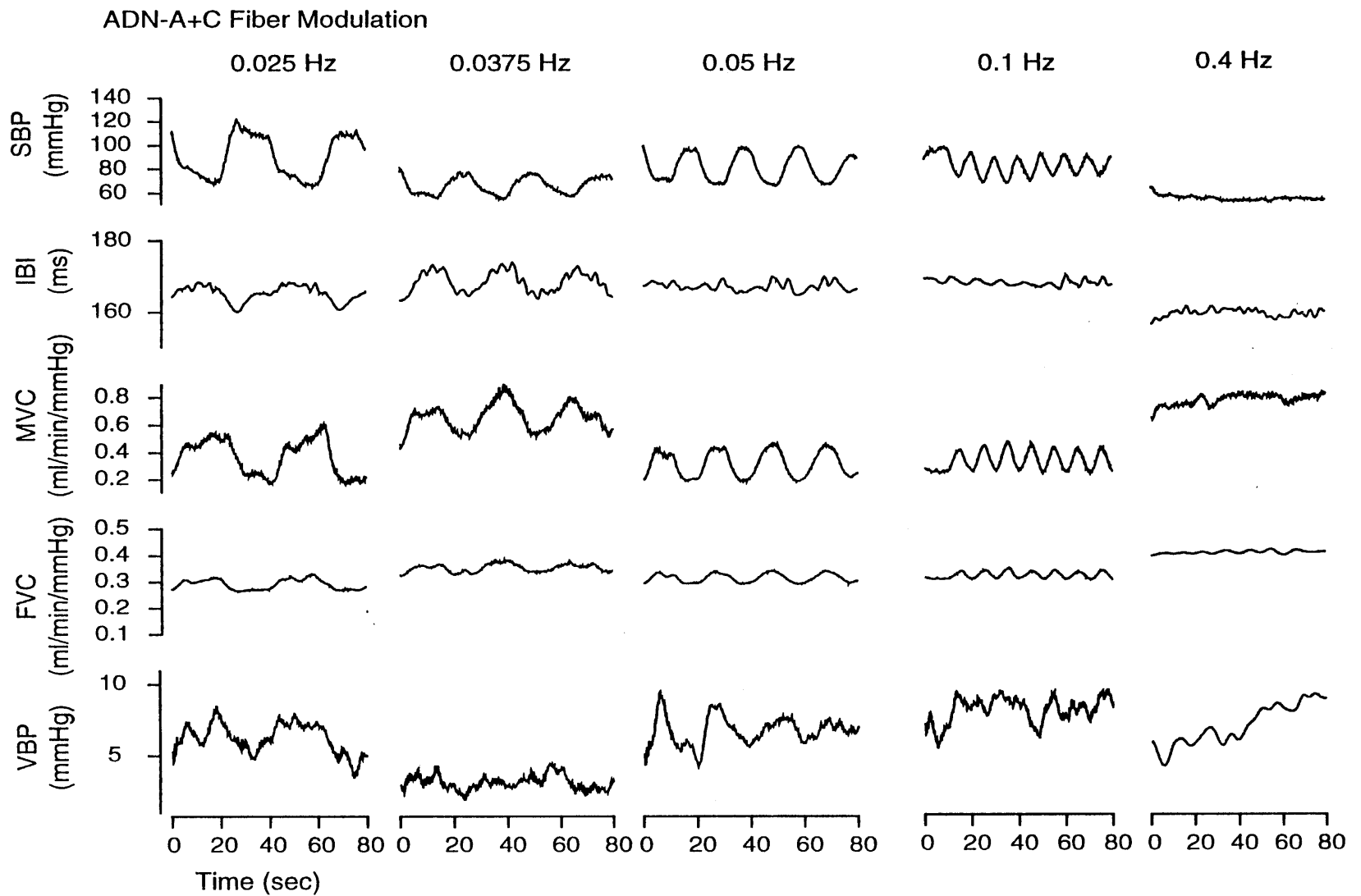**Figure 8.18** Individaul cardiovascular responses to the ADN-A fiber sinusoidal stimulation

Figure 8.19 Individual cardiovascular responses to the ADN-A+C fiber sinusoidal stimulations
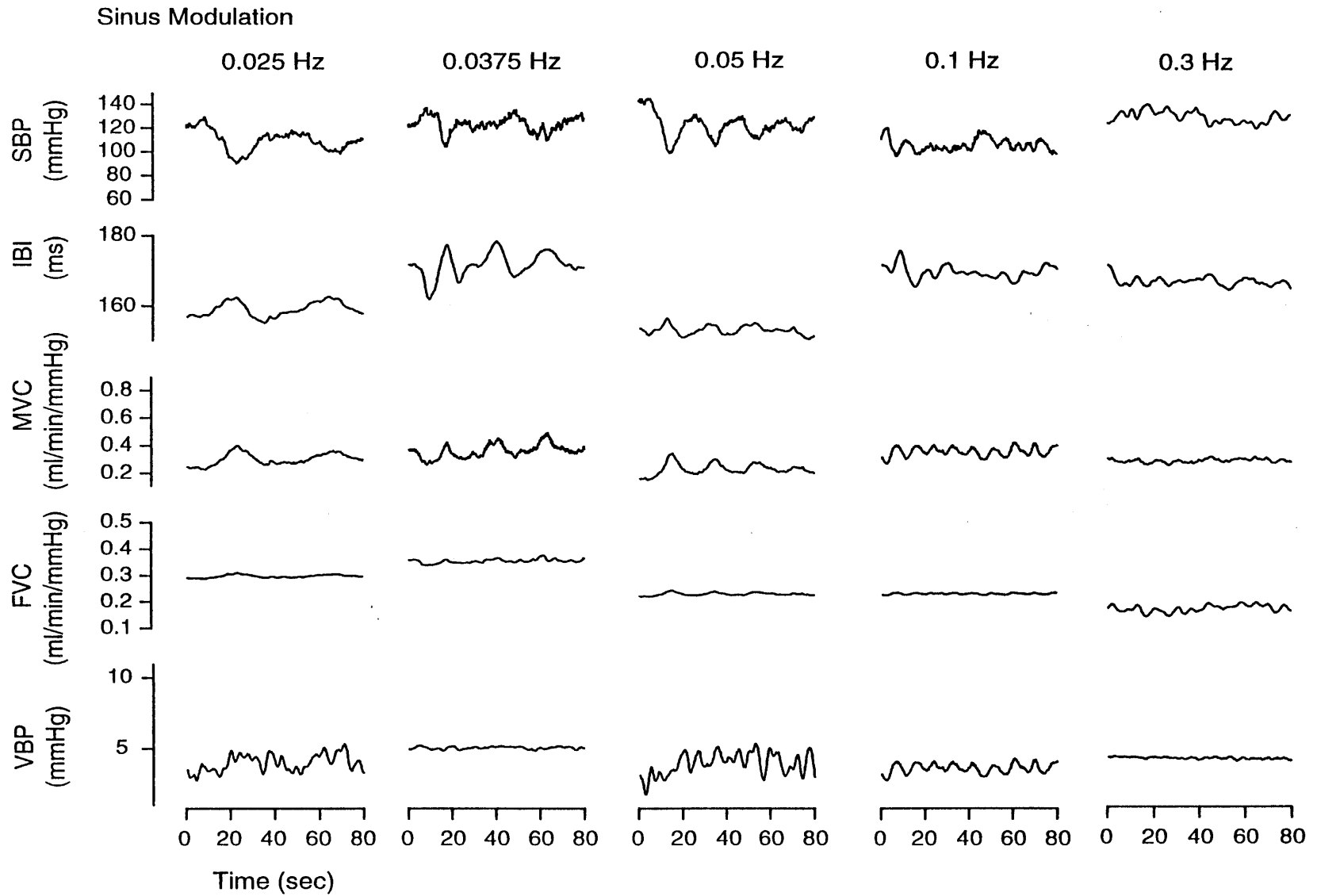
Figure 8.20 Individual cardiovascular responses to the Sinus sinusoidal stimulations

Table 8.6 Effective gains of the baroreflex system derived from the sine fit algorithm

Sinusoidal Fit (Blood Pressure)

| MODE | ADN-A | | | | | | | | | ADN-A+C | | | SINUS | | | | | |
| RAT | EH | | | EC | | | DY | | | EH | | | EH | | | EF | | |
Input Freq(Hz)	AMPL±SD	Output Freq	N	AMPL±SD	Output Freq	N	AMPL±SD	Output Freq	N	AMPL±SD	Output Freq	N	AMPL±SD	Output Freq	N	AMPL±SD	Output Freq	N
0.02	0.98±.01	.021	10	1.00±.01	.020	10												
0.025	1.00±.01	.026	5	0.94±.01	.024	5	1.00±.02	.025	22	1.00±.01	.025	14	1.00±.03	.022	20	0.44±.002	.027	16
0.05	0.84±.02	.050	10	0.87±.01	.050	5	0.81±.02	.050	11	0.70±.01	.050	7	0.84±.03	.050	10	1.00±.002	.050	22
0.075	0.28±.01	.079	5	0.41±.01	.075	10	0.24±.01	.070	11	0.52±.02	.077	7	0.62±.03	.075	10	0.32±.002	.075	8
0.1	0.20±.01	.100	5	0.29±.01	.097	5	0.16±.01	.095	11	0.32±.03	.100	7	0.34±.02	.104	10	0.15±.001	.100	27
0.125	0.15±.02	.126	5	0.34±.02	.123	5	0.28±.02	.126	11	0.10±.01	.126	6	0.49±.03	.123	10	0.11±.002	.121	8
0.15	0.18±.02	.149	5	0.14±.01	.151	5	0.17±.01	.150	15	0.18±.02	.149	5	0.35±.02	.147	22	0.08±.003	.145	10
0.2	0.11±.01	.195	5	0.07±.01	.203	5	0.17±.03	.209	7	0.08±.01	.204	5	0.18±.03	.195	11			
-3dB(Hz)	0.04			0.05			0.04			0.05			0.06			0.054		
-20dB(Hz)	0.25			0.22			0.30			0.13			0.25			0.13		

8.5.3 The Baroreflex Transfer Functions Derived from the Power Spectrum Analysis

The power spectrum algorithm was the third method employed in this thesis to derive the open-loop baroreflex transfer functions. Data were acquired according to protocol 3, described in section 5.4; the analysis procedures were described in section 7.4.3. Figure 8.21 demonstrates the multiple blood pressure spectra at modulation frequencies of 0.025, 0.0375, 0.05,0.075, 0.1, 0.175, 0.2 and 0.4 Hz (0. 3 Hz for the

Sinus) for the ADN-A, ADN-A+C and Sinus modes. The frequencies are plotted on a logarithmic scale, while the amplitudes are plotted on a linear scale; the solid lines represent the spectra of the modulated blood pressure signals and the shaded area are the average blood pressure spectra during the pre-stimulation periods. Data used to create modulation and baseline blood pressure spectra were both 2 minutes long. In all three modes (the ADN-A, ADN-A+C and Sinus modes), when the modulation frequencies were low, the blood pressure spectra showed dominant peaks at the modulation frequencies; with increases of the modulation frequencies, the spectral peaks at the modulation frequencies gradually decreased, and became very small at the frequencies beyond 0.4 Hz. It is noticed that the modulation peak did not monotonically decrease at 0.05Hz, the amplitudes of 0.05 Hz modulation peaks were higher than those at 0.035 Hz.

The key function of the baroreflex system is to regulate the minute-to-minute blood pressure variability; the amplitudes of the modulation peaks in the spectrum represent the relative power of the baroreflex system to regulate the blood pressure variability. In the low frequency region, where the blood pressure variation is high (high blood pressure baseline noise power), the baroreflex contains high regulation power. For example, at 0.025Hz, the modulation peak amplitude is the highest; and the baroreflexes

are assumed to have the highest power to restrain the blood pressure variability at this frequency. Whereas, in the higher frequency region, where blood pressure does not contain too much variability (the blood pressure baseline noise power is low), the baroreflex possesses very low stabilization ability, e.g. the modulation peak amplitude is very low at 0.4 Hz. This is a very interesting feature of the baroreflex system.

Table 8.7 provides detail information of the power spectrum analysis results. Data in the 'AMPL±SD' column are the normalized mean peak amplitude values at each modulation frequency, and their corresponding standard deviations. Data in the '-3dB (Hz)' row are the system -3dB cutoff frequencies derived from the power spectrum algorithm. The -3dB cutoff frequencies, which were <0.1 Hz, derived from the transient step responses, sine fit, and power spectrum analysis were consistent with each other.

8.6. Transportation Lag Estimation

Table 8.8 demonstrates the transportation lags of the baroreflex system determined from 5 rats for the three different stimulation modes. The results were represented as Mean±SE. The values for the Sinus stimuli were slightly larger than the ADN, but this difference was most likely due to mechanical delays in the balloon inflation. The mean lag for the ADN was ≈1.07 s.

8.7 Vagus, Peroneal Nerve and Heart Rate Response Time

Although the Sinus heart rate response is smaller than the ADN (results were presented in section 8.4.3), EH had a measurable Sinus induced heart rate decrease that was clearly related to vagus activity (see figure 8.22). The high resolution vagus recordings of fifteen 3.0 µl Sinus stimulation are shown in figure 8.23. The ensemble average of these, the corresponding peroneal nerve, heart rate traces, and balloon volume are shown in figure 8.24. Because the volume is a ramp, and the baroreceptors are rate sensitive, the stimulus onset was taken as the maximum of the derivative; defining the response as a 3δ (δ: the standard deviation of the baseline vagus activities) increase in vagus activity and 3δ (δ: the standard deviation of the baseline peroneal nerve activities) decrease in peroneal activity, gives a lag ≈ 30 ms for the vagus, and < 20 ms for the peroneal nerve; alternatively, if first detectable change in balloon volume is taken as the onset, the lag ≈ 91 ms for vagus, and ≈ 84 ms for the peroneal nerve. The heart rate change is initiated within one IBI after the vagus peak, or approximately two IBI's from the stimulus onset.
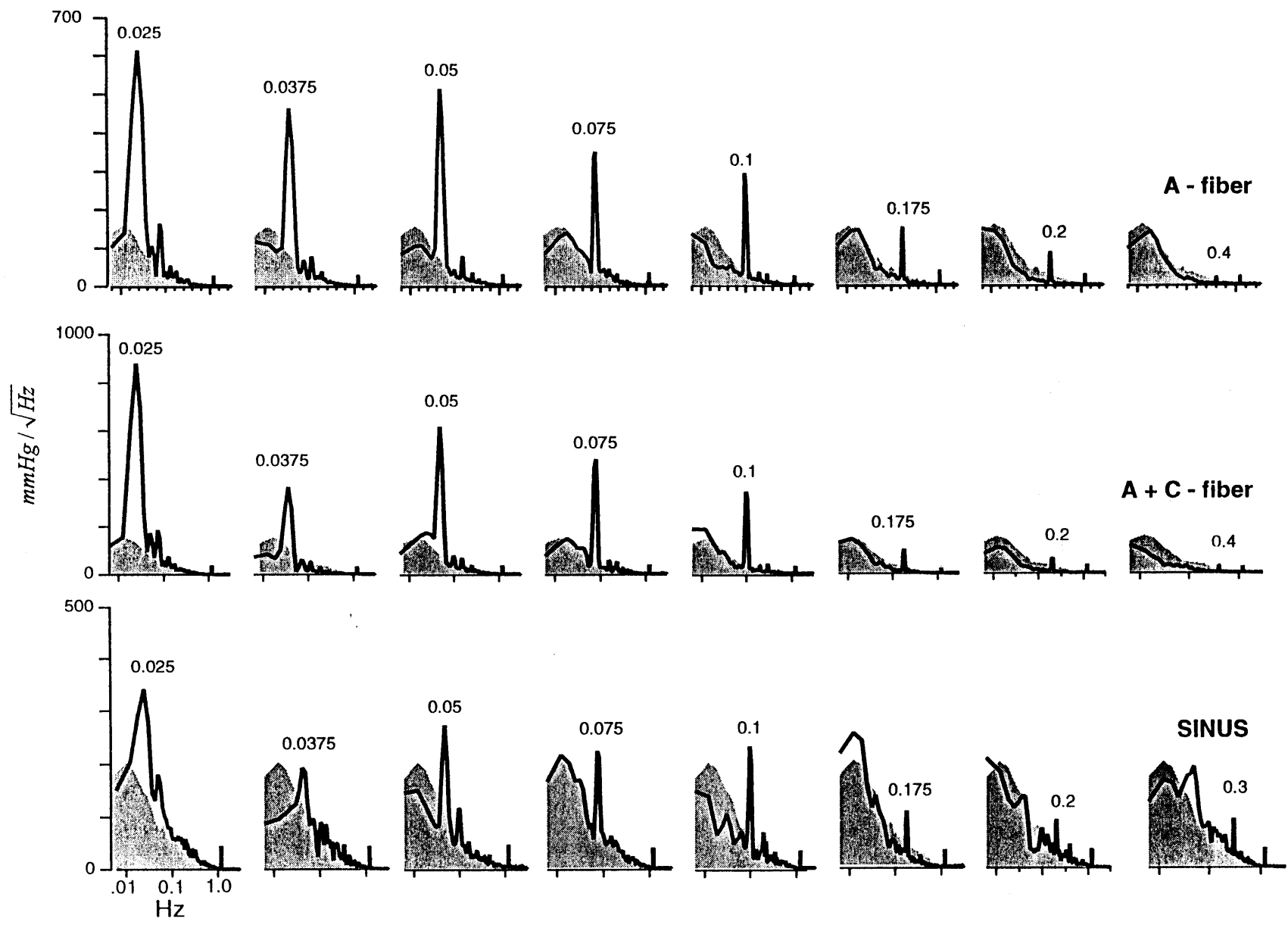
Figure 8.21 Multi-spectra of the sinusoidal stimulation

Table 8.7 Effective gains of the baroreflex system derived from the power spectrum algorithm

FFT Fit (Blood Pressure)

MODE RAT Freq(Hz)	ADN-A EH AMPL±SD	N	ADN-A EC AMPL±SD	N	ADN-A DY AMPL±SD	N	ADN-A+C EH AMPL±SD	N	SINUS EH AMPL±SD	N	SINUS EF AMPL±SD	N
0.02	0.88±0.53	10	1±0.53	10								
0.025	1.00±0.41	5	0.83±0.36	5	0.91±0.79	22	1.00±0.41	14	1.00±1.13	20	0.75±1.24	16
0.05	0.83±0.43	10	0.71±0.31	5	1.00±0.72	11	0.70±0.27	7	0.91±0.39	10	1.00±1.10	22
0.075	0.57±0.38	5	0.56±0.24	10	0.42±0.24	11	0.55±0.23	7	0.76±0.43	10	0.47±0.50	8
0.1	0.48±0.17	5	0.40±0.13	5	0.32±0.18	11	0.39±0.16	7	0.79±0.39	10	0.41±0.47	27
0.125	0.24±0.17	5	0.36±0.13	5	0.43±0.32	11	0.11±0.06	6	0.59±0.22	10	0.26±0.28	8
0.15	0.20±0.16	5	0.22±0.12	5	0.22±0.15	15	0.13±0.07	5	0.27±0.33	22	0.15±0.27	10
0.2	0.14±0.18	5	0.17±0.14	5	0.26±0.29	7	0.07±0.06	5	0.33±0.29	11		
0.4	0.01±0.03	5	0.02±0.02	3			0.03±0.02	5	0.32±0.12	11		
-3dB(Hz)	0.053		0.052		0.054				0.078		0.055	
-20 dB(Hz)	0.278		0.275		0.275						0.25	
0.4 Hz	0.008		0.020						0.31			

Table 8.8 Transportation lag of the baroreceptor reflex loop

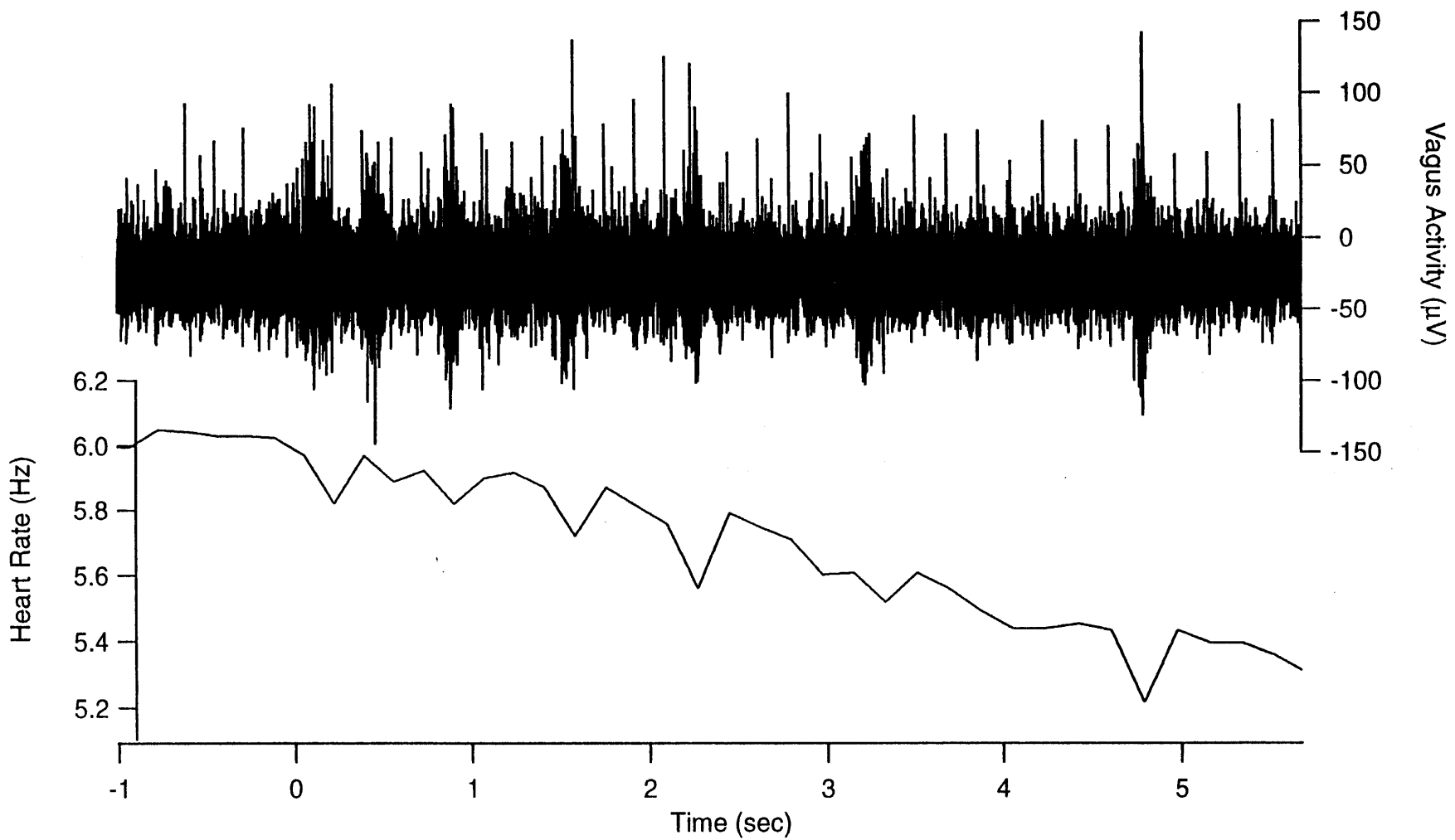|	Mean ± SE (sec)	Number of Trials
EH Sinus	1.108 ± 0.03	34
EH A Fiber	1.050 ± 0.04	25
EH C Fiber	1.010 ± 0.03	27
EF Sinus	1.063 ± 0.03	33
EF A Fiber	0.986 ± 0.04	20
EF C Fiber	1.046 ± 0.03	28
EC A Fiber	1.096 ± 0.03	58
EG A Fiber	1.070 ± 0.06	35
EG C Fiber	1.131 ± 0.07	3
DU Sinus	1.198 ± 0.05	12
DU A Fiber	1.180 ± 0.04	22

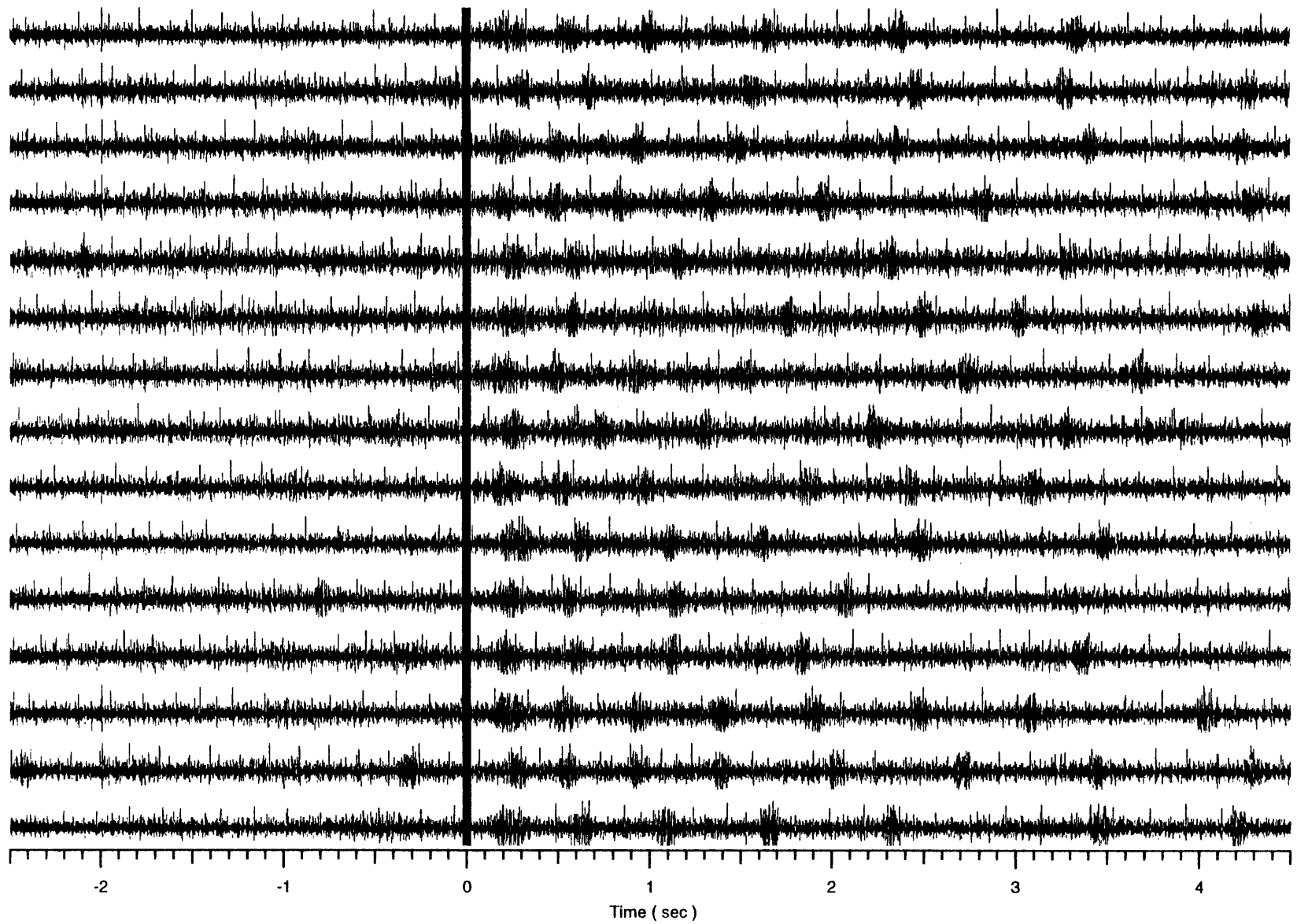**Figure 8.22** Vagus activity related heart rate decreases

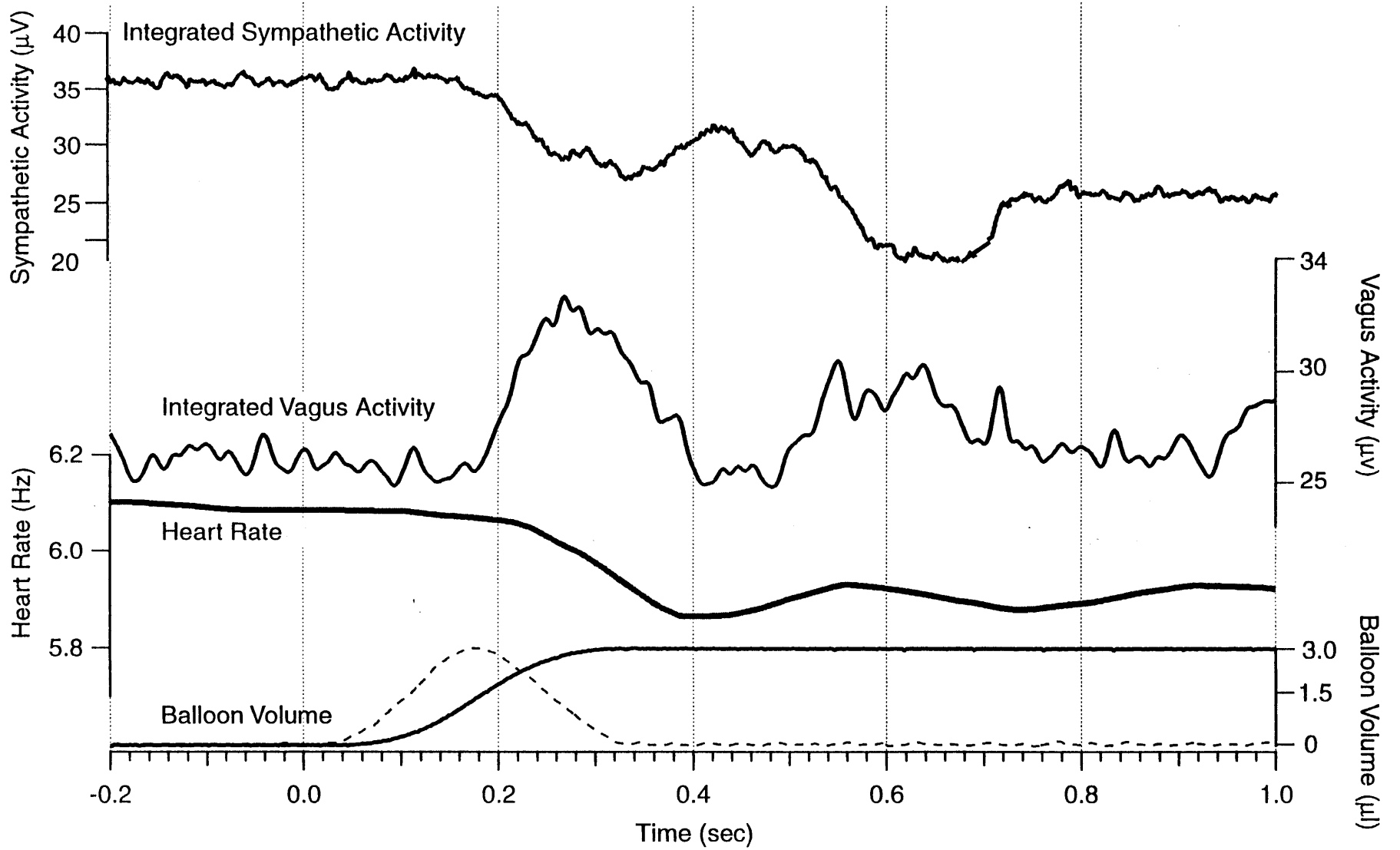**Figure 8.23** Vagus responses to the carotid sinus stimulation

Figure 8.24 The peroneal nerve, vagus nerve and heart rate response times

CHAPTER 9

DISCUSSION

9.1 The Unique Rat Preparation

The positive ventilated, skeletal outflow and autonomic function intact, NMB rats [63] provided unique opportunities for extended observation and precise manipulation of the baroreflex regulatory mechanisms. The neuromuscular block categorically excludes mediation of observed autonomic effects by either skeletal-muscular or respiratory responses. The unusual degree of access, control and stability afforded by the NMB rats enabled completion of complicated experimental designs more rapidly and with far fewer subjects than would be ordinarily required.

9.2 Observations which Implied the Features of the Baroreflex System

SAD substantially increased blood pressure variability. Many phenomenon observed in the variability imply the features of the baroreflex system.

9.2.1 The Substantial Increases of the Post-SAD Blood Pressure Variability

The SAD caused the blood pressure standard deviation to increase by approximately ± 10mmHg, from 6.3 ± 3.5 mmHg to 16.3 ± 2.4 mmHg. The large random variability after denervation is not peculiar to the NMB rat but is generally characteristic of an unanesthetized SAD rat. Jacob et al. reported in freely-moving rats that SAD increased the blood pressure standard deviation by a factor of ≈ 3 over controls [52]. Schreihofer reported in tethered rats that the standard deviation before denervation was $\approx \pm 4$ mmHg, and $\approx \pm 12$ mmHg after [64]. Similarly, Machado et al. reported a pre-denervation SD of

±3.6 mmHg and post of ±13.6 mmHg [65], and Trapani [66] found value of ≈±5 mmHg and ≈±15 mmHg, respectively.

Two groups have explicitly studied the effect of the sampling interval: Alper *et al.* [37] compared 5 second to one minute measurement intervals and found no difference, and Buchholz, Hubbard, and Nathan [45] compared one hour to 24 hour intervals, and also found no difference; in fact, comparing across the studies, there was scarcely any difference over intervals of 5 sec to 24 hours. For samples composed of individual observations, this consistency is to be expected, because if the variability is completely random, the number of observations affects only the confidence interval of the standard deviation estimate, not its central tendency. However, in analyzing the statistics of a blood pressure response measure, we found, that the variance among samples constructed from the differences between 30 s blood pressure means, was similar to that of individual observations. For completely random data, this was not expected. For samples composed of the mean of n observations, the standard deviation of the samples should decrease with increasing of n. A possible explanation of this discrepancy is that the post-SAD blood pressure, although random, has a non-uniform frequency distribution with greater power in the pass band of the '30 s mean difference' filter. The derivation in Appendix B shows that, in time domain, taking 30 s mean difference is equivalent to pass data through a "low-pass" filter, whose pass band is in the region of 0-0.03 Hz. Because only the variability is within the pass band of the '30 s mean difference' filter, the filter is without effect. Thus, from the effects of the '30 s mean difference' on the standard deviation of the blood pressure signal, we can predict that the major power of the blood pressure variability is in the VLF region. The power spectrum analysis of the pre- and post-SAD blood pressure variability confirmed the predication we had for the frequency

features of the blood pressure variability from the time domain observation. A substantial increase of the blood pressure variability after SAD implied a huge power increase of the post-SAD blood pressure spectrum at VLF region.

9.2.2 The Substantial Increases of the VLF Power after SAD

Since the pre- and post-SAD represented two baroreflex states (open and closed loop), we could predict the dynamic characteristics of the baroreflex system from distinct frequency features of the blood pressure spectra from both states. Comparing pre- and post-blood pressure spectra, we noticed that the total power of the post-SAD blood pressure spectra is higher than that of the pre-SAD; the post-SAD blood pressure spectra were not simply the proportional amplification of the pre-SAD spectra. Compared to the pre-SAD spectra, the post-SAD spectra contained significantly increased power in the VLF region (0.00195 – 0.2 Hz), and significantly decreased power in the LF region (0.2 – 0.6 Hz). The post-SAD VLF change was more dominant (the statistical results of the comparison was shown in figure 8.8). It is fundamental that, an element, such as the baroreflex, can oppose and neutralize a disturbance, such as endogenous blood pressure variability, only where the transfer function of the element, and the noise spectrum of the disturbance overlap; it is a corollary, that the spectral change that occurs when an element is removed delineates the element's filter characteristic. Therefore, the substantial increases of the VLF power after SAD implied that the major working area of the baroreflex system is in the VLF region.

9.2.3 The Decrease of the LF Power after the SAD

The 'low-pass' (with cutoff frequency <0.1 Hz) feature of the baroreflex system explained the substantial increases of the VLF power in the blood pressure spectra after the SAD, but did not address the issue of why the SAD caused decreases of the LF power in the blood pressure spectra?

First, since the LF power decreased with the SAD, is the LF band the "marker" of the baroreflex system? This is a paradoxical opinion, because the baroreflex system is a closed loop negative feedback system, which plays an important role to restrain the blood pressure variability, and removing such a system should cause increasing of the blood pressure, instead of decreasing.

Baselli, et al. [67] and Cerutti et al. [53] suggested that the LF frequencies, at around 0.34Hz, may represent the resonant frequency of the feedback system involving one baroreflex loop and the vasculature as the efferent system. Their opinions coincide with our research results.

The transportation lag and transfer function (or effective gain) derived from the present studies provided the solid basis for the understanding of the mechanism behind the decrease of LF power after SAD.

The average pure transportation lag for the baroreflex system derived from the present study was around 1.07 second, (see table 8.8). In the results, the lags derived from the Sinus stimulation were slightly longer (17-98 ms) than that derived from the ADN stimulation, but the difference was not significant. This difference was most likely due to the mechanical delays in the sinus balloon inflation. Charltion et al. reported [68] that the transduction delay of the arterial baroreceptor is negligible compared with the total delay introduced by other components of the reflex arc.

According to control theory, every negative feedback system containing time lags is prone to oscillate, because, as frequency increases, the output signal is progressively delayed from the input signal until, at a particular frequency, it is fed back positively [6].

The baroreflex system can be modeled as a combination of transportation delays and a first-order linear component [55]. For a system of frequency f, the phase lag for a transportation delay Δt_d is $\phi(\Delta t_d) = 2\pi \cdot \Delta t_d f$; in addition, for 1st order linear systems, the phase lag, $\phi_l(f) = \arctan(2\pi f T)$, where T is the time constant, is equivalent to a delay, $\Delta t = \arctan(2\pi f T) / 2\pi f$. Therefore, the total phase delay between the input and feedback signal in the baroreflex system is determined by the formula:

$$\phi(f) = 2\pi \cdot f \cdot T_{total} \tag{9.1}$$

Where $T_{total} = \Delta t_d + \Delta t$, f is the frequency of the input signal; and $\phi(f)$ is the phase shift between input and feedback signals.

With the time constants derived from exponential step responses (Table 8.2) and 1.07 s transportation lag (Table 8.8), it is easy to calculate that the possible oscillation frequency range for the closed loop baroreflex negative feedback system is at the LF region of the blood pressure spectra. Therefore, when the baroreflex is intact, the LF contains resonant power of the baroreflex system, and when the system is denervated, the oscillator is removed, and thus, the LF power is decreased.

Although, several authors [67, 69-71] [72] have suggested that the low frequency component in the blood pressure spectrum might be generated by a resonance

phenomenon of the sympathetic baroreflex control loop, so far, none of these studies have provided solid evidence as we did in our experiments.

Some author in the literature argued that the LF component in the BP spectrum is attributed to the influence of the sympathetic nervous system. For example, in 1991, Cerutti, *et al.*, [72] demonstrated that rats with early destruction of the sympathetic fibers by guanethidine showed large reduction of low frequency power, and rats with acute α-adrenoceptor blockade by phentolamine showed marked decrease of LF power in the blood pressure spectrum. We believe that the real mechanism contributing to the decreases of LF power in the BP spectrum following either destruction or blockade of the sympathetic nervous system was the destruction of the baroreflex loop. Destruction of the sympathetic system opened the baroreflex loop and therefore removed the oscillator source for the LF region, which caused the decreases of the LF power in the BP spectrum.

9.3 Absolute Gain of the Open-Loop Baroreflex System

9.3.1 Derivation of the Absolute Gain of the Open-Loop Baroreflex System

Although the volumetric stimulation of the carotid sinus provided a reliable long-term stimulation method to manipulate the baroreflex system, it lacks the ostensible blood pressure equivalence of barometric stimulation. A similar problem was encountered in the electrical stimulation of the ADN. Thus, the absolute gain of the open-loop baroreflex system was not directly available from the volumetric stimulation of the carotid sinus and electrical stimulation of the ADN methods. However, the absolute gain could be derived from the relationship between the ratio of pre- and post- blood pressure amplitude spectra and the effective gain (normalized transfer function) of the open-loop

baroreflex system. In the following sections, the steps used to derive the absolute gain of the open-loop baroreflex system are described in detail.

Figure 9.1 demonstrates the models used to derive the absolute gain. The top two diagrams in the Figure are the models of the baroreflex system with the loop intact (a) and opened (b1). $G(s)$ represents the baroreflex efferent path, whereas, the $H(s)$ represents the afferent path. $N_1(s)$ is the same in both diagrams, which represents the source of variability or noise input to the CNS. There is a neural summing point in the CNS, which combines $N_1(s)$ with the baroafferents' output, and a reference level in the CNS.

Diagram (b2) illustrates an alternative hypothesis that the noise is an experimental artifact caused by random firing of the damaged, but not destroyed baroreceptors.

The fundamental baroreflex mechanisms implied by Diagram (b2) and (b1) are theoretically different. Diagram (b1) suggests that noise in the baroreflex system is endogenous, and the baroreflex operates continuously to bring the blood pressure into balance, whereas diagram (b2) suggests that the noise is an experimental artifact, and it is likely that the reflex is activated only occasionally, and only in response to specific perturbation, such as postural shifts.

Compelling evidence against the baroreceptor themselves as the noise source is that the lesion of the NTS that destroy both the presynaptic terminals and the second order neurons produce at least as much variability as SAD [45, 48, 73]. Given the anatomically different nature of the lesions, destroying baroreceptors or the second order neurons has similar effects on the blood pressure effects. Thus, the anatomical data suggests that the most enable pre- and post-SAD models are represented by the systems in (a) and (b1)
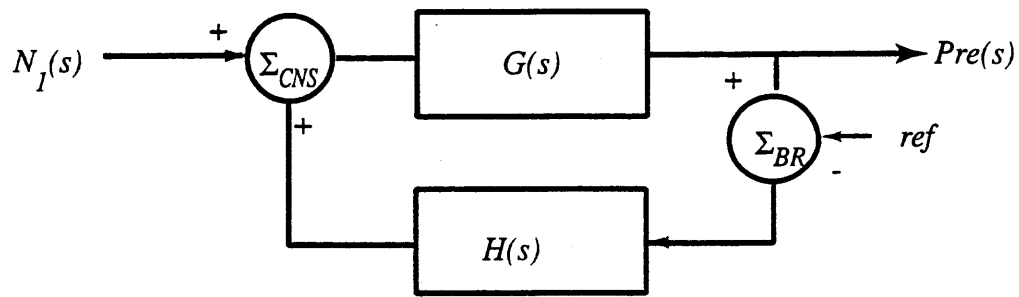
(a)
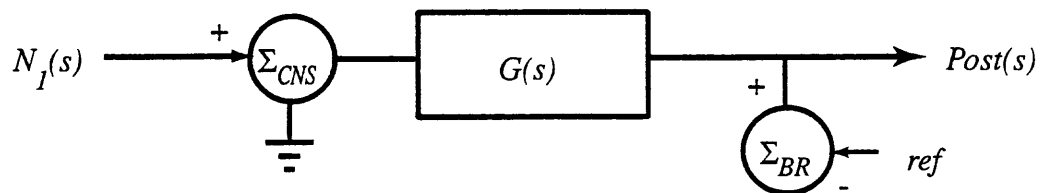
(b1)
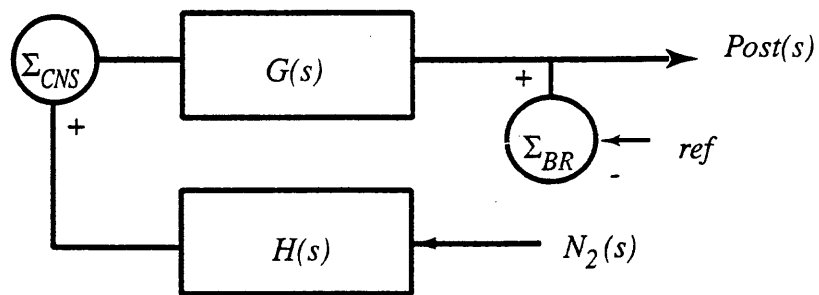
(b2)

Figure 9.1 Models of the baroreflex system; (a) The intact baroreflex system. (b) The SAD baroreflex system. (c) An alternative hypothesis.

Based on the models in diagram (a) and (b1), for (a), the output,

$$\Pr e(s) = \frac{N_1(s)G(s)}{1+GH(s)}$$, and for (b1), the output $Post(s) = N_1(s)G(s)$. Since the

measurements are consecutive, and within the same subject, though the across conditions

phase is random, the magnitudes are fully comparable, Thus:

$$\frac{|Post(s)|}{|\Pr e(s)|} = \frac{|N(s) \cdot G(s)|}{\left| N(s) \cdot \dfrac{G(s)}{1+G(s) \cdot H(s)} \right|}$$

$$= |1 + G(s) \bullet H(s)|$$

(9.2)

Computing the magnitude on the right side and dropping the (s) notation for convenience

gives

$$\frac{|Post(s)|}{|\Pr e(s)|} = \left| 1 + |G| \cdot e^{-j\phi_G} |H| \cdot e^{-j\phi_H} \right|$$

$$= \left| 1 + |GH| \cdot \cos(\phi_{GH}) + |GH| \cdot j \cdot \sin(\phi_{GH}) \right|$$

(9.3)

$$= \sqrt{1 + 2 \cdot |GH| \cdot \cos(\phi_{GH}) + |GH|^2 \cdot \cos^2(\phi_{GH}) + |GH|^2 \cdot \sin^2(\phi_{GH})}$$

$$= \sqrt{1 + 2 \cdot |GH| \cdot \cos(\phi_{GH}) + |GH|^2}$$

Equation (9.3) represents the theoretic relationship between the ratio of the pre-

and post- amplitude spectrum $\dfrac{|Post(s)|}{|\mathrm{Pr}\,e(s)|}$ and the open-loop baroreflex transfer function

$|GH|$. ϕ_{GH} is the system total phase shift caused by the system transportation lag and 1st

order linear system phase lag.

Practically, since the electrical stimulation of the ADN and volumetric stimulation

of the carotid sinus methods only provide us the normalized transfer functions (the

effective gain) of the baroreflex system (for distinctive purpose, we call the effective gain

as GH'), we need to bring a scale factor K to convert the effective gain to the absolute

gain GH. Using scale factor K, and the effective gain GH', we rewrote equation (9.3) as:

$$\frac{|Post(s)|}{|\mathrm{Pr}\,e(s)|} = \sqrt{1 + 2 \cdot |KGH'| \cdot \cos(\phi_{GH}) + |KGH'|^2} + \sqrt{error} \qquad (9.4)$$

where; GH': the normalized open-loop transfer function (the effective gain);

K: the scale factor between GH and GH';

ϕ_{GH}: total phase shift. $\phi_{GH} = 2\pi f(\arctan(2\pi fT)/2\pi f + 1.07)$, where T is the system time

constant, 1.07 is the baroreflex transportation lag (see table 7.8).

$\sqrt{error}$: dummy variable, caused by experimental measurement.

When solved for *error*, as a function of K, (see equation 9.5), and minimized, in the least-

squares sense over all frequencies, yields the value of K that gives the best fit between

the amplitude spectral ratio and open-loop measurements. Multiplying the relative open-

loop gains for each frequency by K gives the absolute gain function of the reflex.

$$error = (\sqrt{1 + 2 \cdot |KGH'| \cdot \cos(\phi_{GH}) + |KGH'|^2} - \frac{|Post(s)|}{|Pr\,e(s)|})^2 \qquad (9.5)$$

The estimated K values in present study were 1.58, 1.83 and 1.71 for rat EH

ADN-A fibers, ADN-A+C fibers and Sinus, respectively, which are comparable to the

reported absolute gain value for the open-loop baroreflex system in rats. [1, 14].

9.3.2 Practical Evaluation of Equation (9.3)

After complete derivation of the relationship between the ratio of the pre- and post-

amplitude spectra, and the open-loop baroreflex transfer function, it is essential to

evaluate the equation (9.3) practically.

Data from rat EH were used for practical evaluation of equation (9.3). The

normalized gain GH', for rat EH, contained three modes; ADN-A, ADN-A+C and Sinus.

The K factors were chosen as the values derived from section 9.3.1, which are 1.58, 1.83,

1.71 for ADN-A, ADN-A+C and Sinus modes, respectively. In the evaluation, shown in

figure 9.2, the left (▲; *lhs*; $|Post(s)|/|Pr\,e(s)|$) and right (●; *rhs*) sides of Equation (9.3)

are plotted as a function of frequency and of on another (●). The graph compare the

directly measured attenuation of blood pressure variability by an intact baroreflex (*lhs*),

with a predicted ratio that is calculated from the open-loop modulation and lag

measurements (*rhs*). Probably because the electrical stimulation was inherently more

accurate and reproducible than mechanical, the total correlation are slightly larger for the

ADN-A fiber than Sinus; however, at ≈ 0.4 Hz, the *lhs* and *rhs* of Equation (9.3) are in

better conformity for the Sinus than the ADN. Since nerve stimulation bypasses natural
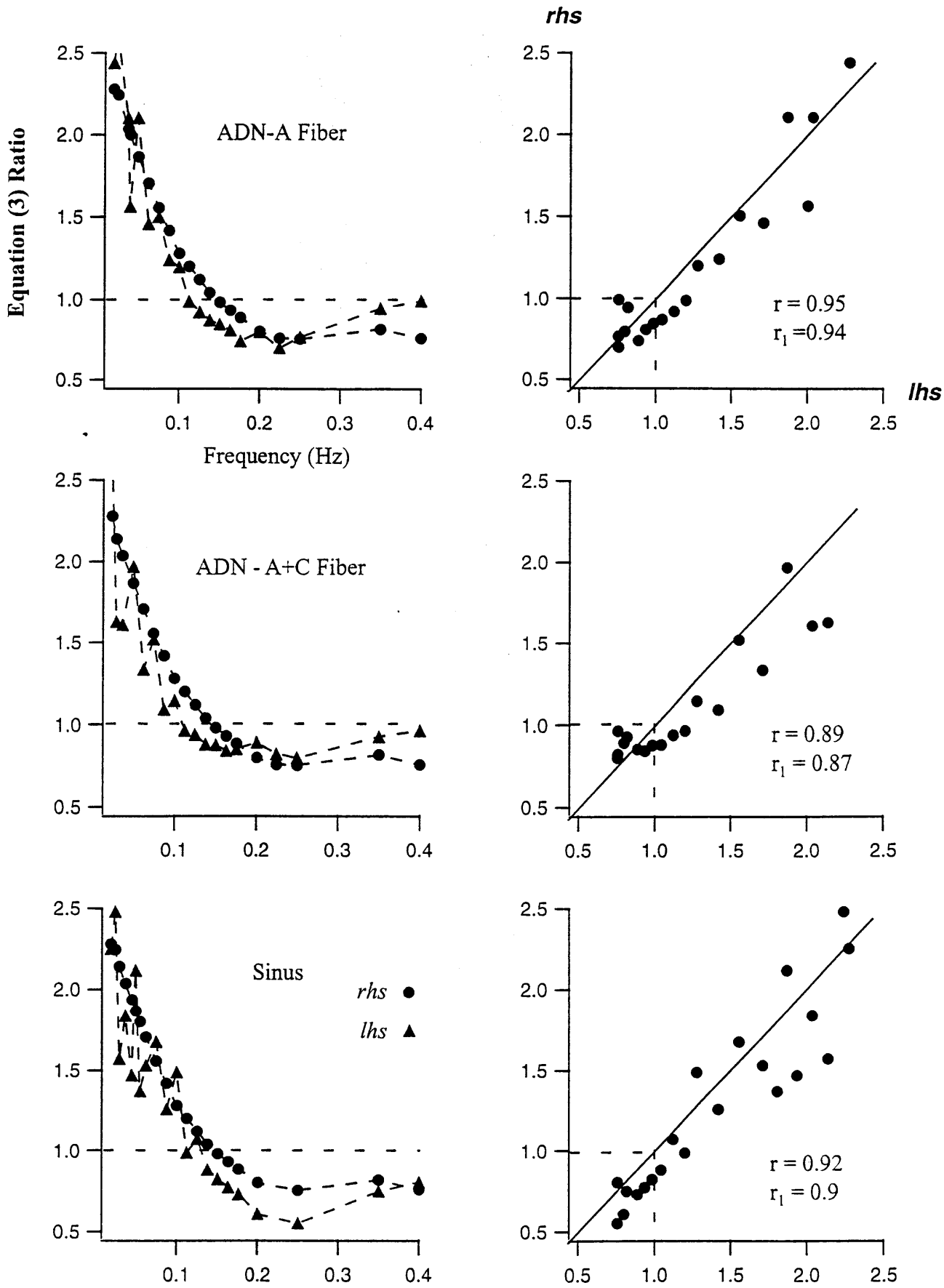
Figure 9.2 The evaluation of the absolute gain equation

stretch endings, while the Sinus stimulus involved the complete natural reflex path, therefore, although the correlation is slightly lower than the ADN-A fiber, overall, the Sinus tracts the direct ratio more consistently than the ADN.

9.4 Approximation of the Effective Gains of the Forward and Backward Loops in the Baroreflex System

Following investigation of the major features of the baroreflex system, which include the steady state, the dynamic features of the complete open-loop baroreflex system, the system absolute gain and transportation lag, we would like to further estimate the effective gain (normalized transfer function) of the forward (G(s)) and backward (H(s)) paths of the baroreflex loop (Figure 9.1 (a)). Figure 9.1, diagram (b1) shows that:

$$|G(s)| = \frac{|Post(s)|}{|N_1(s)|}$$
(9.14)

where $|Post(s)|$ is the amplitude of the post- SAD blood pressure spectrum, and $|N_1(s)|$ is approximated by the amplitude of the sympathetic nerve activity spectrum. The actual sympathetic nerve signal was the peroneal nerve spike counts during the first 75 ms of each cardiac cycle acquired by the HP 3852A system. The normalized $|Post(s)|$, $|N_1(s)|$ amplitude spectra and the effective gain of $|G(s)|$ for EH, EF, EC, EG, DU five rats are shown in figure 9.3. The peroneal nerve spectra are 'flat' for the five rats. The effective gain of $|G(s)|$ behaves as a low pass filter, with cutoff frequency in the VLF region.

With the effective gain of the open-loop baroreflex system $|GH(s)|$ and the effective gain of $|G(s)|$, $|H(s)|$ is then $|GH(s)|/|G(s)|$.

$|H(s)|$ was only derived from rat EH, for three modes. Results are demonstrated in figure 9.4. $|H(s)|$ is relative flat in the very low frequencies, and for the Sinus, which includes the stretch endings, having increasing gain at ≈ 0.4 Hz. The high pass feature of $|H(s)|$ in the Sinus mode may be due to the frequency feature of the baroreceptors.
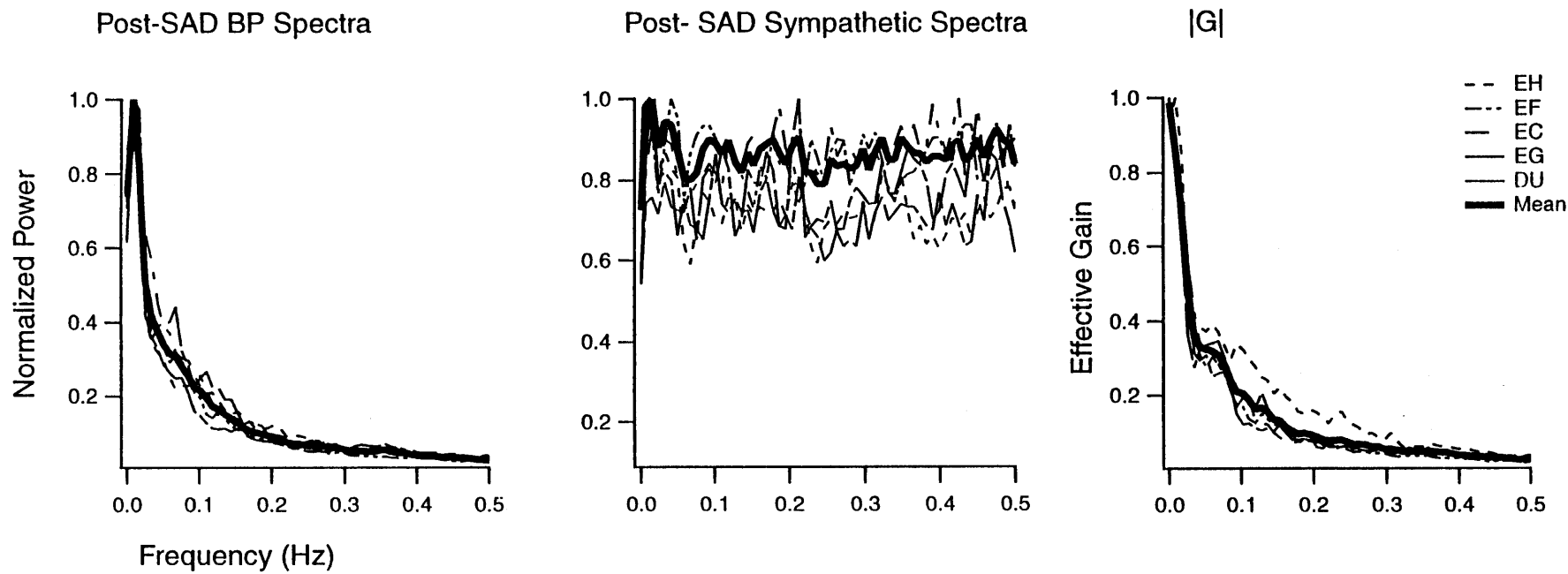
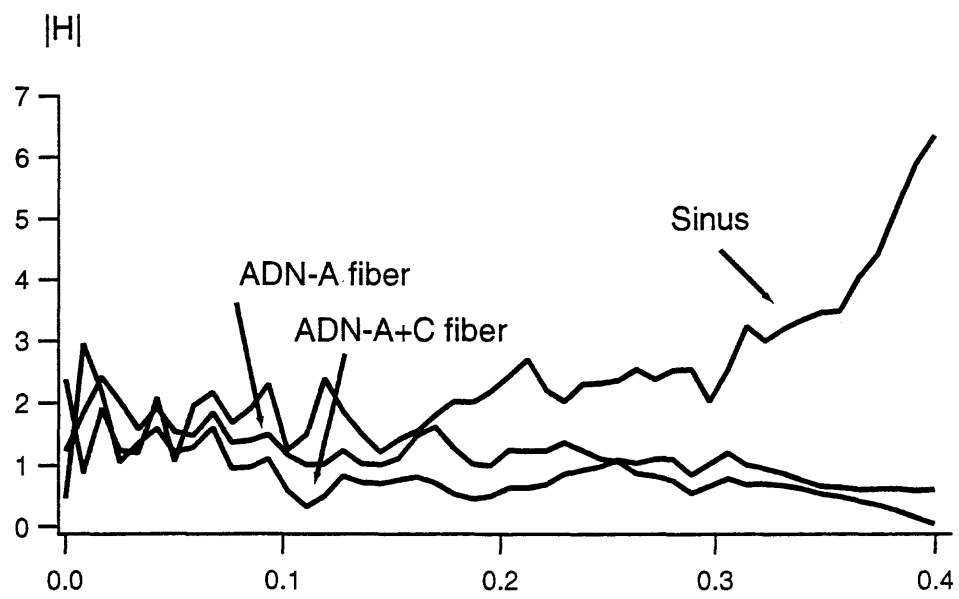**Figure 9.3** Normalized post- SAD BP, sympathetic spectra and the effective gain of G

Figure 9.4 The effective gain of H

CHAPTER 10

CONCLUSIONS

The NMB rats provide unique opportunities for extended, seamless observation and precise manipulation of regulatory mechanisms; and, neuromuscular block categorically excludes mediation of observed autonomic effects by either skeletal-muscular or respiratory responses. We choose the stimulation methods for the studies to optimize the accuracy, consistency and long term stability of the afferent input. Both electrical capacitance stimulation of the ADN, and balloon stimulation of the surgically isolated carotid sinus lent themselves to precision and reproducibility. Based on the above two unique situations, this dissertation work successfully investigated various important features of the baroreflex system, and first time provided solid data to interpret the general mechanisms of the baroreflex system in rats.

The whole work contained three phases. In the first phase of this work, study 1, the effects of the SAD on the blood pressure signals were evaluated. For each rat, the SAD increased the standard deviation of the blood pressure by approximate ± 10 mmHg, from 6.3 ± 3.5 mmHg to 16.3 ± 2.4 mmHg. From an extensive literature search, we argued that the noise in the baroreflex loop is endogenous, this argument is of theoretical important, because, if the noise is endogenous, it implies that the baroreflex normally restrain minute-to-minute variability of the blood pressure, which would suggest that the baroreflex is continuously active and that blood pressure variations are at every instant compensated and brought into balance by the baroreflex. This concept is different from a baroreflex that acts only occasionally in response to specific perturbations, such as thermal stress, postural shifts or hemorrhage.

The blood pressure variability was also investigated using the power spectrum analysis. Results from the power spectrum analysis of the pre- and post- SAD blood pressure variability demonstrated that there was a significant increase of power in the VLF and a significant decrease of power in the LF region after the SAD. The dominant power change after SAD was in the VLF region of the blood pressure spectra.

Phase two contained two sets of studies referred to as the 'study 2' and 'study 3'. In this phase of the work, the steady state and dynamic features of the carotid sinus and the aortic arch baroreflexes were investigated by using hydraulic stimulation of the carotid sinus and electrical stimulation of the ADN. In study 2, step stimulations were applied to the carotid and aortic baroreceptors. For all the sinus data, probably because of combined stimulus and receptor mechanical factors, the stimulus-response curves for each individual cardiovascular component, heart rate, blood pressure, mesenteric vascular conductance and femoral vascular conductance, were in sigmoid shapes; for all the ADN data, the stimulus-responses curves were in quadratic shapes. For all three Sinus and ADN rats (rat EF, EH and DU), the maximum ADN stimulus was substantially more effective than the maximum sinus stimulus in producing blood pressure decreases; the individual component responses, with the exception of ΔIBI, generally reflected the magnitude of the blood pressure effect (see the Mean-Max column of the Table 8.1). For ΔIBI, the ADN-A maximum response (bradycardia) was on average 5 times that of the Sinus, and for rat EF, the ADN-A+C ΔIBI was nearly a factor of 40 times the maximal sinus ΔIBI. The sinus stimulation causes more heart rate effects than the ADN stimulation does. This result is very important for studies that use drugs for analyzing the baroreflex. Because heart rate responses to vasoactive drugs are used extensively to measure baroreflex gain and to confirm denervation, it seems increasing clear, however,

that under some circumstance, stimulation of the carotid sinus can produce a substantial depressor responses with practically no change in heart rate, and correlatively, rats showing almost no heart rate response to a pharmacologically induced blood pressure change, can have completely intact carotid sinus innervation.

In study 2, the blood pressure, heart rate, mesenteric vascular conductance and femoral vascular conductance baroreflex transfer functions were derived from the transient responses of the step stimulations. For all the cardiovascular components, system behaves as a low pass filter, with −3dB cutoff frequency at <0.1 Hz. Heart rate contained the highest cutoff frequency, which implied that the heart rate could respond faster than other cardiovascular components. The cutoff frequency for the blood pressure was lower than that of the heart rate, but higher than those of the mesenteric and femoral vascular conductance. This is because the blood pressure is net effect of the heart rate and vascular responses. The derived low pass feature of the baroreflex system provided a satisfactory explanation for the phenomenon of the substantial power increases in the VLF region in the post-SAD blood pressure spectra. It is fundamental that an element can oppose and neutralize a disturbance only where the transfer function of the element, and the noise spectrum of the disturbance overlap; since the baroreflex is a low pass filter, with cutoff frequency at <0.1 Hz, it is corollary that when the baroreflex is removed, the noise power in the VLF region will change substantially.

The baroreflex transportation lag was derived in study 2 in both sinus and ADN modes. There was no significant difference between the lags derived form the Sinus and ADN modes. The average transportation lag derived from 5 experiment rats, in ADN mode, was 1.07 s.

In the study, the baroreflex system was approximated as a combination of transportation delays and a first-order linear component. With the time constants derived from the transient exponential step responses (Table 8.2) and 1.07 s transportation lag (Table 8.8), study suggested that the baroreflex oscillation frequency region is at $0.2 - 0.6$ Hz, which corresponds to the LF region in the blood pressure spectrum. The decrease of the LF power after SAD is due to the break down of the oscillation path in the feedback system. This dissertation demonstrates for the first time that the primary baroreflex working region is in the VLF, not LF. Before this, much baroreflex research has emphasized the LF component in the blood pressure spectra, now, we say those emphases were not appropriate.

To avoid possible bias in the results, which may be caused simply by using the same data resources or a single analysis method, study 3 varied input and analysis: the stimulations at both carotid sinus and aortic arch baroreceptors were varied sinusoidally in the linear region of the system and the baroreflex blood pressure transfer functions were derived by using the sine fit and power spectral analysis methods. The results from study 3 confirmed that the baroreflex system is a low pass filter, whose cutoff frequency is at <0.1 Hz. The determination of the dynamic features of the baroreflex system has significant practical meanings, for example, since we know that VLF is the major functioning area of the baroreflex system, evaluating blood pressure power at VLF region could help us to evaluate the functionality of the baroreflex.

The last phase of this work provided a new, simple, direct approach to access the absolute gain of the baroreflex system. It is theoretically derived that the relationship between the ratio of the amplitude of the pre- and post- blood pressure spectra and the absolute gain of the baroreflex system follows equation (9.3):

$$\frac{|Post(s)|}{|\Pr e(s)|} = \sqrt{1 + 2 \cdot |KGH'| \cdot \cos(\phi_{GH}) + |KGH'|^2} + \sqrt{error} \qquad (10.1)$$

by minimizing the dummy variable 'error' in equation (10-1), the absolute gain of the baroreflex system can be obtained. This approach has practical significance. The existing methods, reported in the literature, used to evaluate the absolute gain of the baroreflex system involve complicate baroreceptor isolation and stimulation operation procedures, which are very time consuming and difficult. Using the relationship described in equation (10.1), the absolute gain of the baroreflex system can be accessed by simply calculating the ratio of pre- and post- SAD blood pressure amplitude spectra. This approach also overcomes the difficulties associated with surgically isolating and externally stimulating the baroreceptors in very small animals, such as mice. This opens up a new animal model, and one that is potentially feasible for genetic manipulations, for the study of the baroreflex mechanisms.

In conclusion, this thesis demonstrated how control and signal processing engineering techniques can be used to gain new information about real physiological events.

APPENDIX A

PROCEDURES OF THE RAT PREPARATION

A.1 The Beginning of the Experiment

The Experiments started with putting a subject rat into a 20-liter glass jar. 1 ml methoxyflurane, which served as a preanesthetic, was sprayed into the jar from a hole on the lid. After approximately 5 minutes, temperately anesthetized rat was taken out of the jar to be weighted, shaved, and then injected with following five agents: atropine sulfate (0.32 mg/Kg, sc); hydrocortisone sulfate (16 mg/kg, sc); tobramycin sulfate (4.5 mg/Kg, sc); oxacillin sodium (150 mg/Kg, sc); menadial sodium diphosphate (Vitamin K, 0.2 mg/Kg, sc).

A.2 Implantation of EEG Electrodes

The pre-anesthetized rat was put onto a $37^{o}C$ stainless steel surgical table. A 0.7 mm x 1 cm nasal catheter was inserted and temporarily cemented in place. The catheter carried a continuous flow of 97% O_2, and 3% Isoflurane, which maintained a steady level of anesthesia. The rat was then placed into an atraumatic head holder. An incision was made along the middle line of the scalp. Two 0-8 stainless screws are threaded into the scalp at the bregma and lambds. Teflon coded silver wires (28 g) were wrapped around each of the screws. The screws were embedded in dental acrylic for stability and insulation, the scalp incision was closed with a suture, and the head holder was removed. The pair of silver wires was connected to a Xcell-3x4 4-channel microelectrode amplifier (FHC, Inc. Bowdoinham, ME, 04008). The amplified EEG signal was fed into – 28DB/octave digital slot filters, where the signal was separated into δ (0.5-3Hz), θ (6.6-7.5 Hz), α (8.5-18 Hz), and β (20-45 Hz), 4 wave bands. The filter outputs were

rectified, integrated and sent to a voltmeter of both the HP 3852A and Macsym 350 systems to be recorded.

A.3 Corneal Protection

The eyes were covered with a 1 mm layer of Mycostatin ophthalmic ointment, the lids closed, and the rat turned supine with its head resting in a thick sterile cotton pad. The surgical table has an indentation that cradles and supports the head slightly below the surface, so that the spine is in a natural position.

A.4 Tracheal Intubation

A tracheal cannula was made from 316 stainless steel tubes. It was dual lumen coaxial, with separate inspiratory and expiratory pathways. The inspiratory pathway, which was a 19 ga stainless steel tube, was engaged inside the expiratory pathway, a 12 ga stainless steel tube. The inspiratory tube is removable; it is 2 mm beyond the tip of the expiratory lumen. With such design, the cannula did not have functional dead volume, flow is unidirectional for the entire length and tracheal-bronchial secretions are continuously removed with the expiratory gas stream; thus, the cannula is usually self-cleaning. The removability of the inspiratory tube also facilitates the situation when there is a serious obstruction in the respiratory pathway during the experiment. During such situation, the inspiratory tube could be removed and suction could be provided.

Following a midline neck incision and division of the strap muscle, 0.05 ml 1% Xylocaine was injected through an annular ligament of the thyroid cartilage. Guided with a hollow core, "boat" tipped obdurator, the expiratory tube was carefully inserted into the trachea from the mouth and accurately stabilized on a flex bar; the obdurator guide was

withdrawn and replaced with the inspiratory lumen; the nasal catheter was then removed [2].

Initially, the respirator was not engaged and the rat was breathing freely. A continuous "flush" of 2.5% Isoflurane, 47.5% O_2, 47% N_2, and 3% CO_2 was introduced into the expiratory circuit through the inspiratory lumen at a rate of 200 cc/min; the expiratory lumen of the cannula was temporarily connected to one end of 100 cm length of silicone tubing; with the other end left open, the tube formed a reservoir of fresh inspiratory gas that rat could breathe freely.

10-20 min after a 100 μg of α-cobraotoxin (α-CTX) neuromuscular block (NMB) (in 2 ml of saline) was injected through the femoral vein, (when MAP begins to fall and the expired CO2 slightly increased, signaling imparted respiration), the respirator was engaged and the rat was ventilated at 72 beats/min, with 1:2 inspiratory and expiratory ratio, 6 mmHg end expiratory pressure (PEEP), 180-220 ml total minute volume, and periodic (1/600s) hyperinflation (18 mmHg).

A.5 Femoral Arterial and Venous Intubation

The left femoral artery and vein were first dissected free from the surrounding tissues. A 28 ga x 40 mm Teflon tubing with a 45° bevel tip was inserted slowly into the artery for about 2.4 cm, and a renathane tube (Braintree Scientific, Braintree, MA) (0.04 x 0.025, 10 cm long attached to 0.50 x 0.04, 15 cm long renathane tube), with a small bevel, was inserted into femoral vein for about 6cm. Both cannula tubes were secured to the edges of the incision skin, and were attached to continuous infusion pumps and pressure transducers (Baxter PX600, Baxter, Irvine, CA), which were calibrated and connected to the data acquisition systems.

Following infusions were maintained through the entire experimental period: into the femoral artery (.37cc per hour): 50cc H_2O; 50cc .5 N lactated Ringers; 500 IU heparin Na; 1.25g oxacillin NA; 2.8 mg α-cobratoxin (Biotoxins, Miami Fl); .3 mg vitamin K (Synkayvite); 20 mEq K+ (as KCl). Into the femoral vein (.45cc per hour): 50cc H_2O; 50cc . 5N lactated ringers; 300 IU heparin Na; 1.25g oxacillin Na; .5g ticarcillin disodium. The α-cobratoxin concentration in the arterial infusion was equivalent to 125ug/day; this is sufficient to maintain complete paralysis.

A.6 Urinary Bladder Intubation

A bladder cannula was made of a 110 cm long, 0.025x0.047 medical grade silicone tubing with a beveled tip and a collar at 3 cm. (After 48 hours this cannula was replaced by cannulas constructed of .030 x .065 silicone tubing which were changed every 3-5 days). The cannula was autoclaved before the experiment. Before intubation, a small drop of Xylocaine jelly was applied to the tip end of the bladder for initial dilatation. About 5-10 minutes later, the internal flap and the rostral edge of the papilla was located and lifted up gently with a 3-0 tissue forceps, and a 5-0 suture was threaded through the lifted tissues using a fine atraumatic needle. The suture was used to maintain retraction of the flap and to better control the sphincter [2], and the cannula was inserted into the urethra, to the collar. To ensure the bladder cannula was in the right position and not blocked, a gentle pressure was applied on the bladder from the outside to make urine flow through the tube smoothly. Finally, bladder cannula was stabilized to the bladder tip using a drop of super glue (Loctite Corporation, Hartford, CT). The cannula was drained directly into an auto-zeroing strain gauge scale connected to the data acquisition system for urine output measurement.

A.7 Abdominal Surgery

Abdominal surgery was conducted in a high sterile situation and relative high isoflurane level. High anesthesia level was used to minimize bleeding during the abdominal surgery. The shaved abdomen was prepared with Betadine, 70% ethanol, and covered with a sterile surgical incision drape (3M Health Care, St. Paul, MN). Beginning from the xiphoid, a 4-cm incision was made on the abdomen. The cecum was first located and removed. The cecum was isolated from the remaining digestive pathway by placing two sutures at its junction with the ileum, and cut with scissors. Neomycin opthalmic high toxic antibiotic ointment was applied to the incision place.

A gastro duodenal feeding tube was then inserted from the stomach. A 4 mm diameter purse-string of 5-0 silk was placed on the greater curvature ≈ 5 mm oral to the pylorus; then, using a thermal cautery, a 2 mm slit was incised at the center of the purse-string. From the incision site, a 0.030x0.065 medical grade silicon tubing, with a 1 cm dia. fixation collar at 8 cm from the tip, was carefully inserted into the jejunum until the 1-cm dia. collar was into the opening of the stomach. The purse-string was pulled closed, the omentum was wrapped around the closed opening, antibiotic ointment was applied to the incision site and the stomach was flushed with saline. *Nutrition*: Beginning on day 2 and for the duration of the experiment adequate nutrition was maintained with the following intraduodenal infusion at a rate of .58 ml/hr: 100 ml H_2O; 32 g high nitrogen Vivonex (Vivonex TEN, Novarits, Minneapolis, MN); 0.1g Na benzoate; 2g acetyl sulfisoxazole; 4 ml Kaopectate; 5 mEq K+; 25 mg Spironolactone; 1.2 mg Fer-in-sol iron supplement; 100,000 U Nystatin.

A flow probe was attached to the superior mesenteric artery. The superior mesenteric artery was identified on the ventral aorta, between the renal veins,

perpendicular to the dorsal plane. Surrounding tissues were carefully dissected, and a J-shape transonic ultrasonic flow probe (Transonic System Inc., Ithaca NY 14850) was attached to the artery. For rat EH, the abdominal probe was placed directly on the aorta below the superior mesenteric artery to obtain a measure of inferior mesenteric, caudal and lower abdominal skeletal muscle flow.

Finally, a 1 cm x 0.3 mm silicone clothed thermistor probe was fixed in the internal surface of the abdomen to continuously monitor and control intra-abdominal (core) temperature. To prevent adhesions, 5 ml of $37^{o}C$ saline with antibiotics (tobramycin sulfate, 4.5 mg/kg & oxacillin sodium, 150mg/kg) was poured into the abdomen; then the incision was closed in two layers.

A.8 Peroneal Nerve Preparation and Femoral Arterial Flow Probe Attachment

The right femoral artery and peroneal nerve were carefully dissected free from the surrounding tissues. A pre-tested J-shape pulse transit time flow probe (Transonic System Inc., Ithaca, NY) was attached to the artery, the gap between the probe and the vessel was filled with ultrasonic coupling gel.

A pair of Teflon coded twisted silver wires (Ag7/40T, Medwire, Mt. Vernon NY) nerve electrodes, with a spacing of 2 mm, were placed on the nerve. The two-part embedding compounds, Kwik-Cast ^{TM} part A-Catalyst and Kwik-Cast ^{TM} part B-base (World Precision Instruments, Fl), were thoroughly mixed and injected through a 25 ga cannula tip into the field to stabilize the electrode.

A.9 Aortic Depressor Nerve Preparation

ADN preparations contains three main steps: ADN isolation, ADN verification and embedding.

A.9.1 Isolation of the Aortic Depressor Nerve (ADN)

The ADN was located by reference to the superior laryngeal nerve (SLN). The ADN joins the SLN $\approx$ 5 mm from the thyroid cartilage. It enters the main trunk of the SLN through a small "delta" of nerve and connective tissue. Starting with the SLN nerve, carefully dissecting toward the carotid bifurcation, crossing the carotid bifurcation, where SLN adheres to the medio-dorsal surface, and continues dorsal laterally to a confluence with the vagus, the ADN would very likely be found. The ADN enters the SLN $\approx$2 mm central to the bifurcation at a small "delta", which is sometimes obscured by a small pad of yellow fat; the ADN sometimes divided into two or more smaller nerves before entering the SLN.

A.9.2 Electrophysiology Verification of the ADN

For the verification, the ADN was mounted onto a homemade Ta-Ta$_2$O$_5$ field effect electrode (FEE), and stimulated by a current of 30-70 μA, 300 μs pulses at 2-50 Hz under $\cong$ 1.5% light anesthesia. The ADN is verified by producing a gradual (1-5s to develop; 30-90s to asymptote) monotonic frequency and current dependent depressor response, which includes hypotension, bradycardia, and vasodilatation and does not convert to a pressor pattern with very strong (>500 μA) stimulation. The magnitude of the blood pressure decrease is minimally affected by atropine sulfate (.32 mg/kg iv) blockade of the bradycardia.

The fabrication and electrical properties of FEE electrodes are described in reference [7]. Simply, the Ta-Ta$_2$O$_5$ electrode is a non-contactive, capacitative field effect electrode, made from a 0.5 mm diameter anodized slug of sintered tantalum (Ta-Ta$_2$O$_5$), shown in figure A.1. The capacitance of the electrode measured with a conventional capacitance meter in a saline solution using a stainless steel cathode is about 140 nF, with a break down voltage at around 40 V. The peak charge transfer of these electrodes depends upon the net impedance of the *in vivo* stimulation path; for a typical rat aortic nerve, which has a DC impedance of 2-10KΩ, the electrodes sustained square pulses (>1 mA; >5ms) far in excess of what was needed for maximal stimulation.

A.9.3 Embedding

After testing, 3 stabilizing microhooks, functioning as anchors, were placed in the muscle surrounding the electrode site. Shown in figure A.2, the microhooks were constructed by bending 125 μm unannealed 304V spring stainless steel wire (K_SWGX_050) into the shape of a "W" with a 10 mm center peak and 2 mm side wings. The center peak was squeezed into the end of a 22 ga disposable hypodermic needle. When the needle was inserted 4-5 mm into the surrounding muscle, the wings were caught and the needle could be withdrawn, leaving a firmly anchored expanded hook, protruding ≈5 mm above the muscle surface. The two-part embedding compound, Kwik-Cast ^{TM} part A-Catalyst and Kwik-Cast^{TM} part B-base (World Precision Instruments, Fl) were thoroughly mixed in a 1 ml plastic syringe, and injected through a 25 ga cannula tip into the field under the electrode; as the compound rises, it engulfs the electrode and nerve from below, and forms a seal.
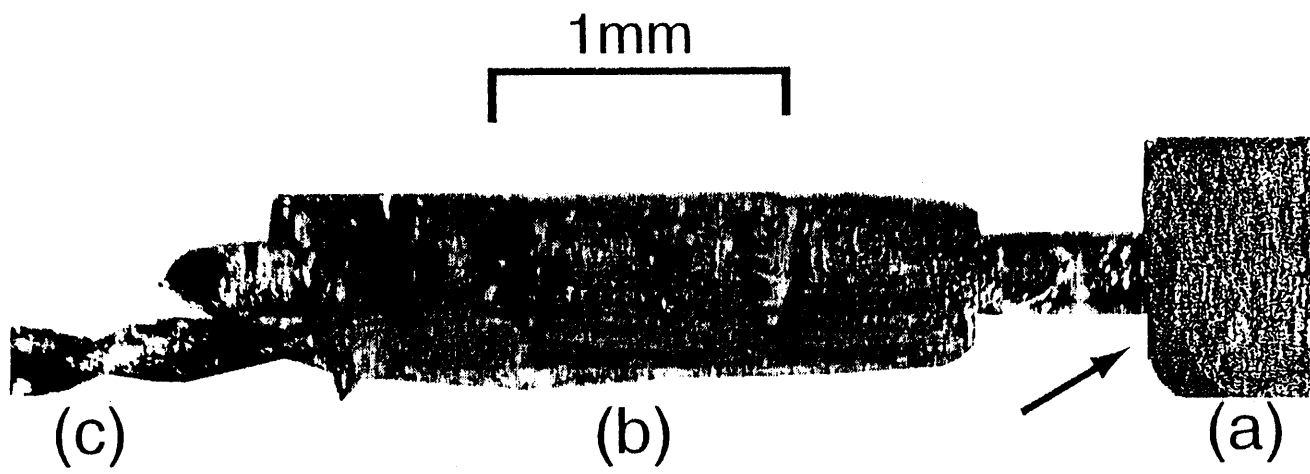
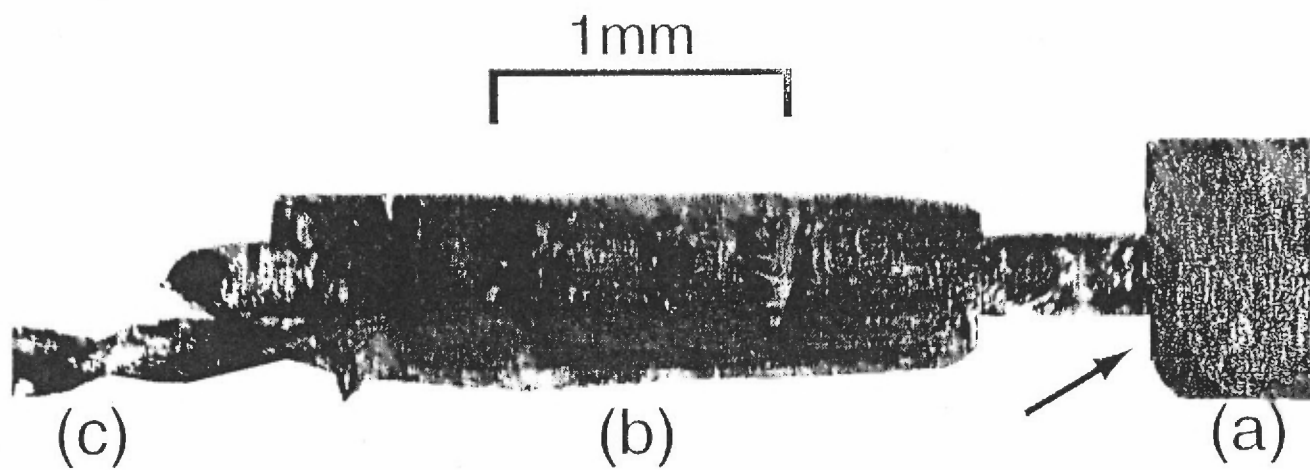**Figure A.1** The Ta-Ta$_2$O$_5$ FEE electrode

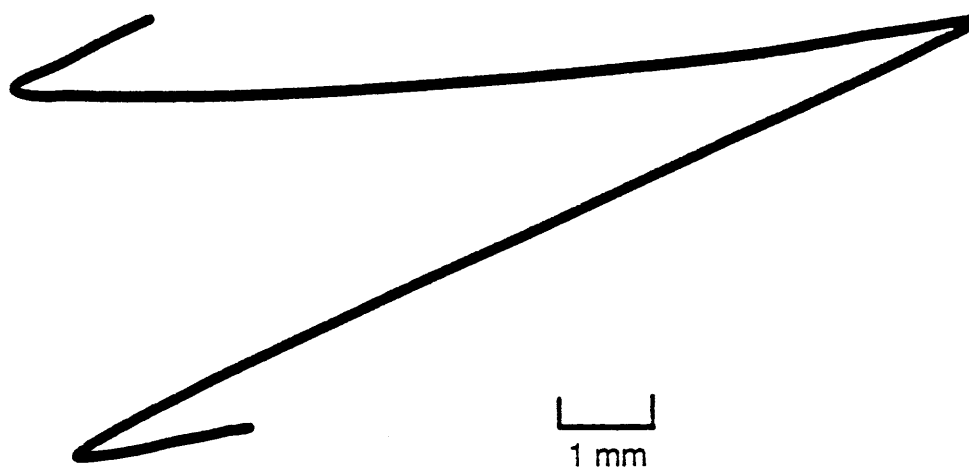**Figure A.1** The Ta-Ta$_2$O$_5$ FEE electrode

Figure A.2 The Micro-hook

A.9.4 ADN Stimulation Circuit

The FEE was driven by a CCIU-8 optically isolated stimulator (Frederic Haer & Co., Bowdoinham, ME). The FEE was connected to the positive output terminal, while a stainless steel indifferent electrode, which was embedded in adjacent tissue, was connected to the negative terminal of the CCIU-8. The CCIU-8 stimulator had an actively switched inter-pulse output shunt, which dissipated the accumulated charges on the electrode between stimulation pulses. The CCIU-8 optical stimulus isolator was connected to a Master-8 eight-channel programmable pulse generator (A. M. P. I Jerusalem, Israel).

A.10 The Carotid Sinus Preparation

The "open-loop" sinus baroreflex stimulation method developed in this study was based on McKeown and Shoukas' plug isolation approach [1, 15]. In order to be able to produce long-term stimulation of the carotid sinus, we substituted a volumetric intra-sinus balloon for a barometric open sinus in Shoukas' technology. A syringe-driven water-filled balloon was used for precise and stable long-term stimulation of the carotid sinus. Details of the surgery procedure and balloon characteristics are introduced below.

A.10.1 Balloon Characteristics

Stimulation of the carotid sinus baroreflex was achieved by uniform distention of the sinus region by a 1 mm x 3. 5 mm cylindrical balloon inserted into the sinus region. The sinus balloon was designed and fabricated from silicone and stainless steel to have the following characteristics: (a) water impermeable; (b) small internal volume, capable of being purged of all air; (c) sufficiently durable to withstand > 1000 inflations without

change in properties or geometry; and, (d) able to be inflated and deflated rapidly. Figure A.3 gives the construction details.

A.10.2 Isolation of the Sinus and Insertion of the Balloon

In the neck, under a surgery video-microscope (WZISS, Germany), the internal, external, common carotid arteries were identified and carefully dissected from the surrounding tissues. At the root of the bifurcation, a 7-0 nylon monofilament suture was threaded through the bifurcation and ligated the external carotid artery near its origin. The common carotid artery was stripped back to the septum, the vagus was carefully isolated with a 7-0 silk suture, ADN was identified and cut, and two 5-0 sutures were placed close to the septum, avoiding damage to the vagus and sympathetic nerves; then, a third suture was tied 2 mm rostral, and a fourth suture passed under the artery further rostral and tied loosely, following which several drops of nitroprusside were applied to the artery. A preliminary cannula of silicone tubing with a polished 45°C beveled stainless steel tip was approximated to the artery, and a micro-vascular clip (003977-01Am Fine Science, Foster City, CA) was placed on the artery at the bifurcation. The cannula was attached via a one-way valve to a glass 5 ml syringe, which was filled with saline, and two .025" (.635mm) 316-stainless steel balls (Salem Specialty Ball, Canton, CT) were held captive in the silicone tube by a small vascular clip placed over the ball, nearest the tip. With slight injection, saline flowed through the valve; around the balls, without dislodging them; completely filling the cannula (any air in the tube could embolize the brain). With the apparatus in place, a small cut was made rostral to, and the artery bisected caudal to, the third suture. The artery was drawn onto the cannula tip and secured with
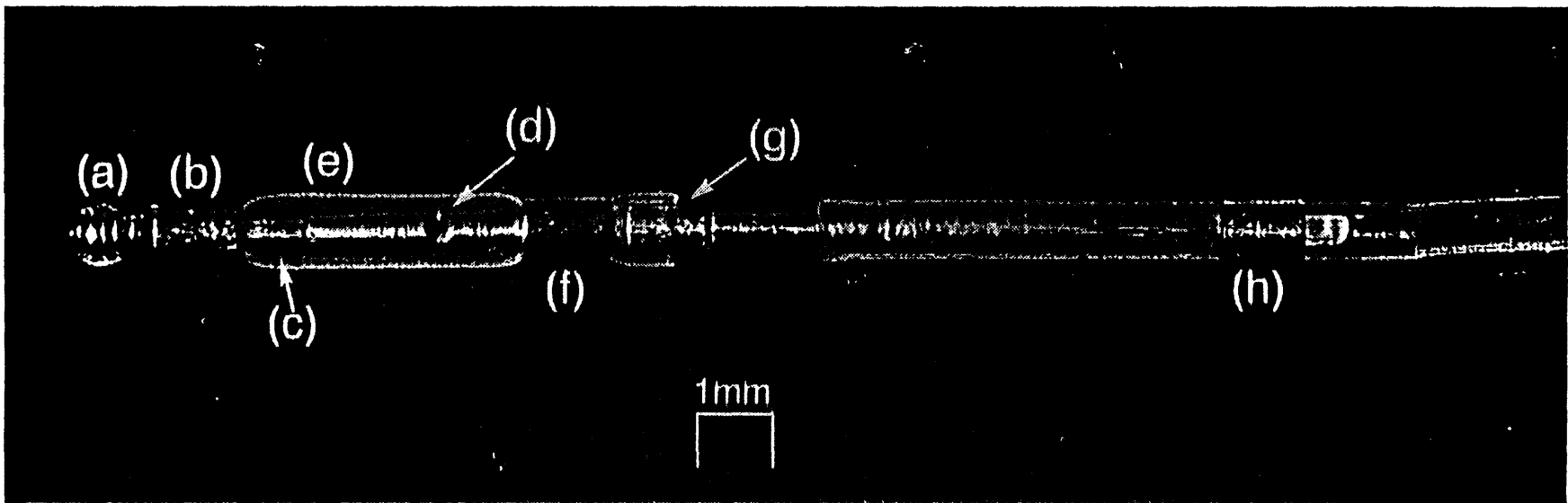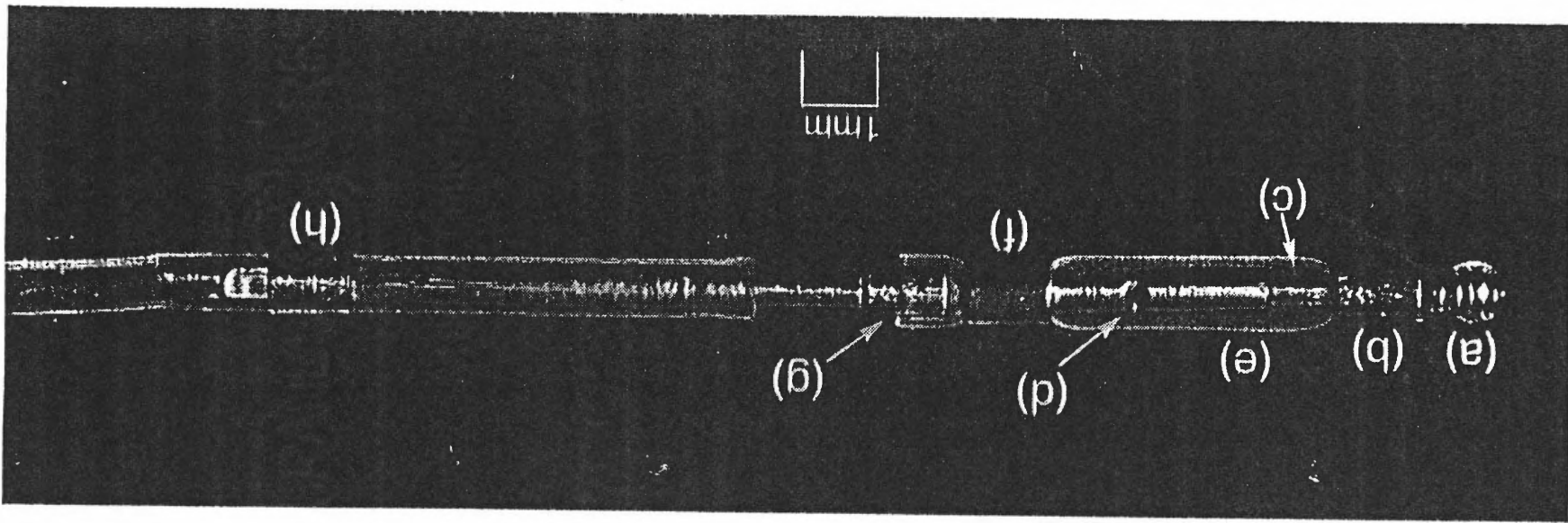
Figure A.3 The carotid sinus balloon construction.

the fourth suture; the micro-vascular clip was released, and the artery was cleared of blood with 2 ml flush of saline; the clip was removed from the ball, and a second low flush ejected both balls from the cannula. The balls fit through the pterygopalatine and cervical portion of the internal carotid, but are too large for the posterior lacerated foramen or carotid canal; thus, the syringe motions stops abruptly, and the artery dilates, as the balls lodge snugly in each of the carotid branches, and complete the isolation of the sinus. The cannula tip was removed, additional nitroprusside applied, and the balloon was introduced and gradually advanced to where the front of the back ferrule was adjacent to the external carotid ligature. A 4-0 suture was passed under the artery and secured behind the ferrule; the 7-0 external carotid suture was then tied, crosswise, into the 4-0 knot, accurately fixing the balloon position relative to the bifurcation. Typically, the sinus response is depressed for 12-24 hr following the surgery, and reaches asymptotic sensitivity and stability within 3 days.

A.10.3 Carotid Sinus Baroreflex Stimulation Setup

Via a 28ga Teflon catheter, the balloon shaft was connected to a Hamilton ultra low volume motorized 3-way valve (Hamilton Company, Reno, Nevada). The second end of the valve was connected to a 10 ul Hamilton gas-tight syringe (Hamilton Company, Reno, Nevada). The third end of the valve was connected to a thin glass tube, which was open to the air. The syringe was tightly mounted on the platform of a modified HP 7035A servo X-Y plotter, and the plunger of the syringe was connected the X-axis drive of the plotter. Before each stimulation, the 3-way valve was closed to the atmosphere end, the balloon and syringe became a sealed system, and the linear motion of the plotter was hydraulically transmitted to the balloon. At the completion of each stimulation, a 3-

way valve was opened to the atmosphere; this procedure avoided the transient negative pressures in the system and re-zeroed the internal volume of the relaxed balloon. The plotter slewing rate was > 37 cm/sec.

Both 3-way valve and plotter were controlled by a Master-8 eight-channel programmable pulse generator. One channel of Master-8 controlled the 3-valve's closing and opening, another channel of the Master-8 controlled the movement to the X-axis of the plotter. Complete sets of stimulation patterns were encoded into the Master-8 in advance.

A.11 Vagus Recording

After completion of the sinus procedure, microhooks, figure 3.2, were placed in the neck muscle on either side of the vagus, approximately 3 mm rostral to the spectrum. A pair of Teflon coded twisted silver wire (Ag7/40T, Medwire, Mt. Vernon NY) electrodes were attached to the vagus nerve. The two-part embedding compounds, Kwik-Cast ^{TM} part A-Catalyst and Kwik-Cast^{TM} part B-base (World Precision Instruments, Fl), were thoroughly mixed in a 1 ml plastic syringe. The mixed embedding compounds were injected through a 25 ga cannula tip into the field under the electrode, and anchored on the microhooks.

A.12 EKG Electrodes

EKG electrodes were constructed by 30 cm long, multi-stranded silver wires (Ag7/40T, Medwire, Mt. Vernon NY) stripped at both ends. The silver wires were threaded through 22-gauge hypodermic needles and attached to the tip of the needle by bending the wire end into a hook shape. EKG electrodes were sutured into the chest,

subcutaneously, at the xyphoid, and ≈1 cm lateral (left and right) to the midline at the level of the fifth rib. A reference electrode was placed 1 cm left or right of the midline and 1 cm above the pubis. The exposed wire and skin were insulated with collodion. The electrodes were connected to a G=1000 preamplifier; the output was split, one branch was applied directly to the high resolution data acquisition system, and another branch was rectified, low-pass filtered, and peak detected (74-60-1A1 FHC Bowdoinham, ME) to form a reliable R-wave trigger.

A.13 Skin Blood Flow

Using an adhesive electrode patch, a Laser Doppler probe (ABLF21, Transonic Systems, Ithaca, NY) was affixed to the flexor surface of the right hindpaw, directly over the three center metatarsals.

APPENDIX B

FILTER CHARACTERISTICS OF THE 30 SECOND MEAN DIFFERENCE

The spectrum of the 30 second mean difference was derived based on the derivative theorem of the *Fourier transform*. According to the theorem, if the *Fourier transform* of a time function $f(t)$ is $F(f)$, then the *Fourier transform* of its first derivative $f'(t)$ equals $j2\pi f F(f)$ [74].

Figure B.1 (a) shows the shape of the equivalent function of the 30 seconds mean difference ($\tau/2=30$, $\tau = 60$) $f(t)$; in the time domain, taking the 30 second mean difference is equivalent to convolution of the original data with this function. (b) is the first derivative of the time function $f(t)$.

$$f(t) = \begin{cases} E & (t < \tau/2) \\ -E & (t < \tau) \end{cases} \qquad (B.1)$$

$$\frac{df(t)}{dt} = E\left[\delta(t) - 2\delta(t - \tau/2) + \delta(t - \tau)\right] \qquad (B.2)$$

Take the *Fourier transform* on both sides of equation (B.2):

$$(j2\pi f)F(f) = E[1 - 2e^{-j\frac{\tau}{2}2\pi f} + e^{-j\tau 2\pi f}]$$

$$(j2\pi f)F(f) = -2Ee^{-j\frac{2\pi f\tau}{2}}\sin^2(\frac{2\pi f\tau}{4}) \qquad (B.3)$$

$$F(f) = \frac{-2Ee^{-j\frac{2\pi f\tau}{2}}}{j2\pi f}\sin^2(\frac{2\pi f\tau}{4})$$

Substitute τ=60, and E=1/30 into equation (B.3), we have:

$$F(f) = -\frac{1}{30j\pi f}e^{-j60\pi f}\sin^2(30\pi f)$$

$$|F(f)| = \frac{1}{30\pi f}\sin^2(30\pi f) \tag{B.4}$$

Figure B.1 (c) demonstrates the equivalent frequency domain filter shape of the 30 second blood pressure mean differences, the major pass band of the filter is at the very low frequency region (0-0.03Hz).
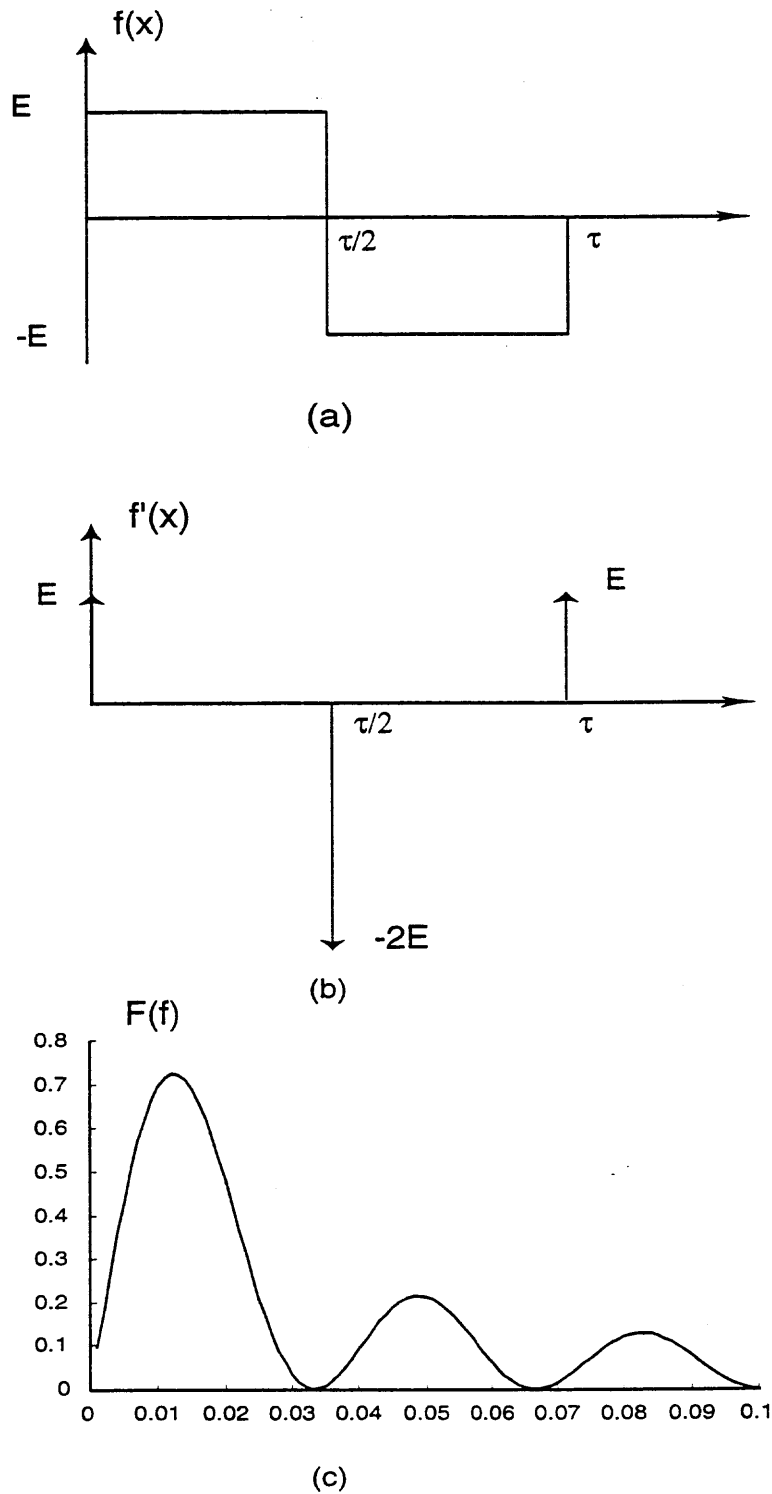
Figure B.1 (a) The shape of convolution signal;
(b) The derivative of the signal; (c) The spectrum of the signal

REFERENCES

1. Sato, T., T. Kawada, H. Miyano, T. Shishido, M. Inagaki, R. Yoshimura, T. Tatewaki, M. Sugimachi, J. JR. Alexander, and K. Sunagawa. 1999. "New Simple Methods for Isolating Baroreceptor Regions of Carotid Sinus and Aortic Depressor Nerves in Rats." *American Journal of Physiology*, 276: H326-H332.

2. Dworkin, B.R, and S. Dworkin. 1990. "Learning of Physiological Responses: I. Habituation, Sensitization, and Classical Conditioning." *Behavioral Neuroscience*, 104: 298-319.

3. Scher, A.M., and A. Young. 1963 "Servoanalysis of Carotid Sinus Reflex Effects on Peripheral Resistance." *Circulation Research*, XII(February): 152-162.

4. Levison, W.H., G.O. Barnett, and W.D. Jackson. 1966 "Non-linear Analysis of the Baroreceptor Reflex System." *Circulation Research*, 18: 673-682.

5. Kubo, T., *et al.*, 1996. "Transfer Function Analysis of Central Arc of Aortic Baroreceptor Reflex in Rabbits." *American Journal of Physiology*, 270: H1054-H1062.

6. Bertram, D., *et al.*, 1998. "The Arterial Baroreceptor Reflex of the Rat Exhibits Positive Feedback Properties at the Frequency of Mayer Waves." *Journal of Physiology*, 513(Pt 1): 251-61.

7. Dworkin, B.R. and S. Dworkin. 1995. "Learning of Physiological Responses: II. Classical Conditioning of the Baroreflex." *Behavioral Neuroscience*, 109: 1119-1136.

8. Angell-James, J.E., 1971. "The Effects of Changes of Extramural, "Introthoracic" Pressure on Aortic Arch Baroreceptors." *Journal of Physiology*, 214: 89-103.

9. Vander, A.J., J.H. Sherman, and D.S. Luciano. 1994. "Human Physiology: The Mechanisms of Body Function." Sixth Edition, New York: McGraw Hill Publishing Company: 167-222, 410-500.

10. Sagawa, K. 1983. "Baroreflex Control of Systemic Arterial Pressure and Vascular Bed." *Handbook of physiology: The cardiovascular system.* American Physiological Society: Bethesda Md. 453-96.

11. Bronk, D.W. and G. Stella. 1932. "Afferent impulses in the carotid sinus nerve. I. The relation of the discharge from single end organs to arterial blood pressure." *Journal of Cell and Comparative Physiology*, 1: 113-130.

12. Allison, J.L., K. Sagawa, and M. Kumada. 1969. "An Open-Loop Analysis of the Aortic Arch Barostatic Reflex." *American Journal of Physiology*, 217: 576-1584.

13. Nosaka, S. and S.C. Wang. 1972, "Carotid Sinus Baroreceptor Functions in the Spontaneously Hypertensive Rat." *American Journal of Physiology,* 222(5): 1079-1084.

14. Shoukas, A.A., *et al.,* 1991. "New Technique to Completely Isolate Carotid Sinus Baroreceptor Regions in Rats.*" American Journal of Physiology.* 260: H300-H303.

15. McKeown, K.P. and A.A. Shoukas. 1998. "Chronic Isolation of Carotid Sinus Baroreceptor Region in Conscious Normotensive and Hypertensive Rats." *American Journal of Physiology,* 275: H322-H329.

16. Neil, E., C.R.M. Redwood, and A. Schweitzer. 1949. "Blood Pressure Response to Electrical Stimulation of the Carotid Sinus Nerve in Dogs and Rabbits." *Journal of Physiology,* 109: 392-401.

17. Douglas, W.W., J.M. Ritchie, and W. Schaumann. 1956. "A Study of the Effect of the Pattern of Electrical Stimulation of the Aortic Nerve on the Reflex Depressor Responses." *Journal of Physiology, London,* 133: 232-242.

18. Jonzon, A., *et al.,* 1973. "Studies of Blood Pressure Regulation in the Unanesthetized Dog. I. The Effects of Constant-Frequency Stimulation of the Carotid Sinus Nerves." *Pfluegers Arch.,* 340: 211-228.

19. Kendrick, J.E., *et al.,* 1973. "The Effect of Stimulus Pattern on the Pressure Response to Electrical Stimulation of the Carotid Sinus Nerve of Cats." *Proceedings of the Society for Experimental Biology and Medicine,* 144: 412-416.

20. Sinnet, H.O., D.F. Peterson, and V.S. Bishop. 1976. "Cardiovascular Responses to Electrocardiogram-Coupled Stimulation of Rabbit Aortic Nerve." *American Journal of Physiology,* 230: 1374-1378.

21. Donald, S.A. and A.J. Edis. 1971 "Comparison of Aortic and Carotid Baroreflexes in the Dog." *Journal of Physiology, London,* 215: 521-538.

22. Kent, B.B., J.W. Drane, and J.W. Manning. 1971 "Suprapontine Contributions to the Carotid Sinus Reflex in the Cat." *Circulation Research,* 29: 534-541.

23. Sagawa, K. and K. Watanabe. 1965. "Summation of Bilateral Carotid Sinus Signals in the Barostatic Reflex." *American Journal of Physiology,* 209: 1278-1286.

24. Scher, A.M. and A.C. Young. 1969 "Nonlinearity in the Control of Blood Pressure and Heart rate." *Annals New York Academic Science,* 156: 722-730.

25. Stegemann, J. and U. Tibes. 1969. "Sinusoidal Stimulation of Carotid Sinus Baroreceptors and Peripheral Blood Pressure in Dogs." *Annals New York Academic Science*, 156: 787-795.

26. Sato, T. and T. Kawada. 1998. "Dynamic Transduction Properties of in situ Baroreceptors of Rabbit Aortic Depressor Nerve." *American Journal of Physiology*, 274: H358-H365.

27. DiBona, G.F. and L.L. Sawin. 1994. "Reflex Regulation of Renal Nerve Activity in Cardiac Failure." *American Journal of Physiology*, 266: R27-R39.

28. Hainsworth, R., J.R. Ledsome, and F. Carswell. 1970. "Reflex Responses from Aortic Baroreceptors." *American Journal of Physiology*, 218: 423-429.

29. Levy, M.N., M.L. Ng, and H. Zieske. 1966. "Cardiac and Respiratory Effects of Aortic Arch Baroreceptor Stimulation." *Circulation Research*, 19: 930-939.

30. Gero, J. and M. Gerova. 1967. "Significance of the Individual Parameters of Pulsating Pressure in Stimulation on Baroreceptors." *Proceeding of International Symposium on Baroreceptors Hypertension*: 17-30.

31. Angell, J.J. and M.D. Daly. 1970. "Comparison of Reflex Vasomotor Responses to Separate and Combined Stimulation of Carotid Sinus and Aortic Arch Baroreceptors by Pulsatile and Non-pulsatile Pressure in the Dog." *Journal of Physiology, London*, 209: 257-293.

32. Ead, H.W., J.N. Green, and Neil. E. 1952. "A Comparison of the Effects of Pulsatile and Non-Pulsatile Blood Flow through the Carotid Sinus on the Reflexogenic Activity of the Sinus Baroreceptors in the Cat." *Journal of Physiology, London*, 118: 509-519.

33. Gero, J. and M. Gerova. 1962. "Dynamics of Carotid Sinus Elasticity During Pressor Reactions." *Circulation Research*, 11: 1010-1020.

34. Ninomya, I., N. Nisimaru, and H. Irisawa. 1971. "Sympathetic Nerve Activity to the Spleen, Kidney and Heart in Response to Baroreceptor Input." *American Journal of Physiology*, 221: 1346-1351.

35. Brooks, A.E. and A.A. Shoukas. 1999. "Baroreceptor Contribution to the Cardiovascular Reflex Responses: Phenylephrine (Ph) and Sodium Nitroprusside (SNP) Effects in the Conscious Rats." *FAFEB*, 13: 1373.

36. Alper, R.H., H.J. Jacob, and M.J. Brody. 1987. "Central and Peripheral Mechanisms of Neurogenic Hypertension and Arterial Pressure Lability." *Canadian Journal of Physiology and Pharmacology*, 65: 1615-1618.

37. Alper, R.H., H.J. Jacob, and M.J. Brody. 1987. "Regulation of Arterial Pressure Lability in Rats with Chronic Sinoaortic Deafferentation." *American Journal of Physiology*, 253: H466-H474.

38. Buchholtz, R.A., J.W. Hubbard, and M.A. Nathan. 1986. "Comparison of 1-hour and 24-hour Blood Pressure Recordings in Central or Peripheral Baroreceptor-Denervated Rats." *Hypertension, Dallas*, 8: 1154-1163.

39. Cowley, A.W., J.F. Liard, and A.C. Guyton. 1973. "Role of Baroreceptor Reflex in the Daily Control of Arterial Pressure and Other Variables in Dogs." *Circulation Research*, 32: 564-576.

40. Heymans, C. and E. Neil. 1958. "Reflexogenic Areas of the Cardiovascular System." Boston: Little, Brown and Company.

41. Ito, C.S. and A.M. Scher. 1981. "Hypertension Following Arterial Baroreceptor Denervation in the Unanesthetized Dog." *Circulation Research*, 1981: 576-586.

42. Jacob, H.J., S.J. Lewis, and M.J. Brody. 1989. "Does Cardiac Output Contribute to Arterial Pressure (APL) in Sinoaortic Deafferented Rats (Abstract)." *FASEB Journal*, 3: A851.

43. Krieger, E.M. 1964. "Neurogenic Hypertension in the Rat." *Circulation Research*. 15: 511-521.

44. Norman, R.G.J., T.G. Colman, and A.C. Dent. 1981. "Continuous Monitoring of Arterial Pressure Indicates Sinoaortic Denervated Rats Are Not Hypertensive." *Hypertension, Dallas,* 3: 119-125.

45. Buchholz, R.A., *et al.*, 1986. "Cardiovascular and Neuroendocrine Responses to Behavioral Stress After Central or Peripheral Barodenervation in Rats." *Brain Research*, 365: 360-364.

46. Barres, C., *et al.*, 1992. "Arterial Pressure Lability and Renal Sympathetic Nerve Activity are Dissociated in SAD Rats." *American Journal of Physiology,* 263: R639-R646.

47. Alper, R.H. and M.J. Brody. 1985 "Neurogenic Regulation of Arterial Pressure Lability in Rats Following Sinoaortic Deafferentation (SAD)." *Society of Neuroscience Abstract*, 11: 999.

48. Buchholz, R.A. and M.A. Nathan. 1984. "Chronic Lability of the Arterial Blood Pressure Produced by Electrolytic Lesions of the Nucleus Tractus Solitarii in the Rat." *Circulation Research*, 54: 227-238.

49.   Alexander, N., M. T.,, M.D. Velasquez, and R.F. Maronde. 1980. "Indices of Sympathetic Activity in the Sinoaortic-Denervated Hypertensive Rat." *American Journal of Physiology*, 238: H521-H526.

50.   Irigoyen, M.C., *et al.*, 1995. "Changes of Renal Sympathetic Activity in Acute and Chronic Conscious Sinoaortic Denervated Rats." *Hypertension,* 26: 1111-1116.

51.   Burgess, D.E., *et al.*, 1997. "Multifiber Renal SNA Recordings Predict Mean Arterial Blood Pressure in Unanesthetized Rat." *American Journal of Physiology*, 273: R851-R857.

52.   Jacob, H.J., *et al.*, 1995. "Spectral Analysis of Arterial Pressure Liability in Rats with Sinoaortic Deafferentation." *American Journal of Physiology,* 269: R1481-R1488.

53.   Cerutti, C., C. Barres, and C. Paultre. 1994. 'Baroreflex Modulation of Blood Pressure and Heart Rate Variabilities in Rats: Assessment by Spectral Analysis." *American Journal of Physiology,* 266: H1993-H2000.

54.   Kenner, T., *et al.*, 1973. "Amplitude Dependence of the Carotid Sinus Reflex." *Pffugers Arch.,* 346: 49-59.

55.   Burgess, D.E., *et al.*, 1997. "First-order Differential-Delay Equation for the Baroreflex Predicts the 0.4-Hz Blood Pressure Rhythm in Rats." *American Journal of Physiology,* 273: R1878-R1884.

56.   Andresen, M. and F. Wei. 1996. "Baroreflex Frequency-Response Characteristics to Aortic Depressor and Carotid Sinus Nerve Stimulation in Rats." *American Journal of Physiology,* 271: H2218-H2227.

57.   Andresen, M. and W. Fan. 1998. "Differential Frequency-Dependent Reflex Integration of Myelinated and Nonmyelinated Rat Aortic Baroreceptors." *American Journal of Physiology*, 275: H632-H640.

58.   Sapru, H.N., E. Gonzalez, and A.J. Krieger. 1981. "Aortic Nerve Stimulation in the Rat: Cardiovascular and Respiratory Responses." *Brain Research Bulletin,* 6: 393-398.

59.   Sapru, H.N. and A.J. Krieger. 1977. "Carotid and Aortic Chemoreceptor Function in the Rat." *Journal of Applied Physiology: Respiratory, Environmental and Exercise Physiology*, 42: 245-250.

60.   Brown, A.M., W.R. Saum, and S. Yasui. 1978. "Baroreceptor Dynamics and Their Relationship to Afferent Fiber Type and Hypertension." *Circulation Research,* 42: 694-702.

61. Coleridge, H.M., J.C.G. Coleridge, and H.D. Schultz. 1987. "Characteristics of C Fiber Baroreceptors in the Carotid Sinus of Dogs." *Journal of Physiology, London,* 394: 291-313.

62. Seagard, J.L., *et al.,* 1993. "Selective Contribution of Two Types of Carotid Sinus Baroreceptors to the Control of Blood Pressure." *Circulation Research,* 72: 1011-1022.

63. Dworkin, B.R. 1991. "The Baroreceptor Reinforcement Instrumental Learning (BR-IL) Model of Essential Hypertension: Biological Data, Quantitative Mechanisms, and Computer Modeling" *Perspectives in behavioral medicine: behavioral aspects of cardiovascular disease.* Lawrence Erlbaum Associates: Hillside NJ. p. 213-45.

64. Schreihofer, A.M. and A.F. Sved. 1994. "Use of Sinoaortic Denervation to Study the Role of Baroreceptors in Cardiovascular Regulation." *American Journal of Physiology,* 266: R1705-R1710.

65. Mauad, H., M.L. Glass, and B.H. Machado. 1992. "Effect of Selective Denervation of Baroreceptors on Pulmonary Ventilation and Arterial Pressure Lability in Rat." *Hypertension,* 19 (suppl II): II-182-II-186.

66. Trapani, A.J., K.W. Barron, and M.J. Brody. 1986. "Analysis of Hemodynamic Variability after Sinoaortic Denervation in the Conscious Rat." *American Journal of Physiology,* 251: R1163-R1169.

67. Baselli, G., *et al.,* 1988. "Cardiovascular Variability Signals: Towards the Identification of a Closed-Loop Model of the Neural Control Mechanisms." *IEEE Transactions on Biomedical Engineering,* 35(12): 1033-46

68. Charlton, J.D. and A.J. Baertschi. 1982. "Responses of Aortic Baroreceptors to Changes of Aortic Blood Flow and Pressure in Rat." *American Journal of Physiology,* 242: H520-525.

69. Julien, C., Z.Q. Zhang, and C. Barres. 1995. "Hemodynamic Analysis of Arterial Pressure Oscillations in Conscious Rats." *Journal of Autonomic Nervous System,* 50: 239-252.

70. Akselrod, S., *et al.,* 1985. *"Hemodynamic Regulation: Investigation by Spectral Analysis." American Journal of Physiology,* 249: H867-H875.

71. De Boer, R.W., J.M. Karemaker, and J. Strackee. 1987. "Hemodynamic Fluctuation and Baroreflex Sensitivity in Humans: A Beat-to-Beat Model." *American Journal of Physiology,* 253: H680-H689.

72.   Cerutti, C., *et al.*, 1991. "Autonomic Nervous System and Cardiovascular Variability in Rats: A Spectral Analysis Approach." *American Journal of Physiology,* 261: H1292-H1299.

73.   Schreihofer, A.M. and A.F. Sved. 1992. "Nucleus Tractus Solitarius and Control of Blood Pressure in Chronic Sinoaortic Denervated Rats." *American Journal of Physiology*, 263: R258-R266.

74.   Bracewell, R.N. 1986. "*The Fourier Transform and Its Applications.*" Second Edition: McGraw-Hill.

75.   Fan, W., J.H. Schild, and M.C. Andresen. 1999. "Graded and Dynamic Reflex Summation of Myelinated and Unmyelinated Rat Aortic Baroreceptors." *American Journal of Physiology,* 277: R748-R756.